UNIVERSITY OF CALIFORNIA, SAN DIEGO

Marine Geophysical Study of Cyclic Sedimentation and Shallow Sill Intrusion in the Floor of the Central Gulf of California

A dissertation submitted in partial satisfaction of the
requirements for the degree Doctor of Philosophy

in

Oceanography

by

Jared W. Kluesner

Committee in Charge:

Professor Peter Lonsdale, Chair
Professor Paterno Castillo
Professor Graham Kent
Professor Falko Kuester
Professor Michael Tryon
Professor Edward Winterer

2011

The Dissertation of Jared W. Kluesner is approved, and it is acceptable in quality and in form for publication on microfilm and electronically:

_____

_____

_____

_____

_____

_____

Chair

University of California, San Diego

2011

To my parents, Tony and Donna Kluesner

and my grandfather James Kluesner

"...Let us go, we said, into the Sea of Cortez,

realizing that we become forever a part of it"

The Log from the Sea of Cortez

John Steinbeck

TABLE OF CONTENTS

LIST OF FIGURES

ACKNOWLEDGMENTS

Firstly, I would like to thank my undergraduate mentor Tony Rathburn. Tony Rathburn introduced me to oceanographic research at Indiana State University, before my arrival at Scripps Institution of Oceanography in the fall of 2006. Tony persuaded me to change my major to geology after three years of majoring in computer science. During my tenure in Tony's paleoceanography lab, I gained invaluable experience and mentoring in the scientific method. I collected data in the field, processed samples, analyzed results, and eventually presented findings at scientific meetings around the nation. I credit Tony for my choice of a career in science and will always be indebted to him. After over two years of working with Tony, he arranged for me to participate in a weeklong multibeam and dredging research cruise offshore Baja California with Barry Eakins and Peter Lonsdale. It was on this research expedition, working with Peter, that I realized I wanted to study the geology of the ocean floor using geophysical methods.

Upon my arrival at Scripps I began working with Peter, and within two weeks I was out at sea in the Gulf of California. Although we were chased by hurricanes and had multiple compressor problems (the exhaust fell off and there was a chronic belt failure), we collected an amazing seismic reflection dataset that became the focus of my research. The cruise would not have been possible without the expertise and resourcefulness of Lee Ellett, who always seemed to have a quick fix for problems that arose, and the crew of the *FRANCISCO DE*

ULLOA, a tiny, but very capable research vessel operated out of CICESE. I thank Antonio González for taking the time to introduce me to processing seismic reflection data and for his help in developing processing methods my first year. I would like to thank my advisor Peter Lonsdale for providing me with this interesting research project and the freedom to investigate my own research interests. Although sometimes stern, Peter provided me with the scientific guidance and discipline needed to take on and complete my own research projects. His guidance and uncanny insight into seafloor geomorphology and geologic processes were crucial in analyzing the data and putting the results into the geological framework on which this dissertation is based. I would also like to thank my thesis committee for their valuable feedback that improved this dissertation.

Additionally, I would like to thank all of my friends from Scripps. In particular, I would like to thank Sandra Kirtland-Turner for her help in developing the climate chapter and for always being somebody off of whom I can bounce ideas. Sandy will always be a close friend and hopefully a colleague for years to come. Second, I would like to thank my officemate Daniel Ebuna for always listening to me propose ideas about my research and providing valuable feedback.

Lastly, I would like to thank my family for always providing support and for believing in me. Ever since I changed my major after 3 years of undergrad, my

parents Tony and Donna Kluesner have been completely supportive of my career path; without their support this dissertation would not have been possible. I thank my father for instilling in me a strong work ethic and my mother for teaching me to always look outside the box. I dedicate this dissertation to them and to my grandfather, James Kluesner, who taught me at a young age to have big dreams and not be afraid to pursue them.

Chapter 2, in full, has been submitted for publication of the material as it may appear in Geosphere, 2012, Kluesner, J., Lonsdale, P., Kirtland, S., and González, A., The dissertation author was the primary investigator and author of this paper.

Chapter 3, in part, is currently being prepared for submission for publication of the material. Kluesner, J., Lonsdale, P., The dissertation author was the primary investigator and author of this paper.

VITA

2003	Associate of Science, Computer Science Vincennes University
2004-2006	Undergraduate Research Assistant Indiana State University
2006	YBRA Geology Field Camp University of Pennsylvania
2006	Bachelor of Science, Geology Indiana State University
2011	Doctor of Philosophy, Oceanography Scripps Institution of Oceanography University of California, San Diego

PUBLICATIONS

Kluesner, J., Lonsdale, P., Kirtland, S., and González, A., 2011, Influence of Glacial-Interglacial Cyclicity on Sedimentation and Axial Rift Structure at the Southern Trough, Geosphere, under review.

Rathburn, A. E., Levin, L.A., Tryon, M., Gieskes, J. M., Martin, J. B., Perez, M. E., Fodrie, F. J., Neira, C., Fryer, G. J., Mendoza, G., McMillan, P. A., Kluesner, J., Adamic, J., Ziebis, W., 2009, Geological and biological heterogeneity of the Aleutian margin (1965-4822 m), Progress In Oceanography, Volume 80, Issues 1-2, p. 22-50.

Basak C., Rathburn, A., Perez, E., Martin, J., Kluesner J., Levin, L., DeDeckker, P., Gieskes, J., and Abriani, M., (2009). Carbon and oxygen isotope geochemistry of live (stained) benthic foraminifera from the Aleutian Margin and the Southern Australian Margin, Marine Micropaleontology, Volume 70, Issues 3-4, p. 89-101.

ABSTRACT OF THE DISSERTATION

Marine Geophysical Study of Cyclic Sedimentation and Shallow Sill Intrusion in the Floor of the Central Gulf of California

by

Jared Kluesner

Doctor of Philosophy in Oceanography

University of California, San Diego, 2011

Professor Peter Lonsdale, Chair

A new marine geophysical study in the central Gulf of California provides new insights into uppercrustal processes associated with the transition from continental rifting to seafloor spreading. This research is based on the collection and processing of multibeam bathymetry, 3.5 kHz profiles, and two multichannel seismic (MCS) reflection grids collected throughout the central Gulf of California. One high-resolution MCS profile collected across the Southern Trough of Guaymas Basin shows alternations of seismically transparent sedimentary units

and horizontally layered strata with high-amplitude internal reflectors. Correlation with DSDP drilling results reveals that reflector alternations are due to cyclical changes between diatomaceous mud turbidites and mud turbidites rich in terrigenous clastics driven by glacial/interglacial cyclicity. This correlation is also supported by the spatial extent of the seismic units, specifically the distance off-axis at which they intercept an intrusion-sediment complex that spreads away from the axis at ~23 km/Myr. Seismic stratigraphy also shows that during glacials, accumulation rates in the southwest part of Guaymas Basin increased significantly, filling the axial trough. During interglacials, greater aridity and higher sea-level reduced the delivery of terrigneous clastics and axial extension outpaced sedimentation, resulting in regeneration of the axial rift relief.

Throughout the central Gulf, analysis of MCS and 3.5 kHz profiles and multibeam bathymetry reveals extensive evidence of shallow, young magmatic intrusions into unconsolidated hemipelagic muds blanketing axial troughs, off-axis oceanic crust, and thinned continental crust. Multiple sills 1-2 km in diameter have a characteristic concave-upwards profile are most common as off-axis intrusions into unconsolidated hemipelagic muds flooring the Guaymas, Carmen, and Farallon Basins, and within the sediment cover of subsided continental crust at the basins' margins. Integration of geophysical datasets suggests that concave-upwards sills have circular to elliptical three-dimensional geometry. Plotting concave upwards sill width against emplacement depth reveals an overall linear trend (deeper = wider sill) and modeling results suggest

emplacement depth as a main control on sill structure. MCS and 3.5 kHz profiles also show extensive evidence of hydrothermal fluid flow and hydrocarbon generation above multiple sills including pipe-like features, pockmarks, acoustic turbidity, bright spots, negative polarities, and eye-like structures interpreted as hydrothermal deposits.

Chapter 1

Introduction

1.1 HIGH-RESOLUTION IMAGING OF RIFT-TO-DRIFT PROCESSES

The process of continental rifting, and possible transition to oceanic seafloor spreading, has been occurring for billions of years and is fundamental to the constant change in the shape and structure of Earth's lithosphere. Previously, continental rifting and the transition to seafloor spreading was thought to be controlled mainly by pre-existing lithospheric conditions, strain rate, and initial geological conditions; however, recent advancement in the understanding of rift evolution has raised a new question: How do fundamental rifting processes (such as tectonics, magmatism, climate and erosion, sediment transport, and sedimentation), and the feedbacks between them, evolve during the transition from continental rifting to seafloor spreading? The inability to address this question has been partly due to the fact that the majority of rifted margins on the planet are now passive margins that have undergone syn- and post-rift magmatism and post-breakup sedimentation, both of which overprint and deeply bury the record of the rift-to-drift transition.

In recent years a large number of deep geophysical studies have focused on old rift systems and rifted continental margins, such as the U.S. east coast (Holbrook et al., 1994; Klitgord et al., 1988) and the North Atlantic Igneous Province (Planke et al., 2000; Bell and Butcher, 2002). Although these studies shed some new light on rift-to-drift processes such as associated magmatism,

their interpretations and conclusions were based on deeply buried (low resolution) end members of processes that have been inactive for millions of years. In contrast to relatively sediment-starved mid-oceanic spreading centers, submerged continental rifted margins are deeply buried beneath the prograding sediments of continental slopes, making high-resolution seismic imaging difficult, predominantly owing to the absorption of higher frequencies and scattering of seismic energy in the overlying, thick layer of sediments (Mosher and Simpkin, 1999). This is problematic, as it limits the ability to image the more intricate geological structures (Hansen and Cartwright, 2007), which are crucial in unlocking the interactions between rifting, sedimentation, magmatism, and fluid flow.

The Gulf of California, in contrast, provides a modern rift-to-drift tectonic setting where one can study, in high resolution, the processes associated with continental rifting and subsequent seafloor spreading. Using high-resolution geophysical tools such as shallow multi-channel-seismic (MCS) profiling and multibeam bathymetry, one can obtain detailed snap-shots of rift-to-drift processes happening at or near the seabed. Sedimentation within the Gulf has a general trend of high sedimentation rates in the northern rifted basins (Dorsey, 2010) to low sedimentation rates in Alarcon Basin located in the mouth of the Gulf (Lonsdale and Kluesner, 2010). Sedimentation rates within the central and southern Gulf are low enough, and the oceanic basins are mature enough, to analyze upper-crustal rift-to-drift processes without having to penetrate through

kilometers of sediment cover. In this study, the processing and analysis of high-resolution MCS profiles, 3.5 kHz acoustic profiles, and multibeam bathymetry collected throughout the central and southern Gulf of California (Figure 1) in order to address fundamental uppercrustal processes and feedbacks operating during the rift-to-drift transition. The following paragraphs will introduce this research and highlight some of the major results and conclusions.

Chapter 2 presents a study of the influence of climatic cyclicity on sediment delivery, seismic stratigraphy, and changes in axial rift structure in the Southern Trough of Guaymas Basin located in the central Gulf. Examination of a high-resolution MCS profile across the 4 km-wide axial rift in southern Guaymas Basin reveals alternations of highly faulted seismically transparent reflector units and horizontally layered high-amplitude reflector units. Correlation of the seismic units to nearby drilling results (Deep Sea Drilling Project Leg 64; Curray, Moore at al., 1982) reveals that transparent units are composed of diatomaceous mud turbidites, whereas high-amplitude reflector units are mud turbidites with thicker, coarser layers of terrigenous silty sand. Limited biostratigraphic data from the drilling results (Schrader, 1982; Aubry, 1982), in combination with observed sediment types (Curray, Moore at al., 1982), indicates that the cyclical pattern in reflector units is a result of glacial-interglacial cyclicity. This correlation is also supported by the spatial extent of reflector units, with transparent units intercepted by sill-sediment complexes at roughly 100 kyr intervals using a half spreading rate of ~23 km/Myr. Analysis of seismic stratigraphy also reveals that

sedimentation rates during glacial periods were much higher than during interglacials, resulting in filling of the axial rift and suppression of the tectonic relief. Sediment grain analysis from nearby drill cores (Van Andel, 1964; Marsaglia, 1991), climate modeling (Kutzback and Wright, 1985; Bartlein et al., 1998), paleobotanical results from Baja California (Rhode, 2002), and the presence of major erosional canyons terminating against the present location of the Southern Trough all indicate that sources for floods of terrigenous clastics during glacial periods were probably both local (erosion of Baja California) and regional (erosion of emergent continental shelves on the mainland side of the Gulf). In contrast, during interglacials, greater aridity and sea-level rise resulted in lower sedimentation rates while axial extension rates stayed the same, resulting in a reestablishment of the axial trough relief. Additional profiles collected across other rift basins in the central and southern Gulf show similar reflector cyclicity; however lack of nearby drilling results limits the ability to correlate alternating units to climatic cycles. Comparison with other seismic reflection studies on tectonic boundaries located in latitudes heavily affected by glacial/interglacial changes suggests that changes in sedimentation caused by 100-kyr glacial/interglacial cyclicity may be common to a variety of heavily sedimented tectonic settings that are located in the mid-latitudes and/or largely affected by orbital-scale climatic cyclicity.

Chapter 3 explores the geologic and hydrologic effects of young magmatic intrusions in the central and southern Gulf of California and also examines the

influence that sediment load has on the structure and depth of intrusive magmatism. Numerous MCS profiles collected across the central and southern Gulf of California display young magmatic sills and associated overburden deformations, fluid migration pathways, and possible feeder networks. Multiple large sills (1-2 km in diameter) display characteristic concave upwards profiles. These shallow, bowl-like sills are most common as off-axis intrusions into unconsolidated hemipelagic muds flooring the Guaymas, Carmen, and Farallon Basins, but some can also be identified in sediment ponded, in at least one of the narrow rift valleys that mark the principal, axial sites of magmatic crustal accretion within these young, actively growing oceanic basins. Clusters of similar sills also occur within the sediment cover of subsided continental crust at the basins' rifted and shearing (transform) margins, where they may mask the geologic boundaries between oceanic and continental crust. In all three settings, several sills are very young, uplifting the seafloor, disrupting turbidite deposition patterns, and creating onlap of the youngest strata, which provides relative ages of intrusions, associated sediment deformation, and fluid-flow structures. Integration of multibeam bathymetry and dense grids of 3.5 kHz profiles over concave-upwards sills imaged on MCS profiles suggest that sills have round to elliptical three-dimensional (3D) geometry. Mapped saucer-shaped sills show a striking resemblance to doleritic saucer-shaped sills imaged with 3D seismics along the North Atlantic Margins (Bell and Butcher, 2002; Smallwood and Maresh, 2002), and similarities with field-mapped saucer-shaped dolerite sills

(Chevallier and Woodford, 1998; Polteau et al., 2008). Plotting width of upturned sills against emplacement depth reveals an overall linear trend (deeper = wider sill) and two distinct slopes that can be separated by geographic location. Modeling results suggest emplacement depth as a main control on sill structure and that development of asymmetrical stress fields above the sill once uplift of the overburden occurs might be responsible for the upturned sill edges. MCS profiles also reveal sub-vertical, cross-cutting reflectors below the sills that differ from seismic artifacts and sideswipes in that they do not resemble out-of-plane diffractions or diffraction ‘smiles’ caused by over-migration and are found only underlying areas of intrusions. Some of these steeply inclined, high-amplitude reflectors can be traced directly below a sill and may represent the inclined tips of older sills, feeding the overlying younger sills. Vertical seismic disturbances called 'chimneys' or 'pipes' leading up from several large sills are probably hydro-fractured pathways that funnel super-heated fluids away from the intrusion-sediment contact zone, some of which terminate directly under pockmarks on the seafloor. Within the heavily faulted axial troughs, fluids utilize fault planes for low-resistant conduits to the seafloor. MCS profiles collected over young sills with no visible fluid pathway to the seafloor, such as faults or ‘pipes’ show extensive evidence for concentrated hydrocarbons and trapping and leakage features. Plainly, in the heavily sedimented central Gulf of California melt is being delivered to the uppermost crust over a broad area, not just to the spreading centers,

resulting in widespread intrusive volcanism and associated hydrothermal fluid-flow.

1.2 REFERENCES

Aubry, M. P., Matoba, Y., Molina-Cruz, A., and Schrader H., 1982, Synthesis of Leg 64 Biostratigraphy: Initial Reports Deep Sea Drilling Program, v. 64, p. 1057-1064.

Bartlein, P. J., Anderson, K. H., Edwards M. E., Mock, C. J., Thompson, R. S., Webb, R. S.,Webb III T., and Whitlock, C., 1998, Paleoclimate simulations for North America over the past 21,000 years: features of the simulated climate and comparisons with paleoenvironmental data: Quaternary Science Reviews, v. 17, p. 549-585.

Bell, B. and Butcher, H., 2002, On the emplacement of sill complexes: evidence from the Faroe-Shetland Basin. In: The North Atlantic Igneous Province: Stratigraphy, Tectonic, Volcanic and Magmatic Processes (D.W. Jolley and B.R. Bell, eds), Geol. Soc. London Spec. Publ., v. 197, p. 307–329.

Chevallier, L. & Woodford, A., 1999, Morpho-tectonics and mechanism of emplacement of the dolerite ring and sills of the western Karoo, South Africa. S. Afr. J. Geol., v. 102, p. 43–52.

Curray, J. R., Moore, D. G., et al., 1982, Guaymas Basin: Sites 477, 478 and 481: Init Repts. DSDP, Initial Report Deep Sea Drilling Program, v. 64, p. 211-415.

Dorsey, R., 2010, Sedimentation and crustal recycling along an active oblique-rift margin: Salton Trough and northern Gulf of California: Geology, v. 38, p. 443-446.

Hansen, D. M., and Cartwright, J., 2007, Reply to comment by K. Thomson on “The three-dimensional geometry and growth of forced folds above

saucer-shaped igneous sills" by Hansen and Cartwright, Journal of Structural Geology, 29, p. 741-744.

Holbrook, S, Reiter, E., Purdy, G., Sawyer, D., Stoffa, P., Austin, J., Oh, J., and Makris, J.,1994, Deep structure of the U.S. Atlantic continental margin, offshore South Carolina, from coincident ocean bottom and multichannel seismic data. JGR, v. 99, p. 9155-9178.

Klitgord, K., Hutchinson, D., and Schouten, H., 1988, U.S. Atlantic continental margin: Structural and tectonic framework, in Sheriden, R. E., and Grow, J. A., eds, The Atlantic continental margin: U.S.: Boulder Colorado, GSA, Geology of North America, Vol. I-2, pp. 19-55.

Kutzback, J.E., and Wright, H.E., 1985, Simulation of the climate 18,000 BP: Results for the North American/North Atlantic/European sector and comparison with the geologic record of North America: Quaternary Science Reviews, v. 4, p. 147-187.

Lonsdale, P., and Kluesner J., 2010, Routing of terrigenous clastics to oceanic basins in the Southern Gulf of California, inherited from features of the pre-spreading protogulf. Fall Meet. Suppl., Abstract T33C-2265.

Marsaglia, K., 1991, Provenance of sands and sandstones from a rifted continental arc, Gulf of California, Mexico: in Fisher, R.V., and Smith, G.A., eds., Sedimentation in volcanic settings: SEPM (Society for Sedimentary Geology) Special Publication 45, p. 237–248.

Mosher, D., and Simpkin, P., 1999, Environmental marine geosciences 1. Status and trends of marine high-resolution seismic reflection profiling: data acquisition. Geoscience Canada, v. 26, p. 174-188.

Planke, S, Symonds, P., Alvestad, E., and Skogseid, J., 2000, Seismic volcanostratigraphy of large-volume basaltic extrusive complexes on rifted margins. Journal of Geophysical Research, v. 105, 19, p. 335-19,351.

Polteau S., Ferré E.C., Planke S., Neumann E.-R., Chevallier L., 2008, How are saucer-shaped sills emplaced? Constraints from the Golden Valley Sill, South Africa: *Journal of Geophysical Research*, v. **113**, B12104, doi: 10.1029/2008JB005620.

Rhode, D., 2002, Early Holocene Juniper woodland and chaparral taxa in the Central Baja California Peninsula, Mexico: Quaternary Research, v. 57, p. 102-108.

Schrader, H., 1982, Diatom Biostratigraphy and Laminated Diatomaceous Sediments from the Gulf of California: Init. Rep. Deep Sea Drilling Program, v. 64, p. 973-981.

Smallwood, J.R. & Maresh, J., 2002, The properties, morphology and distribution of igneous sills: modelling, borehole data and 3D seismic from the Faroe-Shetland area. In: The North Atlantic Igneous Province: Stratigraphy, tectonic, volcanic and magmatic processes (Ed. by D.W Jolley & B.R. Bell), Geol. Soc. London. Spec. Publ., v. 197, p. 271–306.

Van Andel T., 1964, Recent marine sediments of Gulf of California, *in* Van Andel T.,Shor G.G., eds., Marine geology of the Gulf of California: American Association of Petroleum Geologists Memoir 3, p. 216–310.

Figure 1-1. Regional map of the Gulf of California. Map shows major tectonic boundaries between the northern end of the East Pacific Rise (EPR) and the southern end of the San Andreas Fault System (SAFS). Short red lines represent active spreading centers and linking blue lines represent transform faults. Dashed yellow circle marks the region of this study. Large red arrows denote plate motion.

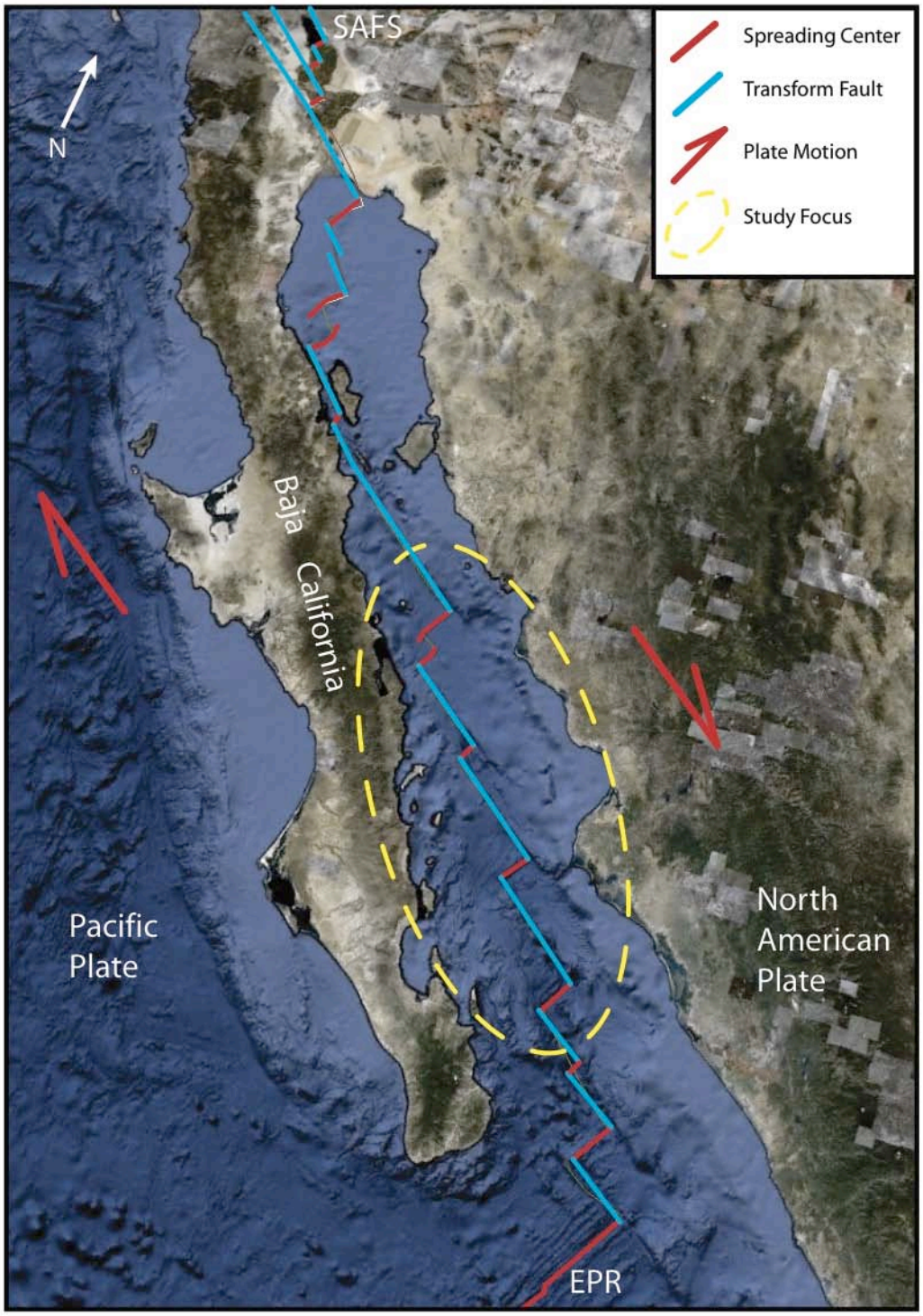
SAFS
N
Spreading Center
Transform Fault
Plate Motion
Study Focus
Baja California
Pacific Plate
North American Plate
EPR

Chapter 2

Influence of Glacial-Interglacial Cyclicity on Sedimentation and Axial Rift Structure at the Southern Trough of Guaymas Basin, Gulf of California

2.1 ABSTRACT

The Southern Trough of Guaymas Basin is a 4 km-wide regenerating axial rift valley along a Gulf of California spreading center that intersects the continental slope of Baja California. A high-resolution seismic reflection traverse across the trough and adjacent basin floor shows alternations of (i) seismically transparent sedimentary units and (ii) horizontally layered strata with high-amplitude internal reflectors. The uppermost stratum, inferred to be of post-glacial age, is a seismically transparent unit of diatomaceous mud turbidites, but within the Southern Trough it does have laterally persistent acoustic (3.5-4 kHz) reflectors, found at Deep Sea Drilling Program (DSDP) Site 477 to be thin layers of clastic sand derived from Baja California. The reflector-rich seismic units, sampled off-axis at DSDP site 478, are also mud turbidites, but with thicker, coarser layers of terrigenous silty sand. Sparse biostratigraphic data from the drill-cores is consistent with a match between the cyclic deposition of reflective and transparent units and the glacial/interglacial climatic cycle. This correlation is also supported by the spatial extent of the seismic units, specifically the distance off-axis at which they intercept acoustic basement, a intrusion-sill complex that spreads away from the axis at ~23 km/Myr. Seismic stratigraphy also shows that while the reflector-rich sandy units were being deposited, turbidite accumulation rates in the southwest part of Guaymas Basin increased significantly. The axial trough was filled, suppressing the tectonic relief that has both channeled and

obstructed turbidity current flows from the continental margins. The principal sources for the floods of terrigenous sediment during the glacial periods were probably both local (enhanced erosion of the wetter Baja California peninsula) and regional (erosion of the sediment cover of emergent continental shelves, especially on the mainland side of the Gulf). With lesser sediment supply during post-glacial periods of greater aridity and higher sea-levels, continued extension and spreading of the oceanic crust reestablished the axial rift-valley relief. Some profiles across tectonically active depocenters elsewhere in the plate boundary zone in the central and southern Gulf show similar apparently cyclical effects, but their correlation with the glacial/interglacial timescale is more tenuous because of the lack of drill-core samples. Those basins supplied with terrigenous sediment mainly from the mainland margin show less obvious cyclicity in their seismic stratigraphy, probably because delivery of coarse clastics by rivers draining the high Sierra Madre Occidental persisted throughout glacial/interglacial cycles.

2.2 INTRODUCTION

The Gulf of California occupies part of a 1750km-long obliquely opening rift zone and is floored by a chain of post-Miocene oceanic basins surrounded by stretched and subsided continental crust (Lonsdale, 1989). Spreading centers at the basin axes are of three structural types (Figure 1), which accrete different types of upper oceanic crust. The one in the southernmost (Alarcon) basin has a structure similar to that of the East Pacific Rise (EPR) crest, with an elevated

axial zone of eruptive fissural volcanism and a lava-flow upper crust like that of the EPR (Castillo et al., 2002). At the shallow northern end of the Gulf, spreading centers in Wagner and Upper Delfin Basins (Persaud et al., 2003) occupy broad depressions with gently inclined side-slopes interrupted by a few low fault scarps; their upper crusts are thick sections of sparsely intruded Colorado Delta sediments (Dorsey, 2010) as at comparable subaerial sites in the Salton Trough. The seven gulf spreading centers between these two extreme types are all marked by rift valleys, or “axial troughs”, with 3-5 km-wide floors 150 m (Guaymas Basin)-1200 m (Farallon Basin) below the general level of the adjacent basin floors. These narrow enclosed depressions act as depocenters for sediment delivered by density flows, especially turbidity currents (Einsele and Kelts, 1982). Gravitationally focused accumulation of low-density turbidites right at the axes of crustal accretion is inferred to hamper the rise, and particularly the eruption, of magma injected into the neovolcanic zones, and is thereby held responsible for the distinctive composition of the crust accreted at these axes (igneous dikes and other intrusions combined with variably baked sediment, referred to by Einsele (1985) as a sill-sediment complex), and for their distinctive structure (Moore, 1973)). Contrary to initial interpretations that the axial troughs are simple grabens created by recent local subsidence of initially flat, unfaulted basin floors (e.g., Moore, 1973: Bischoff and Henyey, 1974), it is now generally accepted (e.g. Einsele, 1985; Lonsdale and Becker, 1985) that they are regenerating rifts like the axial rift valleys of slow-spreading mid-ocean ridges,

where newly accreted crust moves upwards and outwards from the trough floors (Atwater and Mudie, 1968; Tapponnier and Francheteau, 1978), though in the Gulf sediment loading of the basin floor may suppress isostatic uplift of the rift shoulders. Regenerating rift valleys have been described as “steady-state” features, but because their structure is controlled by a balance of tectonic, magmatic, and sedimentary forces it can alter if these forces change in a cyclical or secular fashion. This is seen on slow-spreading ridges by cyclical development of low-angle detachments (e.g., Escartin et al., 2008), and in the Gulf by changes in the sediment input to the spreading axes. Curray, Moore et al. (1980, p. 257) suggested that “during times of glacial maxima and low sea-levels” higher inputs of terrigenous sediment to the floor of Guaymas Basin may “completely fill the (axial) troughs, forming a single depositional basin plain”; at these times the axial structure in the central gulf may have resembled the gently sloping depressions of the present northernmost gulf, where huge inputs of Colorado River sediments continued through interglacial periods.

Mineralogy of seafloor sediment in Guyamas Basin (Van Andel, 1964; Calvert, 1966; Einsele and Kelts, 1982; Marsaglia, 1991), and its pattern of submarine fans and channels (Figure 1), indicates t hat most of the terrigenous sand and silt in Guaymas Basin enters the gulf via two permanent mainland rivers, the Yaqui and the Mayo, whose tributaries drain the well watered deeply incised Sierra Madre Occidental plateau, 100-150 km inland. A bathymetrically defined, and apparently still active channel on the Mayo fan extends to within 100

km of the basin's Southern Trough (Figure 1), and there is a continuous downhill gradient from the end of this channel into the trough. There is other geomorphic evidence for another, more local, source of terrigenous clastics for the Southern Trough; it intersects the Baja California continental slope off the mountainous Concepcion Peninsula. Seaward of Concepcion Peninsula is an integrated system of high-gradient (80 m/km) channels, ephemeral washes on the now-arid peninsula continuing downslope as submarine canyons to the basin floor (Figure 2), including two canyons that lead directly to the southwest end of this axial trough. In addition to the coarser terrigenous clastics delivered as the bed-load of turbidity currents, terrigenous clay size particles are major components of the mud turbidites of Guaymas Basin (Einsele and Kelts, 1982). They enter the basin as the suspended load of rivers and as fall-out from wind-borne dust, in both cases derived mainly from the mainland side of the Gulf (Baba et al., 1991; Baumgartner et al., 1991), but widely dispersed across the basin as the suspended load of surface currents and (after reworking) turbidity currents.

Multichannel seismic (MCS) reflection profiles are here examined for evidence of glacial-interglacial cyclicity in delivery of terrigenous sediments to the floors of central gulf basins, and for evidence of resulting changes in the structure of regenerating axial troughs. These structural changes may in turn affect sediment dispersal routes and thereby the seismic stratigraphy. Also considered are secular (non-cyclical) changes in sediment delivery to this widening basin, caused by the predictable movement of axial troughs away from rifted margins

and along shearing (transform) margins. We also evaluate possible effects of cyclical changes in the other principal source of deep-sea sediment in Guaymas Basin: algal blooms that are stimulated by wind-driven upwelling of nutrient-rich water, and are most prolific along the mainland continental margin (Douglas et al., 2007). The blooms produce rains of planktonic debris; principally low bulk-density siliceous diatom frustules and calcareous coccoliths that are widely dispersed by surface and bottom currents to depositional sites throughout the basin.

2.3 GEOPHYSICAL DATA

In September 2006, 2500 km of high-resolution MCS reflection profiles were collected throughout the southern Gulf of California, with a few additional profiles further north across Guaymas and Carmen Basins (Figure 1). The survey vessel was CICESE's ship *FRANCISCO DE ULLOA*, firing a small (45+105 cubic inches) G.I. gun. Collection of 8-fold seismic data was with the Scripps Institution of Oceanography's 48-channel, 12.5 m-group-spacing, streamer. A shooting interval of 12 seconds traveling at an average of 6 knots was used, with a sampling interval of 1.00 msec. The dominant frequency is approximately 80 Hz and using a mean velocity of 1600 m/s at a depth of 2,000 m results in a post-migrated vertical resolution of about 5 m and a migrated horizontal resolution of approximately 100 m. This resolution decreases with depth due to absorption of higher frequencies. We also use a MCS profile collected across Guaymas Basin

in 1978 during the site-survey cruise for DSDP Leg 64. It crosses DSDP core sites 477 and 478, and thereby allows correlation of profiling and coring results. The site survey profiling used a 24-channel streamer with nonlinear hydrophone spacing, and an array of 3 Bolt airguns (20, 120, and 40 cubic inches) firing every 15 seconds at an average ship speed of 6 kts. Sampling intervals were 1.5 and 2.0 msec. Data processing on both MCS data sets was done using Seismic Unix and SIOSEIS software, and included common-depth-point sorting, bandpass filtering, dip filtering, semblance velocity analysis, predictive deconvolution, normal move-out correction, partial pre-stack migration (dip move-out correction), stacking, post-stack migration with a variable velocity model, water column muting, and time-varied gain. An average velocity of 1.6 km/s is used to convert Two-Way-Travel-Time (TWTT) to meters of sediment thickness. This value is based on physical property and acoustic loss tests conducted on core samples during DSDP drilling leg 64 in Guaymas Basin (Einsele and Niemitz, 1982), together with interval velocities calculated from semblance velocities picked from the recently collected high-resolution, MCS data. Multibeam bathymetry data was collected during various cruises led by P. Lonsdale over the past decade, using the EM120 sonar of *R/V ROGER REVELLE* and the Seabeam 2112 sonar of *R/V ATLANTIS*.

2.4 RESULTS AND INTERPRETATIONS

2.4.1 Seismic Stratigraphy

MCS images of the seabed flanking the Southern Trough have three noteworthy characteristics:

1. A cyclic alternation of (i) 10-100 m –thick sedimentary units (labeled A, B, and C in Figure 3) that are almost transparent at seismic frequencies, with just a few low-amplitude internal reflectors, and (ii) intervening units with close-spaced high-amplitude internal reflectors, typical of classic turbidite sequences where textural differences between texturally heterogeneous graded beds provide sharp acoustic impedance contrasts (Sangree and Widmier, 1977).

2. A thickening of the reflector-rich units toward the spreading axis, most abruptly where they onlap steeply dipping and step-faulted parts of the underlying transparent units.

3. A seismic basement that is a diffuse and irregular surface, intersected by units B and C at successively greater distance from the spreading axis.

Definition of the seismic stratigraphy of the axial trough floor is hampered by recent tectonic deformation and shallow intrusive volcanism (Kluesner and Lonsdale, 2008). In our interpretation of MCS Profile 1 (Figure 3), the superficial “transparent” unit A is considerably thicker within the trough than on the flanks, and has more internal reflectors. The underlying well-stratified unit has inclined, discontinuous reflectors. Surface-ship and near-bottom 3.5-4 kHz profiles along and across the trough floor (e.g., Lonsdale and Lawver, 1980, Figure 2; Lonsdale and Becker, 1985, Figure 3, with their Profile 3C being very close to our MCS

Profile 1) provide a higher resolution description of the acoustic stratigraphy of the upper 100 m of the trough fill. A 20-80 m-deep pond of sediment with several laterally persistent and slightly deformed internal reflectors hosts large hydrothermal mounds and active hydrothermal and hydrocarbon vents. It unconformably overlies the higher relief surface of a more deformed sedimentary section that has been locally uplifted to form islands of semi-lithified mudstone within the superficial pond of unconsolidated sediment (Lonsdale and Lawver, 1980).

2.4.2 Lithology and Age of the Seismic Stratigraphy Units

Coring at DSDP Site 477, in the axis of the Southern Trough within 1 km of MCS Profile 2, recovered unconsolidated diatomaceous ooze and hemipelagic mud turbidites above a basaltic sill at 58 m sub-bottom (Curray, Moore at al., 1982). Sedimentologic analysis concluded that even the ooze, as well as the visibly graded mud turbidites, were deposited by thick, slow low-concentration turbidity flows (Einsele and Kelts, 1982), perhaps with a higher velocity basal flow that accounts for the several 2-3 cm thick basal sandy silt layers found in the drill core. Mineralogic analysis by Marsaglia (1991) determined that these turbidite sands had a Baja California source, consistent with van Andel's (1964) interpretation of heavy mineral assemblages in superficial (gravity core) samples, and inferred that they were brought to the trough floor by channeled flow down canyons in the steep continental slope (Figure 2). Though core recovery was

very incomplete, and the sandy layers are very thin, three of them match the depths of widespread internal reflectors on acoustic (4 kHz) profiles across the superficial sediment pond (Lonsdale and Becker, 1980). The very shallow sills sampled at DSDP Site 477 and nearby DSDP Site 477A produce strong reflectors on acoustic and seismic profiles (e.g., Figure 4). Deeper reflectors within unit A in other parts of the trough floor where the shallowest sills are at greater sub-bottom depth or are thin enough to allow seismic imaging of sub-sill strata (e.g., on MCS Profile 1; Figure 3), and in the deformed section imaged below the sediment pond on acoustic profiles, are probably caused by variably indurated claystone, dolostone, siltstone, and sandstone beds within an older, hydrothermally altered section, like the one cored at 100-270 m sub-bottom, beneath the shallow sills, at DSDP Sites 477 and 477A (Currray, Moore et al., 1982).

Cores from DSDP Site 478, approximately 12 km northwest of the Southern Trough axis (Figure 2), provide the best evidence for lithology and age of the alternating transparent and reflective seismic units of the trough flanks. The youngest seismically defined transparent unit (A) pinches out at or near this relatively elevated drill site (Figure 5), but may be represented by the “gelatinous diatom ooze” in the upper few meters of the core (Curray, Moore et al., 1982, p. 240). The underlying reflector-rich unit, with a base 0.15 seconds TWTT sub-bottom (120 m at a sonic velocity of 1600 m/sec) is identified with Subunit 1A, base at 127 m, of the core description: muddy diatomaceous oozes interlayed

with graded turbidites with basal layers of silty sand, mainly composed of terrigenous clastics including coarse feldspathic sands (e.g., Figure 32 of Curray, Moore et al., 1982), and an overall mineralogy indicative of a mainland Mexico source (Marsaglia, 1991). Transparent seismic unit B, at 0.15-0.22 seconds TWTT (120-176 m, at a sonic velocity of 1600 m/sec), corresponds to the "uniform diatomaceous silty mud" of the upper part (127-164 m) of Subunit 1B in the core description; the "1-2 m- and 3-m-thick sand turbidites with interlayered diatom oozes and muds " in the lower part (164-188 m) of this subunit (Curray, Moore et al., 1982, p. 241) are probably responsible for the upper reflectors in the reflector-rich unit below transparent unit B. Unit 2 of the core description (Figure 5) has alternations of igneous sills, dewatered indurated claystones and siltstones, and unconsolidated sediments. Recovery of the latter was minimal, and on seismic Profile 2 (Figure 5) we see few coherent reflectors below the level of the sill intrusions, so correlation of the seismic reflectors with cored lithologies is difficult. Core recovery was better in the underlying 80 m-thick Unit 3, which at 340 m overlies a diabase sill more than 100 m thick. Layers of terrigenous sand are common in the upper half of Unit 3, but at 295 m there is a transition to diatom-rich partly laminated muds (Curray, Moore, et al., 1982). At a comparable distance from the spreading axis on the higher resolution seismic Profile 1 (Figures 3 and 5), 4 km to the southwest of Profile 2, there is no seismic evidence of sill intrusions (abruptly ending, high-amplitude reflectors) as shallow as those at DSDP Site 478, and reflector-rich units are separated by a well

defined transparent unit C, at ~300-350 m subbottom. This seismic unit may correspond to the diatomaceous mud overlying the thick sill in which drilling terminated at Site 478.

All three of the DSDP sites on the floor of Guaymas Basin are located on crust that accreted within the past 0.4 Myr, so it is not suprising that biostratigraphy of the drill-cores establishes that all their sediments were deposited during the Late Quaternary (Curray, Moore, et al., 1982). Using micropaleontology to establish a finer scale stratigraphy, and in particular to identify deposits from specific glacial and interglacial periods, has proven more difficult. Problems include poor fossil preservation in some key core sections, and the relatively slow evolution of the two most abundant fossil groups (coccoliths and diatoms), but the major problem may be that so much of the sediment and its microfossils have been reworked from their original deposition sites, especially by turbidity currents. Two biostratigraphic datum levels were recognized in Site 478 cores from the inter-sill part of the section: (i) the ~260 ka last appearance of the diatom *Nitzchia fossilis* at 315 m, in the diatomaceous muds, with mainly “warm water forms” (Schrader, 1982) that we correlate with seismic transparent Unit C; and (ii) the ~270 ka last appearance of the coccolith *Emiliania huxleyi*, in the overlying sand-rich zone at 285 m subbottom (Aubry, 1982). If the diatom datum gives a valid age for deposition of unit C, that would support deposition of this unit during the penultimate (pre-Illinoian) interglacial [~250-200 ka (Gibbard et al., 2007)], consistent with the seismic stratigraphy (Figure 3), and with the

prevalence of “warm water forms” (Curray, Moore et al., 1982, p. 242). However, reworking of older calcareous microfossils is needed to explain the presence of pre-270 ka forms in the overlying sandy turbidites, more plausibly attributed to the post-200 ka Illinoian glacial period.

To summarize the core-derived evidence for the composition, derivation, and age of the seismically defined stratigraphic units:

1. Most of the sediments beneath the floor and flanks of the Southern Trough are diatomaceous mud turbidites. Deposition from turbidity currents was responsible for both the reflector-rich units and the seismically transparent units (A, B, and C).

2. Turbidite beds within the highly reflective units have Bouma sequences (Bouma, 1962) that include sandy basal layers, composed mainly of terrigenous clastics; we infer that impedance contrasts between these layers and intervening finer grained muds and oozes are responsible for most of the internal reflectors. Turbidites in the transparent units lack such sandy layers, or, as in the superficial turbidite pond of the Southern Trough floor, have laterally extensive layers of clastic sands so thin as to be invisible at seismic frequencies, though they are imaged by higher frequency acoustic profiles.

3. The terrigeneous clastics that form thin sandy layers in young sediments of the Southern Trough floor were derived from subaerial erosion of the adjacent Baja California peninsula. Older sandy turbidites sampled in the

basin floor outside of the axial trough, at DSDP Site 478, have a mainland Mexico provenance.

4. Where magma has intruded the diatomaceous mud turbidites, variable amounts of dewatering and hydrothermal diagenesis (Einsele et al., 1980), and patchy formation of thermogenic hydrocarbons (Simoneit and Lonsdale, 1982), have modified and obscured the original seismic stratigraphy. Sedimentary strata below igneous sills are faintly imaged, if at all, by our low energy (one 45+105 cubic inches air gun) seismic profiling. Gas accumulations in the seabed rapidly attenuate seismic energy, giving a “transparent” aspect even to strata with strong impedance contrasts (Judd and Hovland, 1992). These “gas wipe-outs” can be distinguished from seismic transparency caused by sediment homogeneity, our coring-supported interpretation for the transparency of the laterally extensive units A, B, and C, because gas attenuation masks all reflectors deeper than the gas-rich horizon, whereas strong internal reflections, like those observed beneath A, B, and C (Figure 3), can be recorded below gas-free homogenous seismic units.

5. Sparse biostratigraphic evidence indicates that transparent seismic unit C was deposited, at least in part, during the penultimate (Pre-Illinoisan) interglacial; the thickness and superficial position of unit A is consistent with postglacial (Holocene) deposition; and interpolation suggests a last interglacial (Sangamonian) age for unit B. These age assignments imply that the intervening reflector-rich units were deposited during glacial periods. We infer that the

defining seismic transparency of units A, B, and C, caused by the absence of thick sandy basal layers in their turbidite sequences, results from diminished supply of coarse terrigenous clastics to the southwestern Guaymas Basin during both interglacial and postglacial times.

Similar cyclic changes in Quaternary seismic stratigraphy that correlate with orbitally forced glacial/interglacial cyclicity have been reported previously from several other widely scattered mid-latitude sites of near-shore Pleistocene marine deposition. Perissoratis et al. (2000) describe alternations of glacial-stage reflector-rich turbidites and interglacial seismically transparent muds in the bed of the Gulf of Corinth, but there the cyclicity derived directly from glacio-eustatic sea-level change: sediment-depositing turbidity currents were restricted to glacial low sea-levels when the shallow sill separating that gulf from the Mediterranean was emergent, creating a fresh-water lake with under-flows of denser turbid river water. Off the U.S. west coast across Santa Barbara Basin, Peterson et al. (2009) correlated changes in seismic reflector amplitudes to orbital-to-sub orbital climate cyclicity. Weigelt and Uenzelmann-Neben (2007) correlated cyclicity of reflector strength in seismic profiles from the continental slope of southwest Africa with orbitally driven climatic variations, and proposed that the linkage there was via climatically controlled changes in plankton populations that changed the bulk density, and thereby the acoustic impedance, of the biogenous slope sediment. Perhaps the closest reported analog to the situation we describe in Guaymas Basin involves trench-floor turbidites that onlap a tectonically tilted

ocean-basin sediment blanket at 36-38° S in the Chile Trench. Several (but not all) MCS profiles show four 200-300 m-thick glacial-stage units with high amplitude internal reflectors, separated by interglacial units with reflectors of much lower amplitude (Rauch, 2005; Völker et al., 2006); climatic changes affecting rates of denudation in the Andes is inferred to be the principal control of trench-floor cyclical stratigraphy, though Völker et al, (2006) suggested that seismogenic cycles provoking slumping of the continental slope could also be a factor.

To estimate the approximate ages of the strongly and weakly reflective facies in the turbidite fill of the Chile Trench, in the absence of drill-core samples, Rauch (2005) used a plate stratigraphy technique: he measured the distances on trench-normal MCS profiles between the outboard margin of the turbidite plain and points where flat-lying reflectors beneath the plain onlap the ocean-basin sediment blanket, and assuming the width of the axial turbidite plain did not vary with time, those distances divided by the known convergence rate between the oceanic plate and the trench axis yielded estimates of the reflectors' age. We used a similar method to provide further age constraints, augmenting core biostratigraphy, for seismic-stratigraphic units in the southwestern part of Guaymas Basin, where new oceanic crust is being accreted at an axial trough and ages away from that trough at a predictable rate. A crustal accretion rate (full spreading rate) of 46+/-2 m/kyr in the Southern Trough can be calculated from the geodetically established vector for the present motion of Baja California with

respect to North America (Plattner et al., 2007), a vector that matches the post-1 Ma average spreading rate recorded by lineated magnetic anomalies at the thinly sedimented Alarcon Rise in the southern Gulf (de Mets et al., 1995). Our estimates of oceanic basement ages along MCS Profile 1, presented in Figure 3, assume symmetric spreading at 2.3 m/kyr on each flank from a 1 km-wide crustal accretion zone along the axis of the Southern Trough. Symmetry of spreading is assumed because we have been unable to identify lineated magnetic anomalies that might indicate otherwise. We use 1 km as the width of the "zero age" zone of focused dike injection (into sediment and preexisting intrusions) that creates the upper crust because this is the width of the neovolcanic zone at the crests of Alarcon Rise (Castillo et al., 2002) and of the Pacific-Rivera East Pacific Rise in the mouth of the Gulf (Spiess et al., 1980), and because on most seismic profiles across the Southern Trough (e.g., Figure 3) intrusive disturbance of the uppermost sediments is largely confined to the central 1km of the trough floor. On the northwest flank of the trough, transparent seismic units B and C intersect the intrusion-sediment oceanic basement (acoustic basement) where the latter has estimated ages (~100 ka, ~200 ka) that match the Sangamonian and Pre-Illinoisan interglacials. On the southeast flank it is difficult to identify unit C (a likely reason is discussed below), and the intersection of unit B with oceanic basement plausibly occurs at crust of Sangamonian age, but is obscured by seismic wipe-outs inferred to be caused by interstitial gas. This small-scale application of "plate stratigraphy," a technique generally applied over much

longer spatial and temporal scales (e.g., Berger and Winterer, 1974) has several uncertainties (Was spreading really symmetric? Did the intersecting intrusion-sediment “basement” originate at the spreading axis or at off-axis intrusions? Should the entire width of the axial trough floor, rather than just its central 1km, be taken as the “zero age” crustal accretion zone?), but does offer some corroboration of the age assignments derived from core biostratigraphy.

2.4.3 Record of Tectonic Deformation and Axial Trough Filling

Because most of the sediments in and around the Southern Trough were deposited by turbidity currents, their seismic stratigraphy provides a good record of post-depositional tectonic deformation and clear evidence for temporal changes in the geomorphic expression of the spreading center, namely a cyclic alternation between a narrow, scarp-bounded axial trough and a broader, shallower axial basin.

The turbidite basal beds responsible for reflectors within the reflector-rich units were probably deposited horizontally, but few of the reflectors imaged on the Figure 3 transect have maintained that attitude; their present tilts record local vertical deformation within the plate boundary zone, and regional flexure of the rift flanks. Local deformation includes uplift over multiple dike intrusions along the spreading axis; inward tilting by 5-6° in the outer parts of the rift floor (e.g., 1-2 km off-axis in Figure 3), caused by continuous subsidence of newly accreted brittle crust as it is tectonically extended (Francheteau and Tapponnier, 1978);

and slight outward tilting as trough-floor turbidites climb out of the rift valley on the back-tilted fault blocks of the rift walls (e.g. ~3 km off-axis on Figure 3), as observed in other turbidite-smothered axial rifts (Atwater and Mudie, 1973). Within sparsely faulted parts of reflector-rich units that were deposited outside of the axial trough (e.g., turbidites assigned to the Wisconsin and Illinoisan glacials that are now more than 5-6 km off-axis) reflectors have a regional dip of ~2° toward the axis. This slight inward tilt is attributed to broad isostatic uplift, over a region wider than the entire length of Profile 1, as young oceanic lithosphere is "unloaded" by continuous rift-valley formation, the mechanism that on thinly sedimented mid-ocean ridges (and at some sediment-starved Gulf axes, as noted below for the North Pescadero axis) typically raises "rift mountains" alongside axial rift valleys (Francheteau and Tapponnier, 1978). We infer that isostatic uplift on the flanks of the Southern Trough is much more modest because it is suppressed by loading of rapidly accumulated sediment.

For enclosed marine basins in which turbidity currents pond, local variations in the rate of turbidite deposition (beyond the marginal channeled fans) are strongly controlled by seafloor relief, with higher rates on deeper seafloor (where the cloud of suspended particles in a ponded turbidity current is thicker), and especially in the deepest topographically accessible depressions (where bedload is preferentially deposited as the sediment-rich basal flow stops). In the axial parts of Guaymas Basin, straddling active zones of plate divergence, most of the seafloor relief with which turbidity currents interact is tectonic in origin,

notably the pair of axial troughs, which are terminal depocenters with floors now more than 100 m deeper than any other parts of the basin floor. At MCS Profile 1 (Figure 3) the still-accumulating (post-glacial) transparent unit A is twice as thick in the floor of the Southern Trough, where it has thin sandy layers interpreted as turbidity current bedload, as it is outside of the rift valley, where the mud turbidites thin gradually as the seafloor shoals away from the spreading center (Figs., 3 and 5). The older units B and C show little if any thinning away from the axis, but the thickness of any coeval axial-depression deposits have been masked by intrusions and gas wipe-outs. Near-axis parts of the reflector-rich units beneath transparent layers B and C have lower halves that form thick turbidite ponds with steep outer margins, on the northwest flank at 2.5-4.5 km off-axis for the unit over layer B, and 4.5-6 km off-axis for the unit over unit C. At these steep margins, circled in red on Figure 5, there is clear onlap of the transparent facies by the reflector-rich facies, over a vertical distance of approximately 200 m. Deposition of the upper halves of these reflector-rich units was not restricted to the axial ponds, but extends widely across the basin floor beyond 4.5-6 km off-axis, with apparently conformable contacts with units B and (where present) C.

Our geological interpretation of the cyclical signal recorded by seismic stratigraphy in the southwestern part of Guaymas Basis is sketched in Figure 6. During Late Pleistocene interglacials, as in the present postglacial period, slow, low-density turbidity currents spread their loads of suspended sediment

composed of fine-grained terrigenous and low-density biogenous particles, probably reworked by slumping off the steep sides of the basin (Lonsdale and Lawver, 1980), across the basin floor. Accumulation of the diatomaceous mud turbidites was fastest in the deepest part of the region, the floor of the Southern Trough, but was not fast enough to overwhelm the active tectonic processes that maintained the axial rift valley, or to suppress the shallow intrusive volcanism that (in postglacial times) has emplaced sills less than 40 m below the trough floor (e.g. at DSDP Site 477A; Curray, Moore, et al., 1982). Most of the postglacial and interglacial turbidites are seismically transparent because of their lack of thick sandy beds, though thin sands in postglacial sediments of the Southern Trough do indicate some infrequent bedload transport of coarse locally derived terrigenous clastics into this terminal depocenter, probably following passage of hurricanes, which have historically flooded adjacent parts of the Baja California coast about once a decade (e.g., during our 2006 seismic reflection survey!). The apparent absence in the seabed southeast of the Southern Trough of any seismically transparent counterpart of unit C on its northwestern side (Figure 3) may record that turbidity currents during the penultimate (Pre-Illinoisan) interglacial brought enough sandy turbidite bedload to the southeastern side to deposit a reflector-rich seismic facies there, while suspended-load deposition was building a transparent facies (unit C) on the other side of the axial rift valley. This would be a predictable outcome of turbidity currents rich in mainland-derived coarse clastics sweeping down the Mayo Fan via slightly longer antecedents of

the fan channel that exists today (Figure 1), and dropping all their remaining coarse load when basal parts of the flows ponded in the Southern Trough.

Transitions from interglacial to glacial periods were accompanied by a greater influx of sediment, especially terrigenous clastics, to the southwestern part of this inter-continental marine basin, because of changes in local climate and in eustatic sea level, as discussed later. Early in the last (Wisconsin) glacial, sediment-rich basal layers of turbidity currents were channeled into the Southern Trough, and ponded there. Deposition of the reflector-rich turbidite facies was initially restricted to the trough floor, so we infer that suspended-load deposition continued to accumulate the seismically transparent facies in the early part of the glacial stage, perhaps explaining why unit B in the basin floor does not thin away from the axis in the way that postglacial unit A does (Figure 3). Focused deposition of most of the enhanced sediment input eventually filled the Southern Trough, as evidenced by onlap by the reflector-rich facies at steep slopes that represent former rift-valley walls; this sediment-smothered central Gulf spreading axis then probably resembled, in geomorphology and structure, the sediment-smothered axes present today in the northernmost Gulf, i.e., broad depressions with gently inclined side-slopes interrupted by just a few low fault scarps, and axial zones of crustal accretion with few shallow (<500 m subbottom) intrusions to disturb the reflector-rich trough fill. In the absence of a deep valley to focus turbidite deposition, especially bed-load deposition, at the spreading axis, sandy turbidites were then deposited over a much broader region of the basin floor,

including areas beyond the plate-boundary zone, as evidenced by the extensive sections of never-faulted reflector-rich facies on MCS Profile 1 (Figure 3). The thickest (300 m) section of reflective turbidites assigned to the ~60 kyrs of the Wisconsin glacial stage (e.g., at 2.7 km northwest of the present axis) accumulated at an average rate of 5 m/kyr, but the onlapping lower two-thirds of that section was deposited, presumably at a much higher rate, during the initial phase of focused deposition in the rapidly filling axial rift valley. On MCS Profile 1, less than 75 m of reflective Wisconsin turbidites were deposited above transparent B at sites beyond the infilled rift valley (e.g., at 5 km off-axis on Figure 3), but we are not sure what fraction of the Wisconsin stage they represent.

Seismic stratigraphy reveals the same history, of trough filling followed by expansion of the area of rapid bedload deposition, at the end of the earlier Illinoisan glacial stage, except that sandy turbidites derived from the Mayo Fan at the mainland rifted margin (Figure 1) seem to have accumulated on the northeast side of the Southern Trough, and perhaps even on the trough floor, even during the preceding interglacial. We assume that the Northern Trough, which now intersects the mainland margin, was also filled with sediment during glacial periods; the lack of that deep valley, which now intercepts turbidity currents from that margin, and accommodates much of their sediment load (Lonsdale and Lawver, 1980), would have allowed wider dispersal of mainland-derived

terrigenous clastics to southwestern parts of Guaymas Basin, e.g., to the site of the DSDP 178 drill-core.

At the Guaymas Basin spreading centers, the extensional tectonic processes driven by plate separation continued, of course, throughout the sediment-smothering glacial periods. As these periods ended, decreased rates of axial deposition allowed steep-sided axial rift valleys to be maintained, and the Northern and Southern Troughs were regenerated.

In addition to the glacial/interglacial changes in sediment supply that have affected tectonic geomorphology of the plate boundary zone, in turn changing patterns of turbidite deposition, we also note that even within the brief duration of the Late Pleistocene there have been secular (non-cyclical) tectonic processes that probably also affected sediment dispersal on the basin floor. Because of its active spreading in the widening Guaymas Basin, the separation of the Southern Trough from potential sources of terrigenous sediment at the rifted continental margins has steadily increased. This might explain why sand-bearing turbidity currents from the mainland (Mayo Fan) margin seem to have reached the Southern Trough during the penultimate interglacial, but not during subsequent non-glacial periods. A clearer tectonic effect derives from the southeastern migration of the Southern Trough along the sheared Baja California continental margin that it intersects. Figure 2 illustrates how far the trough has moved along this margin since 500 ka, assuming the spreading center within the trough accretes crust to the Baja California plate at 23 km/Myr (the half spreading rate).

In that time the trough has shifted from intersecting the mouth of a canyon system linked to washes that drain the highest parts of the adjacent Concepcion Peninsula, past a 12 km gap in canyons on the continental slope, to its present location off the mouth of canyons draining a smaller, lower part of the peninsula. We infer, as discussed below, that orographic rainfall on this peninsula during glacial, but not postglacial, periods was important for creating the cyclic sedimentation in the Southern Trough, so even this relatively small migration may have caused significantly different rates of sediment supply in successive glacial periods.

2.5 INFLUENCE OF GLACIAL/INTERGLACIAL CYCLICITY ON GUAYMAS BASIN SEDIMENTATION

How did orbitally forced cyclicity bring about the alternations of turbidite facies observed in the seabed of the southwestern Guaymas Basin, where seismically transparent mud turbidites alternate with glacial-stage turbidites rich in high-amplitude reflectors that, based on coring evidence, are probably caused by thick sand interbeds at the bases of graded sequences? Our preferred explanations for the sandier composition of glacial-stage turbidites are (i) a larger local supply of coarse terrigenous clastics because of faster fluvial denudation of a wetter Baja California, and (ii) a regional increase in the rate at which terrigenous sediment was delivered to the basin floor, as glacio-eustatic lower

sea-levels changed coastal geography and seafloor bathymetry in ways that fostered long-distance sediment dispersal from the mainland continental margin.

As noted earlier, the narrow (25-30 km-wide) strip of Baja California that drains (episodically) toward Guaymas Basin, lying northeast of the dissected escarpment marking the peninsular divide (Figure 1), is now arid; coastal weather stations record average rainfalls of 10-12 cm, almost all from late summer thunderstorms and infrequent hurricanes (Hastings and Turner, 1965). During the last glacial period, however, climatic models (Kutzback and Wright, 1985; Bartlein et al., 1998), lake levels in southwestern North America (Allen and Anderson, 1993; Menking et al., 2004) and Cuenca de Mexico (Bradbury, 1989; 1997), and paleobotanical data (Rhode, 2002) indicate that the region had a wet-winter “mediterranean” climate similar to that of present-day Southern California. Paleoclimate simulations for the ~70-14 Ma period when the Laurentide Ice Sheet covered much of North America (e.g., Kutzbach and Wright, 1985; Broccoli and Manabe; 1987) portray southward displacement of the average jet stream, and of the mid-latitude depressions that it steers within the westerlies, by as much as 2000 km. This would have extended the winter storm belt that now affects northernmost Baja California well into central parts of the peninsula, and Rhode (2002) reports that typical Mediterranean chaparral and juniper woodland persisted as recently as 10.2 Ma near the now-arid peninsular divide at 27.5° N. We assume that a similar climate prevailed during earlier glacial stages, and infer that the winter rains that watered these forests also carved the canyons on

Concepcion Peninsula (Figure 2), and washed the erosion products to the heads of submarine canyons that led to the Southern Trough of Guaymas Basin.

The Sonoran coastal plain bordering Guaymas Basin is much wetter than the peninsular Gulf coast, receiving highly seasonal rainfall (60-70% in July-September) from the North American monsoon system (Adams and Comrie, 1997). Peak rainfall from this system is along the western escarpment of the Sierra Madre Occidental, in a belt drained by the headwaters of large rivers that (before being comprehensively dammed) supplied clastic sediments that built large coastal deltas and beach ridges; average rainfall totals diminish southeast to northwest: ~70 cm/yr for the Rio Mayo headwaters, 65-30 cm for the R.Yaqui , 25cm/yr for the R. Sonora (Arbingast et al., 1975), and the share of precipitation brought by winter storms increases in the same direction. There are no good estimates of rainfall totals for these drainage basins during glacial periods, when the monsoonal flow was suppressed and westerly storm tracks were displaced further south (Metcalfe et al., 1997), but it seems probable that unlike now the northern tributaries of the R. Yaqui, which extend to the U.S. border, had higher flows and sediment yields than its southern tributaries, or the R. Mayo, and that the R. Sonora, which seldom flowed into the Gulf even before recent damming, may have contributed significant terrigenous sand and silt to northern parts of Guaymas Basin (its delta is labeled on Figure 1). So cyclic glacial/interglacial climate change probably changed the seasonality and distribution of fluvial sediment delivered to the central Gulf from its mainland coast, but how it

changed the overall supply rate is uncertain. We infer that the more important reason for an increased glacial-stage supply of terrigenous sediment from the mainland margin to sites of turbidite deposition on the deep basin floor was glacio-eustatic sea-level change.

A regression caused by a ~120 m fall in sea-level (Figure 3, lower panel) would have exposed a 15-30 km-wide strip of continental shelf along the mainland margin; the geological effects would have been much less at the Baja Californian margin, where the shelf is much narrower or, off the Concepcion Peninsula, nonexistent (Figure 2). Subaerial erosion of biogenic and terrigenous neritic sediment from a newly emergent shelf would provide a temporary increase in sediment supply to the Gulf, but there are also longer term consequences of the shift of the shoreline to the crest of a continental slope that is very steep off southern Sonora. Fluvial sediment from the mouths of the Mayo and Yaqui would be delivered directly to the steep gullied fronts of their now partly submerged deltas, rather than being stored as at present in coastal lagoons and large coastal sand spits (Though the large cuspate sand spit that forms Punta Lobos on the Yaqui Delta [Figure 1], shaped by convergence of southward longshore drift in the winter and northward drift in the summer, has prograded to the shelf break, and the submarine canyon that heads at the tip of the spit implies that littoral sand is still being supplied to the deep basin). Slumping of unstable rapidly deposited sediment accumulations on the steep earthquake-shaken upper slope are presumed to still generate turbidity currents that build the channeled

fans mapped at the foot of the continental slope (Figure 1); with sediment being delivered to the upper slope at a faster rate during low stands of sea-level, slumps and the turbidity currents that they spawned would be predictably larger and/or more frequent.

In addition to effects of astronomically forced climatic and eustatic cyclicity on the nature, location and rate of terrigenous inputs to Guaymas Basin, and hence on the seismic stratigraphy of turbidites on the basin floor, can any effects of cyclic variations in plankton productivity be recognized in these diatom-rich sediments? The best and most studied sedimentary record of postglacial climatic change, short-term cyclicity, and seasonality in Guaymas Basin is not in the reworked muds of basin-floor turbidites that we studied, but in hemipelagic sediments deposited on the basin margins in the 500-900 m depth range of the oxygen-minimum zone, where the inherently low oxygen content of Pacific Intermediate Water is exacerbated by decomposition of sinking organic matter. The alternations of biogenic-rich and terrigenous-rich laminae that are preserved as annual varves under these low-oxygen conditions have been explained as seasonal (spring diatom bloom) peaks in planktonic debris added to a steady terrigenous supply (Byrne, 1957), or to summer peaks of terrigenous input added to steady deposition of planktonic debris (Calvert, 1966); sediment-trap data (Thunell, 1997; 1998) show that at present seasonal variation in both biogenic and terrigenous fluxes play a role in varve formation, and that the short-term cyclicity of the El Nino-Southern Oscillation also causes cyclic changes in the

supply of biogenic debris. Barron et al. (2003) attribute 200 yr cyclicity observed in diatom abundance in a 2000 yr record of a varved core to cyclic astronomic forcing of plankton productivity, tuned to the solar minimum/maximum cycle. Whether changes in the biogenic/terrigenous ratio of basin-margin cores deposited prior to the Flandrian transgression reflect changes in inputs of biogenic or of terrigenous debris is more problematic, because of the complicating effects of sea-level change (e.g., changing the spatial pattern of diatom blooms), but Cheshire et al. (2005) present evidence for drastic basin-wide decrease in diatom productivity during the cold periods Younger Dryas stadial (12.8-11.5 ka) and the Last Glacial Maximum (26.5-19 ka). The controlling factor for seasonal and short-term cyclical changes in postglacial plankton productivity is the seasonal presence or absence, or cyclical variations in strength, of northwest winds that channel down the Gulf at the eastern margin of the Pacific Subtropical Anticyclone, and increase surface water fertility by thickening the surface mixed layer in the fall, and promoting upwelling in the spring (Douglas et al., 2007). In the postglacial period these winds fail in the summer, as the Subtropical High moves north of the Gulf; Cheshire et al. (2005) suggest they failed during the Younger Dryas and Last Glacial Maximum, resulting in low biogenic input at these times, when the High, along with the westerly depressions discussed above, was displaced to the south. If absence of upwelling in Guaymas Basin because of displacement of the Subtropical High was a persistent feature of glacial periods, then we might expect orbitally forced

changes in biogenic input to be a contributing, though difficult to recognize, factor explaining the observed alternation of transparent and reflective facies on the basin floor. However, the presence of varved sediment throughout much of the Wisconsin-glacial section in a core that sampled sediment as old as ~40 ka indicates that upwelling-induced high productivity did not cease during this glacial period (Cheshire et al., 2005); those authors suggested that with the average position of the Subtropical High being displaced to the south during glacials, northwest winds and upwelling in the Gulf may have occurred during the summer season, when the High migrated north. We are left unsure whether sediment deposited on Guaymas Basin slopes during glacial periods had a smaller biogenic fraction than in non-glacial periods because of orbitally forced lower planktonic productivity, not just because of a higher rate of terrigenous supply, and even more uncertain whether any such changes in productivity affected the composition of the reworked sediment deposited as basin-floor turbidites in ways that contribute to their observed cyclical seismic stratigraphy.

2.6 CYCLIC SEISMIC STRATIGRAPHY ELSEWHERE ALONG THE GULF OF CALIFORNIA PLATE BOUNDARY

Establishing the presence or absence of alternating reflective and transparent facies or cyclic variations of reflector strength in other turbidite-

floored basins in the Gulf may help determine the environmental conditions needed for development of these distinctive seismic stratigraphies.

MCS Profile 3 across Carmen Basin (Figure 7) shows cyclical acoustic stratigraphy similar to that around the nearby Southern Trough of Guaymas Basin, except that seismically transparent units make up the majority of the sediment overlying shallow magmatic intrusions on the flanks of the Carmen axial rift valley. Only thin reflector-rich packages separate successive transparent units, suggesting that even during glacial periods few turbidity currents delivered terrigenous clastics there. The Carmen axis has been protected from turbidity currents from the eastern margin (e.g. from the Mayo Fan) by tectonic uplift of a transverse ridge along the Carmen transform fault, and only a few small turbidity current channels approach the axis via a circuitous route from the Baja California margin (Figure 7). Slow postglacial deposition within the present axial trough has allowed intrusion of very shallow (<30 m subbottom) sills and eruption of small pillow-lava cones in the crust-accreting neovolcanic zone (Figure 7B).

In the southern Gulf, our multibeam coverage, MCS profiles and seabed sampling show that the North Pescadero Basin also has a topographically protected, sediment-starved and locally eruptive axial trough. A few small channels do approach the northeastern end of this rift valley, but there it intersects a transform valley opened by transtension along the North Pescadero transform (Figure 8). This structurally deeper amagmatic valley has been the primary site for gravitationally focused turbidite deposition. Seismic

Profile 4 across the 4 km-wide floor of this transform valley imaged a thick turbidite pond with alternating almost-transparent and reflector-rich units that are bisected by the active North Pescadero transform fault, which separates mainland continental crust from young oceanic crust. At this transect, 15 km from the axial neovolcanic zone, the estimated age of oceanic basement on the southwest side of the fault is ~600 ka, and at least 5, possibly 6, transitions from reflective to transparent facies occur in the overlying turbidites (Figure 8). This would be consistent with the ~100 ka frequency of Late Pleistocene glacial/interglacial cyclicity, but we have no direct age information from these unsampled sediments. That they were deposited by density flows, i.e. turbidity currents, is demonstrated by the way each stratigraphic unit almost doubles in thickness as it crosses from oceanic to continental crust at the strike-slip fault zone, which forms only a very low (~10 m) monoclinal step in the otherwise flat valley floor. The seismic stratigraphy of Profile 4 (Figure 8) records differential density-flow deposition that maintained an almost flat sediment plain even as the oceanic half of the valley floor was being steadily uplifted, by ~350 m since deposition of transparent unit 5 began (at ~500 ka?). Shoaling of young oceanic basement by hundreds of meters as it climbs from the floor of the regenerating axial rift valley to the flanking rift mountains is held responsible for uplift of the oceanic half of the transform valley floor.

Major submarine canyon systems and fan channels provide turbidity currents from delta fronts and deep-sea fans on the mainland margin with direct

access to the axial regions of the other enclosed depocenters of the southern Gulf, Farallon and South Pescadero Basins; terrigenous clastics, brought to the Gulf by large permanent rivers draining and eroding the SMO, have constituted much of the sediment load of these turbidity currents (Lonsdale and Kluesner, 2010). Our high-resolution MCS profiles across the floors and axial troughs of these basins show little evidence of seismically transparent units within their thick sedimentary sections, though the pervasive reflector-rich turbidite facies do have subtle cyclic variations in reflector strength, less marked than those correlated with climatic cyclicity in the Chile Trench (Rauch, 2005), that we have not investigated fully. We infer that continued rapid erosion of the Sierra Madre Occidental, during both glacial and interglacial stages, led to deposition of sandy mud turbidites in the adjacent accessible Gulf basins throughout Late Pleistocene and post-glacial times (as discussed above to account for the apparent absence of transparent unit C on the southeast side of the Southern Trough). This description also seems to apply to the northeastern parts of Guaymas Basin, where a turbidite fan at the foot of the delta built by the SMO-draining Yaqui River extends to within 40 km of the Northern Trough (Figure1). However, Yaqui Fan is contained within an indentation of the continental margin, none of its channels extend to the northern spreading axis, and acoustic profiles across the Northern Trough (Lonsdale and Lawver, 1980) show a 50 m-thick pond of mostly transparent turbidites (with a few internal reflectors) very much like the one in the Southern Trough. No seismically transparent units or cyclic variation of reflector

strength are clearly defined by available MCS profiles across the flanks of the Northern Trough, but all profiles (e.g., those collected during the 1978 DSDP site survey, which also provided our Profile 2 across the Southern Trough) have lower resolution than those from our 2006 survey, which did not cover this region. Another factor that may preclude identification of transparent layers and paleo-rift turbidite ponds beneath the flanks of the Northern Trough is masking by the abundant off-axis intrusions and gas accumulations (Kluesner and Lonsdale, 2008; Lizarralde et al., 2010).

There is no shortage of high-resolution MCS profiles across the plate boundary zone in the northern Gulf of California, where a 1999 *ULLOA* survey (Persaud et al., 2003) collected data along 3500 km of track. Lower Delfin Basin, the southernmost in this region (Figure 1, inset), is near the limit of the submerged delta of the Colorado River, and has an axial rift valley similar in geomorphology and structure to those in Guaymas Basin. Steckler et al. (2009) found that sediments on the flanks of the Lower Delfin Trough exhibited cyclic variation in reflector strength that could be ascribed to 100,000 yr glacial/interglacial cyclicity, with eustatic sea-level changes probably exerting the main influence on sediment deposition in this shallow (<900 m-deep) region.

Our interpretation of the distribution of cyclic turbidite facies in the axial basins of the Gulf of California is that some signature of cyclicity probably occurs in all those basins that now have axial troughs at their spreading centers, troughs known or inferred to have been filled during glacial periods of faster sediment

accumulation. A clear-cut alternation of interglacial seismically transparent and glacial reflector-rich units is limited to those basins (South Guaymas, Carmen) that in the present postglacial stage, and we infer in past interglacials, have received turbidity currents from the arid Baja California margin, rather than from the more prolific sources of coarse-grained terrigenous clastics at the mainland margin. Basin floors supplied by turbidity currents from the North American mainland margin, and adjacent to fans or submerged deltas, may have reflector-rich turbidites with a cyclic variation in reflector amplitudes (high for glacial-stage, low for interglacial), as described near the margins of turbidite fans in the Chile Trench (Rauch, 2005), but in the Gulf this is well documented only for the northern Lower Delfin Basin. An intermediate style of turbidite cyclicity, with transparent layers well defined, but containing a few low amplitude seismic reflectors, occurs in the Carmen transform valley, which has received a sparse sediment supply from the mainland margin.

2.7 SUMMARY OF CONCLUSIONS

The pair of offset spreading centers in Guaymas Basin is now occupied by axial rift valleys with floors 75-150 m below the general level of the muddy basin floor; the Northern Trough intersects the mainland (Sonoran) continental margin, the Southern Trough the peninsular (Baja Californian) margin. A new high-resolution MCS profile across the Southern Trough and adjacent basin floor imaged a seismically transparent superficial layer of sediment underlain in parts

of the trough floor by a sequence with close-spaced high-amplitude internal reflectors, and on the older flanking crust by several alternations of the transparent and reflector-rich seismic facies. These alternations are distinct enough to be recognizable in (reprocessed) lower resolution MCS data collected three decades ago for a DSDP site survey that includes a profile close enough to DSDP coring sites to allow correlation of basin-floor and trough-floor seismic stratigraphy with sampled sediment. Most of the cored sediment is diatomaceous mud turbidite interpreted as fall-out from the suspended loads of thick, slow turbidity currents (Einsele and Kelts, 1982), and the seismically transparent units correlate with parts of the cored sections where sandy beds at the base of (often subtly) graded sequences are very thin or absent. Mineralogy indicates that thin sandy layers in postglacial turbidites in the Southern Trough floor were derived from the adjacent continent, and probably delivered via submarine canyons that lead down the Baja Californian continental slope directly into the trough. Thick beds of silty sand terrigenous clastics, most apparently from mainland sources, occur in drill-cores from approximately 8 km northwest of the trough at the subbottom depths of reflector-rich seismic facies. We conclude that the seismically imaged alternation of reflective and transparent turbidite units was generally caused by alternation between periods when turbidity currents carried coarse terrigenous bedloads and deposited them in layers thick enough to create impedance contrasts detectable at seismic profiler frequencies, and periods when they did not.

Biostratigraphic interpretation of the DSDP cores from the floor of Guaymas Basin was hampered by a combination of very rapid sediment accumulation, patchy microfossil preservation, and massive reworking of microfossils in the turbidity currents that brought them to their final sites of deposition, but published age estimates and interpolated deposition rates (Aubry et al., 1982) are consistent with interglacial-stage deposition of the two seismically transparent layers imaged within the seabed. The still-accumulating superficial transparent unit must be, at least in part, of postglacial age. Deposition of the buried transparent units during the last and the penultimate Pleistocene interglacials (centered at ~100 ka and ~200 ka) is corroborated by the observation that these units intersect basement crust, i.e., directly overlie it, where the geophysically estimated crustal ages are ~100 ka and ~200 ka.

Recognizing that most high-amplitude internal reflectors (other than localized reflectors caused directly or indirectly by volcanic intrusions) result from bedload deposition from turbidity currents, and were therefore originally almost flat-lying, with a tendency to infill enclosed depressions, allows them to be used as records of post-depositional deformation and pre-depositional bathymetry. At this crust-accreting plate boundary zone the deformation record is of tilting of the trough floor toward the axis as the midline of the regenerating axial rift valley subsides, followed by back-tilting as fault slices climb the rift walls out of the valley floor, locally accompanied by uplift and doming over shallow spreading-axis and off-axis intrusions. The most significant bathymetric change recorded by

seismic stratigraphy of the turbidites is infilling of the axial trough at the beginning of the two most recent glacial stages. For these times, our profiles record that bathymetrically focused trough-floor accumulation of sandy turbidites outpaced axial tectonic subsidence, causing turbidite ponds of the reflective facies to onlap faulted transparent facies at the steep rift-valley walls. Once the axial troughs of Guaymas Basin had been filled and deposition of turbidity current bedload was less restricted to enclosed axial deeps, reflector-rich turbidite facies sourced from both margins extended broadly across the basin floor. These accreting plate boundary zones in the central Gulf then resembled, in geomorphology and structure, those in the present northernmost Gulf that are still smothered by Colorado River sediment. When post-glacial conditions slowed the supply of sediment, especially of coarse terrigenous clastics, to the floor of Guaymas Basin, the pre-glacial axial topography, of narrow, scarp-bounded troughs with floors deformed by shallow igneous intrusions, was reestablished.

We conclude that there were two principal causes of increased terrigenous sediment supply during glacial periods. Enhanced supply of coarse clastics from the Baja Californian margin resulted from climatic change that greatly increased the previously very low rainfall on the coastal mountains. At the Sonoran margin, changes in rainfall patterns probably altered the relative importance of the large rivers that brought sediment from the deeply eroded Sierra Madre Occidental, but lower glacial-stage sea-levels probably had a greater overall effect. Low sea-levels exposed to erosion sediment that had accumulated on broad continental

shelves, and brought river mouths, delta fronts and coastal sand spits to the top of steep continental slopes, thereby promoting slumping of fluvial and littoral silts and sands down the basin sides and turbidity current dispersal of these sediments (as well as planktonic sediment reworked from basin-margin sites of deposition) across the low-gradient basin floor. Given the small catchment areas of streams draining into the Gulf from the peninsula, it is unlikely that increased fluvial erosional during glacial stages of now-arid parts of Baja California had a major effect on the overall sediment budget of Guaymas Basin. Its significance is that by introducing coarse clastics to parts of the basin floor that received very little of this type of sediment before or after glacial periods (because of remoteness from the principal mainland sources) there is such a clear distinction in the region around the Southern Trough between glacial-stage reflective turbidite facies and 'interglacial' transparent facies. (Note that because seismic stratigraphy indicates that the reflective facies did not spread over the basin floor until it had filled the axial trough, some of the transparent facies on the basin floor was deposited from the suspended load of turbidity currents while their coarser bedloads were filling the trough, i.e., early in the glacial stages.)

During our high-resolution MCS survey of the central and southern Gulf, comparably distinct alternations of transparent and reflector-rich turbidites were imaged only around the axial trough of Carmen Basin, which is also remote and topographically protected from turbidity currents originating at the mainland margin. At other basins that receive most of their reworked sediment from the

mainland margin during both glacial and non-glacial stages (as evidenced by fans and fan-channels extending from that margin) we observed a cyclicity in turbidite reflector amplitude that may be matched to orbitally driven climatic or sea-level cyclicity (resulting in coarser or thicker sand layers during glacial periods), as has been inferred in several other mid-latitude sites of near-shore turbidite deposition, including a basin in the northern Gulf of California. We suspect that such a pattern prevails around the Northern Trough of Guaymas Basin, but we collected no high-resolution profiles that could have resolved cyclic variation in reflector amplitude there; low resolution MCS profiles show no clear cyclic alternation of turbidites in this region, though such alternation is imaged where some of these same profiles cross the Southern Trough.

Our results, in combination with similar seismic reflection studies from other mid-latitude regions, suggest that significant changes in sedimentation caused by 100-kyr glacial/interglacial cyclicity might be common to a variety of heavily sedimented tectonic settings that are largely affected by orbital-scale climate cyclicity, and that high-resolution seismic reflection profiling could provide a practical way to cross-correlate sediment packages to glacial/interglacial periods.

2.8 ACKNOWLEDGMENTS

We thank the captain and crew of the Mexican research vessel *FRANCISCO DE ULLOA*, and Scripps geophysical engineer Lee Ellett, for their

skill and perseverance while conducting the seismic survey. Dr. Barry Eakins helped prepare the bathymetric maps that guided the survey, and are used in this paper. Figures were prepared using Generic Mapping Tools (GMT) and IVS Fledermaus software packages. Dr. Neil Mitchell and Dr. Heather Cheshire are thanked for helpful and constructive reviews of an early version of the manuscript. Funding was by grants from the U.S. NSF (OCE-0203348, OCE-0646563) and its Mexican partner CONACYT.

Text and figures in this chapter have been submitted for publication in: Geosphere, 2011, Kluesner, J., Lonsdale, P., Kirtland, S., and González, A., The dissertation author was the primary investigator and author of this paper.

2.9 REFERENCES

Adams, D.A., aand Comrie A. C., The North American monsoon, Bull. Amer. Meteor. Soc.,v. 78, p. 2197-2213.

Allen, B. D., and Anderson, R. Y., 1993, Evidence from western North America for rapid shifts in climate during the Last Glacial Maximum: Science, v. 260, p. 1920-1923.

Arbingast, S., Blair, C. P., and Buchanan, J. R., 1975, Atlas of Mexico, Universityof Texas Press, 167 p.

Atwater T., and Mudie J.D., 1973, Detailed near-bottom geophysical study of the Gorda Rise. Journal of Geophysical Research, v. 78, p. 8665–8686.

Aubry, M. P., Matoba, Y., Molina-Cruz, A., and Schrader H., 1982, Synthesis of Leg 64 Biostratigraphy: Initial Reports Deep Sea Drilling Program, v. 64, p. 1057-1064.

Baba, J., Peterson, C.D., Schrader, H.J., 1991, Modern fine-grained sediments in the Gulf of California. In: Dauphin, J.P., Simoneit, B.R.T. (Eds.), The Gulf and Peninsular Province of the Californias. Am. Assoc. Pet. Geol. Mem. 47, p. 569–587.

Barron, J. A., Bukry, D., and Bischoff, J. L., 2004, High resolution paleoceanography of the Guaymas Basin, Gulf of California, during the past 15,000 years: Marine Micropaleontology, v. 50, p. 185-207.

Bartlein, P. J., Anderson, K. H., Edwards M. E., Mock, C. J., Thompson, R. S., Webb, R. S.,Webb III T., and Whitlock, C., 1998, Paleoclimate simulations for North America over the past 21,000 years: features of the simulated climate and comparisons with paleoenvironmental data: Quaternary Science Reviews, v. 17, p. 549-585.

Baumgartner, T.R., Ferreira-Bartrina, V., and Moreno-Hentz, P., 1991, Varve formation in the central Gulf of California: a reconsideration of the origin of the dark laminae from the 20th Century varve record, J.P. Dauphin, B.R.T. Simoneit, Editors, The Gulf and Peninsular Province of the Californias. American Association of Petroleum Geologists Memoir, v. 47, American Association of Petroleum Geologists, Tulsa p. 617–635.

Berger, W.H., and Winterer, E.L., 1974, Plate stratigraphy and the fluctuating carbonate line. International Association of Sedimentologists (Special Publication), v. 1, p. 11–48.

Bintanja, R., van de Wal, R. S. W., and Oerlemans, J., 2005, Modeled atmospheric temperatures and global sea levels over the past million years: Nature, v. 437, p. 125–128.

Bouma, A.H., 1962, Sedimentology of some flysch deposits: a graphic approach to facies interpretation. PhD Thesis, Amsterdam, 168 p.

Bischoff, J. L., and Henyey, T. L., 1974, Tectonic elements of the central part of the Gulf of California: Geological Society of America Bulletin, v. 85, p. 1893-1904.

Bradbury, J. P., 1989, Late Quaternary lacustrine paleoenvironments in the Cuenca De Mexico: Quaternary Science Reviews, v. 8, p. 75-100.

Bradbury, J. P., 1997, Sources of glacial moisture in Mesoamerica. Quaternary International, v. 43/44, p. 97-110.

Broccoli, A. J. and Manabe, S., 1987, The effects of the Laurentide Ice Sheet on North American Climate during the Last Glacial Maximum: Geographie physique et Quaternaire, v. 41, p. 291-299.

Byrne, J., 1957, The marine geology of the Gulf of California (Ph,D, dissertation), University of Southern California, Los Angeles, 289 p.

Calvert, S. E., 1966, Accumulation of Diatomaceous Silica in the Sediments of the Gulf of California: Geological Society of America Bulletin, v. 77, p. 569-596.

Castillo, P.R., Hawkins, J.W., Lonsdale, P.F., Hilton, D.R., Shaw, A.M., and Glascock, M.D., 2002, Petrology of Alarcon Rise lavas, Gulf of California: nascent intracontinental ocean crust: Journal of Geophysical Research, v. 107 p. 2222-2237.

Cheshire, H., Thurow, J., Nederbragt, A. J., 2005, Late Quaternary climate change recorded from two long sediment cores from Guaymas Basin, Gulf of California: Journal of Quaternary Science, v. 20, p. 457-469.

Curray, J. R., Moore, D. G., et al., 1982, Guaymas Basin: Sites 477, 478 and 481: Init Repts. DSDP, Initial Report Deep Sea Drilling Program, v. 64, p. 211-415.

DeMets, C., 1995, A reappraisal of seafloor spreading lineations in the Gulf of California: Implications for the transfer of Baja California to the Pacific Plate and estimates of Pacific-North America motion. Geophys. Res. Lett., v. 22(24), p. 3545–3548.

Dorsey, R., 2010, Sedimentation and crustal recycling along an active oblique-rift margin: Salton Trough and northern Gulf of California: Geology, v. 38, p. 443-446.

Douglas, R., Gonzalez-Yajimovich, O., Ledesma-Vazquez, J., and Stainess-Urias, F., 2007, Climate forcing, primary production and the distribution of Holocene biogenic sediments in the Gulf of California: Quaternary Science Review, v. 26 p. 15–129.

Einsele, G., and Kelts, K., 1982, Pliocene and Quaternary mud turbidites in the Gulf of California: sedimentology, mass physical properties and significance: Init. Rep. Deep Sea Drilling Program: v. 64, p. 511–528.

Einsele, G., 1985, Basaltic sill-sediment complexes in young spreading centers: Genesis and Significance, Geology, v. 13 p. 249–252.

Escartin, J., Smith, D., Cann, J., Schouten, H., Langmuir, C., and Escrig, S., 2008, Central role of detachment faults in accretion of slow-spreading oceanic lithosphere: Nature, v. 455, p. 790-795.

Gibbard, P.L., Boreham, S., Cohen A.C., and Moscarriello, A., 2004, Global chronostratigraphical correlation table for the last 2.7 million years (http://www.quaternary.stratigraphy.org.uk) 1p.

Hastings J. R. and Turner, R. M., 1965, Seasonal precipitation regimes in Baja California, Mexico, Geografiska Annaler, v. 47A, p. 204-223.

Judd, A., Hovlnd M., 1992, The evidence of shallow gas in marine sediments: Continental Shelf Research, v. 12, no. 10, p. 1081-1095.

Kluesner, J., and Lonsdale, P., 2008, Young saucer-shaped sills within rapidly accumulated sediments of the central Gulf of California: Eos Trans, AGU, 89 (53), Fall Meet. Suppl., Abstract T11A-1847.

Kutzback, J.E., and Wright, H.E., 1985, Simulation of the climate 18,000 BP: Results for the North American/North Atlantic/European sector and comparison with the geologic record of North America: Quaternary Science Reviews, v. 4, p. 147-187.

Lizarralde D., Soule, A., Seewald., J., and Proskurowski, G., 2010, Carbon release by off-axis magmatism in a young sedimented centre: Nature Geoscience, v. 4, p. 50-54. doi:10.1038/NGEO1006.

Lonsdale, P., and Becker, K., 1985, Hydrothermal plumes, hot springs, and conductive heat flow in the southern trough of Guaymas Basin: Earth and Planetary Science Letters, v. 73 p. 211–225.

Lonsdale, P., and Kluesner J., 2010, Routing of terrigenous clastics to oceanic basins in the Southern Gulf of California, inherited from features of the pre-spreading protogulf. AGU Fall Meet. Suppl., Abstract T33C-2265.

Lonsdale, P., and Lawver, L.A., 1980, Immature plate boundary zones studied with a submersible in the Gulf of California. Geol. Soc. Am. Bull., v. 91, p. 555–569.

Lonsdale, P., 1989, Geology and tectonic history of the Gulf of California, In: Winterer, E.L., Hussong, D.M., Decker, R.W. (Eds.), The Eastern Pacific Ocean and Hawaii: The Geology of North America N. Geological Society of America, Boulder, CO, p. 499–521.

Marsaglia, K., 1991, Provenance of sands and sandstones from a rifted continental arc, Gulf of California, Mexico: in Fisher, R.V., and Smith, G.A.,

eds., Sedimentation in volcanic settings: SEPM (Society for Sedimentary Geology) Special Publication 45, p. 237–248.

Menking, K. M., Anderson R. A., Shafike N. G., Syed K. H., and Allen, B. D., 2004, Wetter or colder during the Last Glacial Maximum? Revisiting the pluvial lake question in southwestern North America: Quaternary Research, v. 62, p. 280-288.

Metcalfe, S., Bimpson, A., Courtice A., O'Hara S., and Taylor, D., 1997, Climate change at the monsoon/Westerly boundary in Northern Mexico, J. Paleolimnology, v.17, p. 155-171.

Moore, D., 1973, Plate-Edge Deformation and Crustal Growth, Gulf of California Structural Province: Geological Society of America Bulletin June, v. 84, p. 1883-906.

Perissoratis, C., Piper, D.J.W., and Lykousis, V., 2000, Alternating marine and lacustrine sedimentation during late Quaternary in the Gulf of Corinth rift basin, central Greece: Marine Geology, v. 167 p. 391-411.

Persaud, P., Stock, J.M., Steckler, M.S., Martin-Barajas, A., Diebold, J.B., González-Fernández, A. & Mountain, G.S., 2003, Active deformation and shallow structure of the Wagner, Consag and Delfín Basins, Northern Gulf of California: Mexico, J. Geophys. Res., v. 108(B7), p. 2355-2377.

Peterson, C., Behl, R., Nicholson, C., Lisiecki, L., and Sorlien, C., 2009, Orbital- to Sub-Orbital-Scale Cyclicity in Seismic Reflection and Sediment Character in Early to Middle Pliestocene Mudstone, Santa Barbara Basin, California: GSA Abstracts with Programs, v. 42, No. 4, p. 77.

Plattner, C., Malservisi, R., Dixon, T., Sella, G., Lafemina, P., Fletcher J., and Suarez-Vidal, F., 2007, New constraints on relative motion between the Pacific plate and Baja California microplate (Mexico) from GPS measurements. Geophys. J. Int., p. 1373–1380.

Rauch, K., 2005, Cyclicity of Peru-Chile trench sediments between 36° and 38°S: A footprint of paleoclimatic variations?: Geophysical Research Letters, v. 32, L08302, p. 1-4. doi:10.1029/2004/GL022196.

Rhode, D., 2002, Early Holocene Juniper woodland and chaparral taxa in the Central Baja California Peninsula, Mexico: Quaternary Research, v. 57, p. 102-108.

Sangree, J.B., and Widmier, J.M, 1977, Seismic stratigraphic interpretation of clastic depositional facies, pp.165-184 of Seismic Stratigraphy - applications to hydrocarbon exploration, Am. Assn. Petrol. Geol. Memoir 26, 516 p.

Schrader, H., 1982, Diatom Biostratigraphy and Laminated Diatomaceous Sediments from the Gulf of California: Init. Rep. Deep Sea Drilling Program, v. 64, p. 973-981.

Simoneit, B.R.T., and Lonsdale, P.F., Hydrothermal petroleum in mineralized mounds at the seabed of Guaymas Basin. Nature, v. 295, p. 198–202.

Spiess, R. N., et al. 1980, East Pacific Rise: Hot springs and geophysical experiments, Science, v. 207, p. 1421–1433, doi:10.1126/science.207.4438.1421.

Steckler, M., Sagy, Y., Mountain, G., Stock, J., and Martin Barajas, A., 2009, Seismic-Stratigraphic Framework for the Northern Gulf of California: Eos, Trans. AGU, 90 (52), Fall Meet. Suppl., Abstract T31A-1785.

Tapponnier, P., and Francheteau, J., 1978, Necking of the lithosphere and the mechanics of slowly accreting plate boundaries: Journal of Geophysical Research, v. 83, p. 3955-3970.

Thunell, R., 1997, Continental margin particle flux – seasonal cycles and archives of global change: Oceanus, v. 40, p. 20–23.

Thunell, R., 1998, Seasonal and annual variability in particle fluxes in the Gulf of California: A response to climate forcing: Deep Sea Research I, v. 45, p. 2059-2083.

Van Andel T., 1964, Recent marine sediments of Gulf of California, in Van Andel T.,Shor G.G., eds., Marine geology of the Gulf of California: American Association of Petroleum Geologists Memoir 3, p. 216–310.

Völker, D., Wiedicke, M., Ladage, S., Gaedicke, C., Reichert, C., Rauch, K., Kramer W., and Heubeck, C., 2006, Latitudinal variations in sedimentary processes in the Peru-Chile trench off Central Chile. In: Oncken, G.C.O., Franz, G., Giese, P., Götze, H.-J., Ramos, V.A., Strecker, M.R., and Wigger, P., Editors, The Andes—Active Subduction Orogeny: Springer-Verlag, p. 193–216.

Weigelt, W., Uenzelmann-Neben, G., 2007, Orbital forced cyclicity of reflector strength in seismic records of the Cape Basin: Geophysical Research Letters, v. 34, p. 1-4 L01702, doi:10.1029/2006GL028376.

Figure 2-1. Topography of Guaymas and Carmen Basins. Bathymetry is from Multibeam surveys, supplemented in shallow water by contour interpolation of archival soundings; subaerial relief from satellite altimetry. Blue lines represent principal channels used for transport of terrigenous clastics: subaerial rivers, and submarine canyons, slope gullies, and fan channels. Brown lines on Baja California locate primary and secondary (dashed) drainage divides. Dashed black and orange boxes locate areas shown in more detail in Figures 2 and 7A. Numbered circles locate DSDP coring sites discussed in the text. Labeled contours are in hundreds of meters (10 = 1000 m). C.P.=Concepcion Peninsula. Inset: Pattern of the plate boundary throughout the Gulf, with spreading centers labeled: W-Wagner, UD-Upper Delfin, LD- Lower Delfin, G-Guaymas, C-Carmen, F-Farallon, NP- North Pescadero, SP-South Pescadero, A-Alarcon, EPR-East Pacific Rise. Land is dark grey, newly accreted crust light grey; dashed blue box locates area of main map.

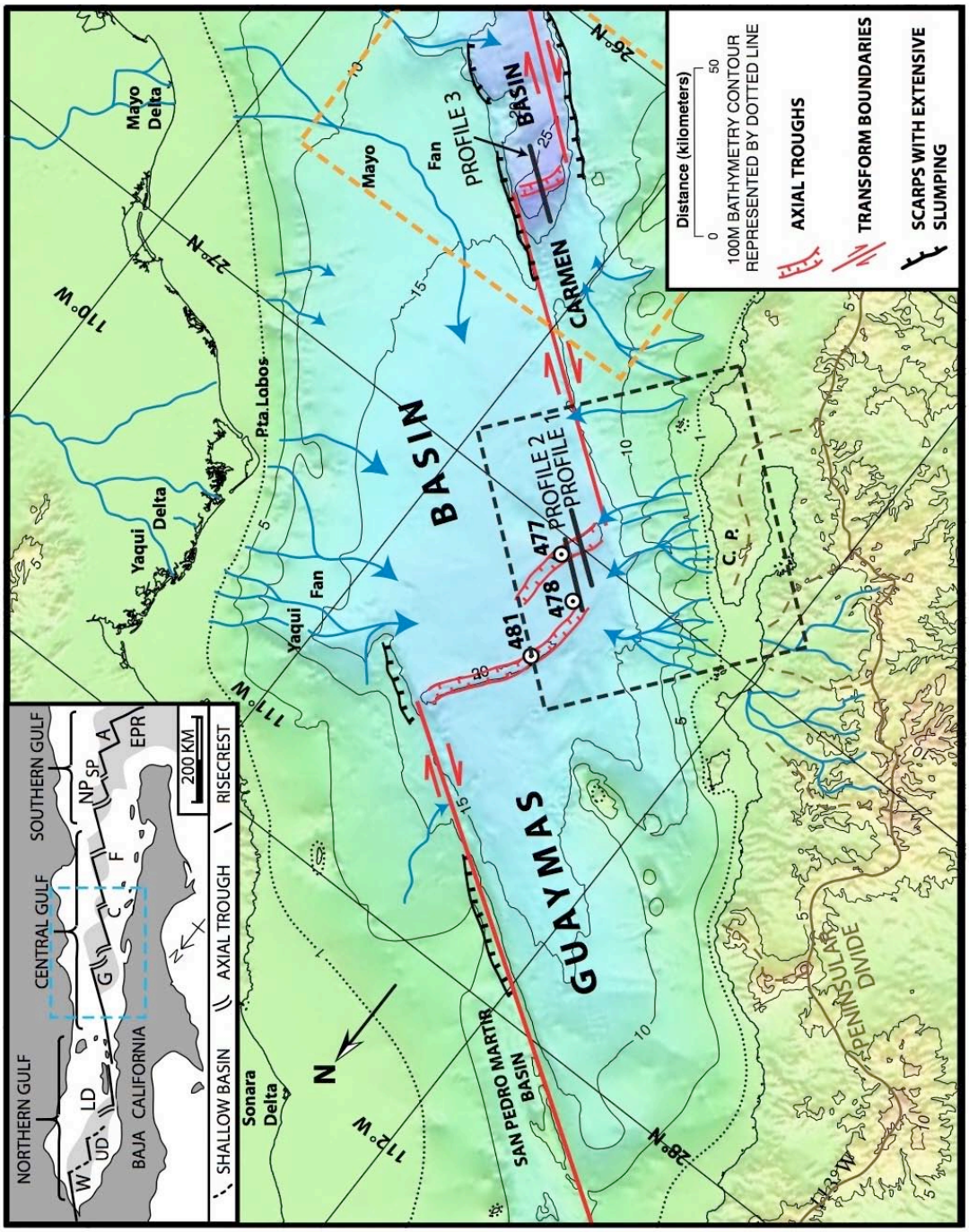
NORTHERN GULF
CENTRAL GULF
SOUTHERN GULF
BAJA CALIFORNIA
LD
UD
G
C
F
NP
SP
A
EPR
200 KM
SHALLOW BASIN
AXIAL TROUGH
RISECREST
Sonara Delta
Yaqui Delta
Mayo Delta
Pta.Lobos
Yaqui Fan
Mayo Fan
PROFILE 3
PROFILE 2
PROFILE 1
BASIN
GUAYMAS
CARMEN
SAN PEDRO MARTIR BASIN
481
478
477
C. P.
PENINSULAR DIVIDE
N
111°W
110°W
112°W
27°N
28°N
26°N
Distance (kilometers)
0
50
100M BATHYMETRY CONTOUR REPRESENTED BY DOTTED LINE
AXIAL TROUGHS
TRANSFORM BOUNDARIES
SCARPS WITH EXTENSIVE SLUMPING

Figure 2-2. Multibeam bathymetry of study area in southwestern Guaymas Basin, and the adjacent Baja California continental slope (located in Figure 1). Contour interval (offshore and onshore) is 100 m, 250 m where interpolated (dashed lines). Blue lines are now ephemeral washes onshore, slope gullies and submarine canyons offshore; possible links between them (dashed lines) are hypothetical, in the absence of high-resolution shallow-water bathymetry. Dashed yellow lines show estimated location of the Southern Trough relative to Baja California at 500 ka (see text).

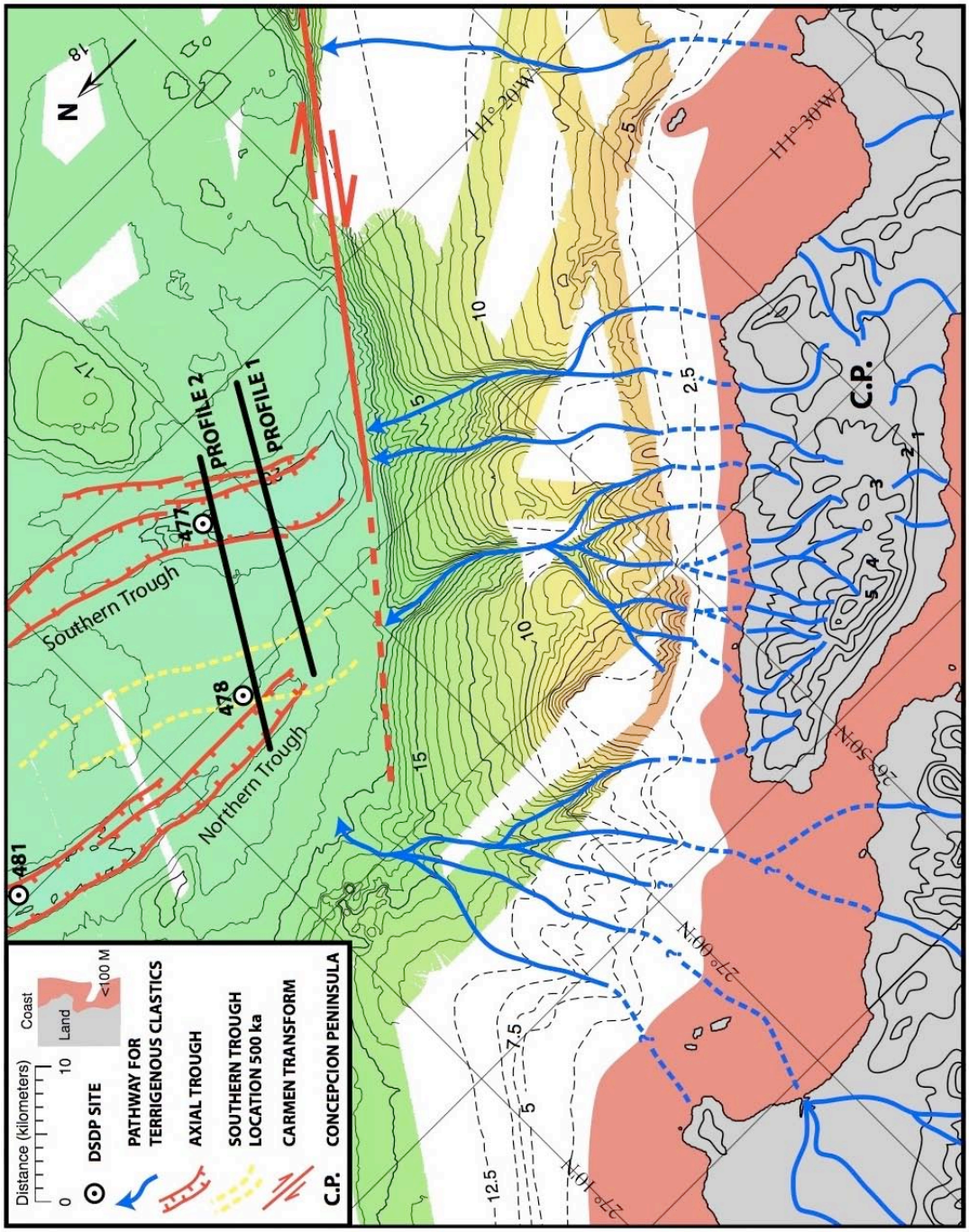
Distance (kilometers)
0
10
Coast
Land
<100 M
DSDP SITE
PATHWAY FOR TERRIGENOUS CLASTICS
AXIAL TROUGH
SOUTHERN TROUGH LOCATION 500 ka
CARMEN TRANSFORM
C.P.
CONCEPCION PENINSULA
N
481
477
478
PROFILE 2
PROFILE 1
Southern Trough
Northern Trough
C.P.
111° 30'W
111° 20'W
27° 50'N
27° 00'N
26° 50'N
26° 40'N
5
10
15
2.5
12.5
7.5
3
2
1
4

Figure 2-3. 3D cutaway of MCS Profile 1 and multibeam bathymetry, crossing the Southern Trough of Guaymas Basin (located in Figures 1 and 2). Dashed black line represents Profile 2 shown in Figure 4. Superficial layer A is the youngest transparent unit; buried B and C are seismically similar older units. Principal faults are identified using sub-vertical black lines. A paleo-sealevel reconstruction (Bintanja et al., 2005), with glacial (blue labels) and interglacial (green) stages identified, has its horizontal scale (age, ka) adjusted to match the estimated age of oceanic basement in the profile directly above it (assuming symmetric spreading at 23 m/kyr from a 1 km-wide crustal accretion zone). Dashed green lines are drawn vertically from the apparent intersection of seismically transparent sedimentary units with oceanic basement, allowing an estimate of the ages of those units; on the northwest flank, units B and C seem to have been deposited on oceanic basement during high stands of sea-level, i.e. during interglacial stages.

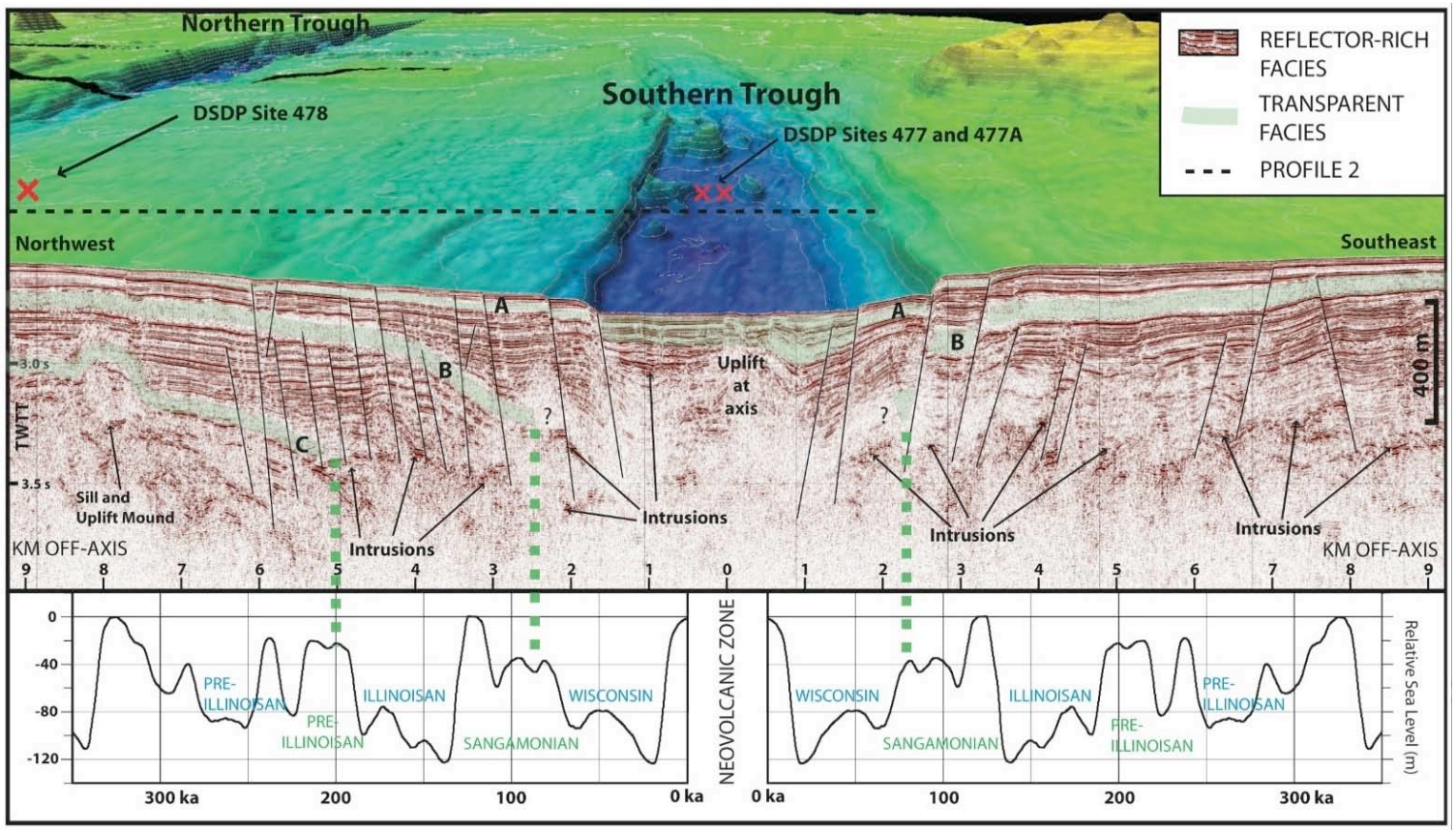
Northern Trough
Southern Trough
DSDP Site 478
DSDP Sites 477 and 477A
REFLECTOR-RICH FACIES
TRANSPARENT FACIES
PROFILE 2
Northwest
Southeast
A
B
C
Uplift at axis
3.0 s
3.5 s
TWTT
400 m
Sill and Uplift Mound
Intrusions
KM OFF-AXIS
9 8 7 6 5 4 3 2 1 0 1 2 3 4 5 6 7 8 9
0
-40
-80
-120
PRE-ILLINOISAN
ILLINOISAN
SANGAMONIAN
WISCONSIN
NEOVOLCANIC ZONE
Relative Sea Level (m)
300 ka 200 100 0 ka
0 ka 100 200 300 ka

Figure 2-4. MCS Profile 2. A 24-channel seismic profile collected between the Northern and Southern Troughs of Guaymas Basin during the site-survey cruise for DSDP leg 64. Gaps within the line are from changing recording tapes during data collection; the abrupt decrease in amplitudes at time 0845 is due to failure of part of the airgun array. Layer B is highlighted in blue and represents diatomaceous mud. High-amplitude, layered reflector unit above Layer B is composed of sandy turbidites and diatomaceous mud. Identification of shallow intrusive sills near DSDP site 477 is based on drilling results.

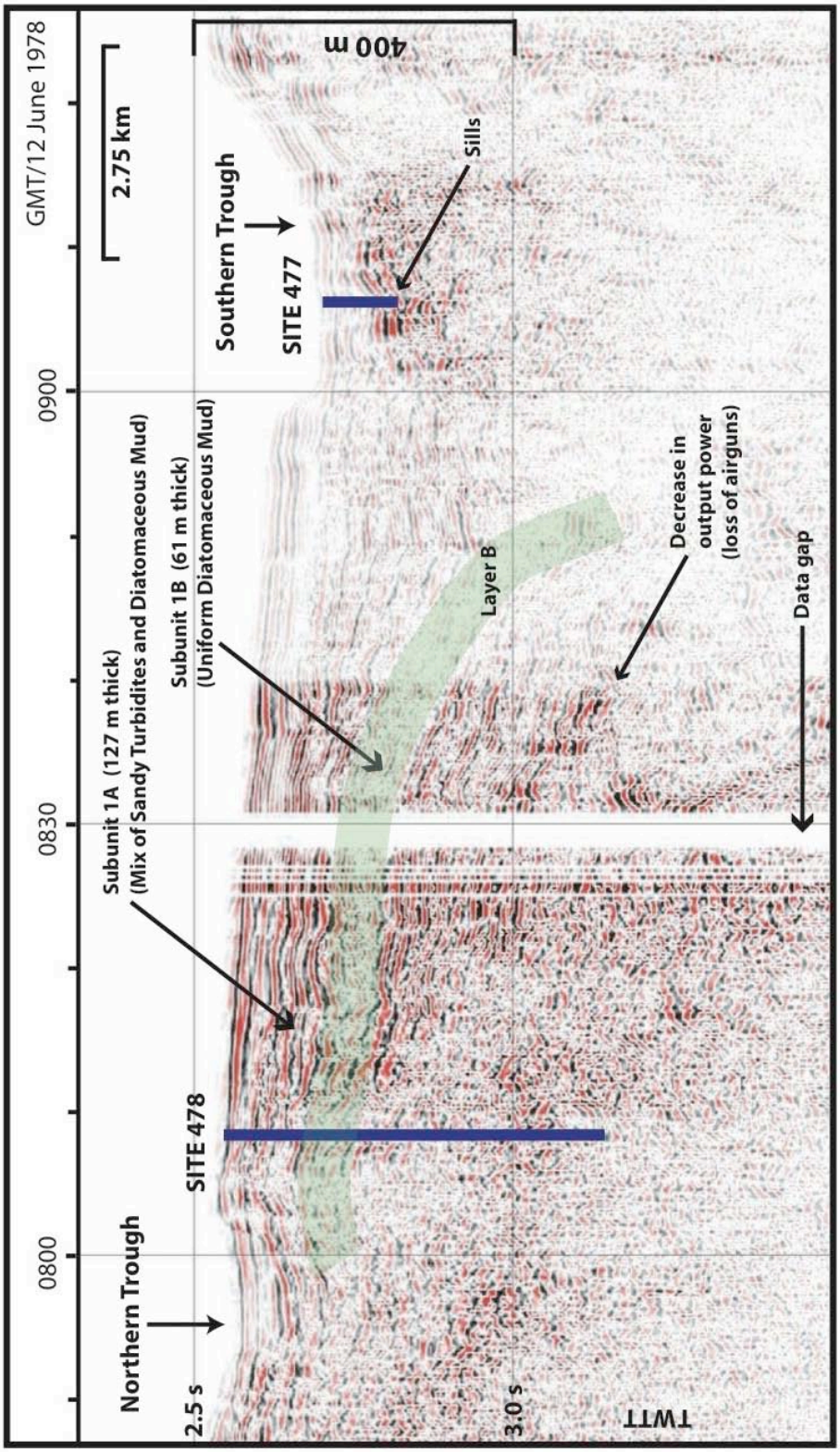
GMT/12 June 1978
0800
0830
0900
2.5 s
3.0 s
TWTT
Northern Trough
SITE 478
Subunit 1A (127 m thick)
(Mix of Sandy Turbidites and Diatomaceous Mud)
Subunit 1B (61 m thick)
(Uniform Diatomaceous Mud)
Layer B
Decrease in
output power
(loss of airguns)
Data gap
Southern Trough
SITE 477
Sills
2.75 km
400 m

Figure 2-5. Northwestern sections of MCS Lines 1 and 2 tied to DSDP Site 478 drilling results. Highlighted yellow layers represent acoustically transparent units A, B, and C. Section of homogenous muddy diatomaceous turbidites (Subunit 1B at Site 478) are correlated to transparent unit B in unit 2 and tied to Line 1 based on similar acoustic character, depth-below-seafloor, thickness, extent, structure, and proximity. Using the same logic, high-amplitude reflector wedges between acoustic units A and B on Lines 1 and 2 are correlated to sandy turbidites interbedded with diatomaceous mud turbidites (Subunit 1A in DSDP Site 478). Note onlap of relatively flat high-amplitude reflectors onto identified transparent layers.

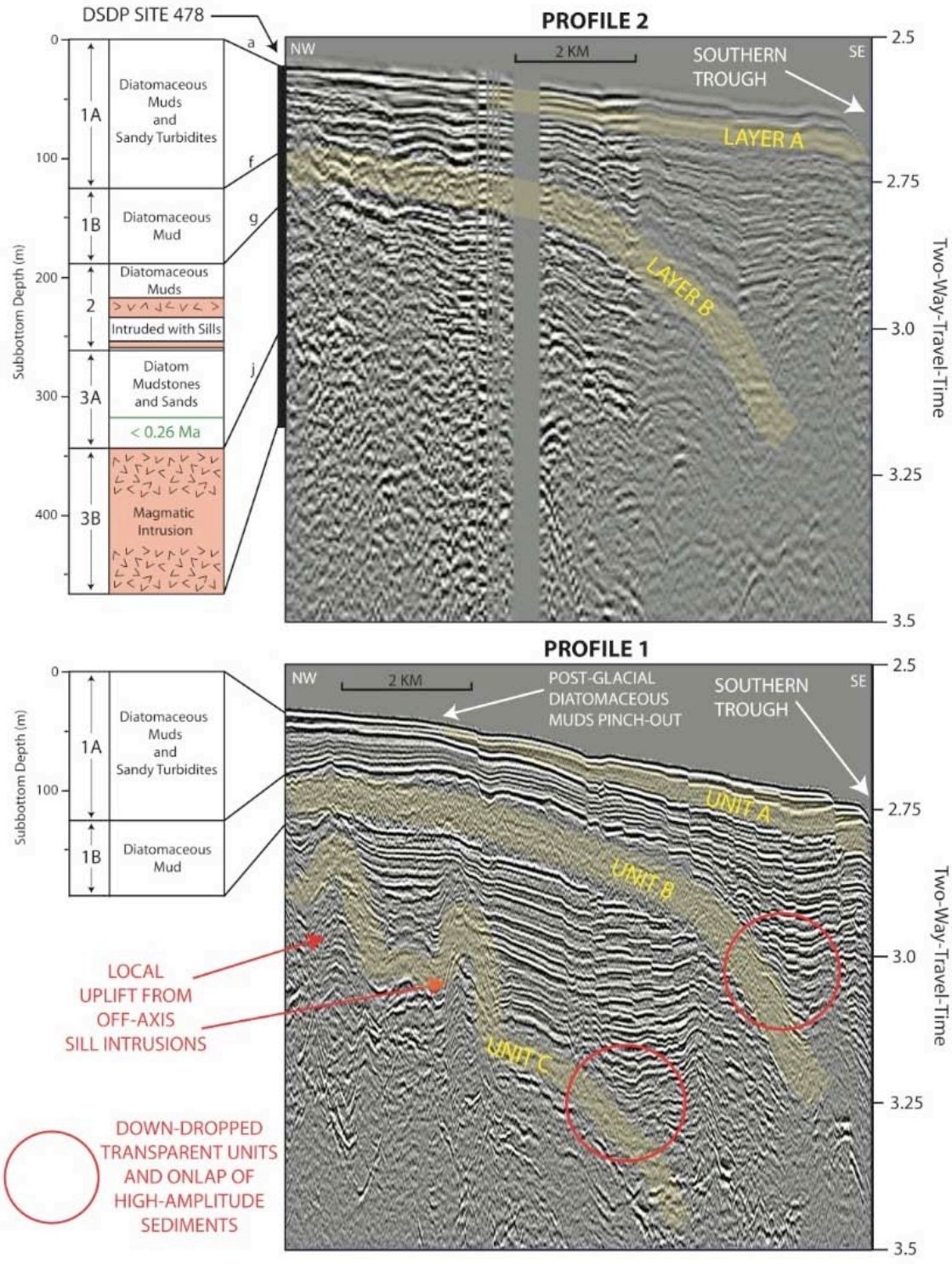
DSDP SITE 478
PROFILE 2
Subbottom Depth (m)
0
100
200
300
400
1A
Diatomaceous Muds and Sandy Turbidites
1B
Diatomaceous Mud
2
Diatomaceous Muds
Intruded with Sills
3A
Diatom Mudstones and Sands
< 0.26 Ma
3B
Magmatic Intrusion
a
f
g
j
NW
2 KM
SOUTHERN TROUGH
SE
LAYER A
LAYER B
2.5
2.75
3.0
3.25
3.5
Two-Way-Travel-Time
PROFILE 1
POST-GLACIAL DIATOMACEOUS MUDS PINCH-OUT
UNIT A
UNIT B
UNIT C
LOCAL UPLIFT FROM OFF-AXIS SILL INTRUSIONS
DOWN-DROPPED TRANSPARENT UNITS AND ONLAP OF HIGH-AMPLITUDE SEDIMENTS

Figure 2-6**.** Simplified rift evolution model for the southern trough in Guaymas Basin. Three panels represent axial rift structure during different time periods: 1---100,000 yr (Last Interglacial); 2---20,000 yr (Last Glacial Maximum); and 3---present (Current Interglacial). BP = before present. Arrows denote spreading direction and indicate a constant spreading rate over the past 100,000 yr. Thin green units (interglacial sediments) are alphabetically labeled with unit A being the youngest (present day deposition) and E representing the oldest. Thick brown wedges of sediment represent deposition of terrigenous turbidites during glacial periods. Letter F traces a distinct fault through time and demonstrates how crust is accreted and rafted away from the spreading axis, preserving the paleo-rift structure on the rift flanks. Shaded layer at depth signifies sill and dike intruded sediments. Shallow intrusions on panel 3 represent off-axis intrusions, which acoustically mask structures below (these are removed from panels 1 and 2 in order to clearly show rift structure). Note how sediment load is modulated by glacial-interglacial periods, filling the trough during glacial periods (sea-level low stands). As spreading continues, sedimentary units are split by diking and extension and rafted away from the spreading axis at the half-spreading rate.

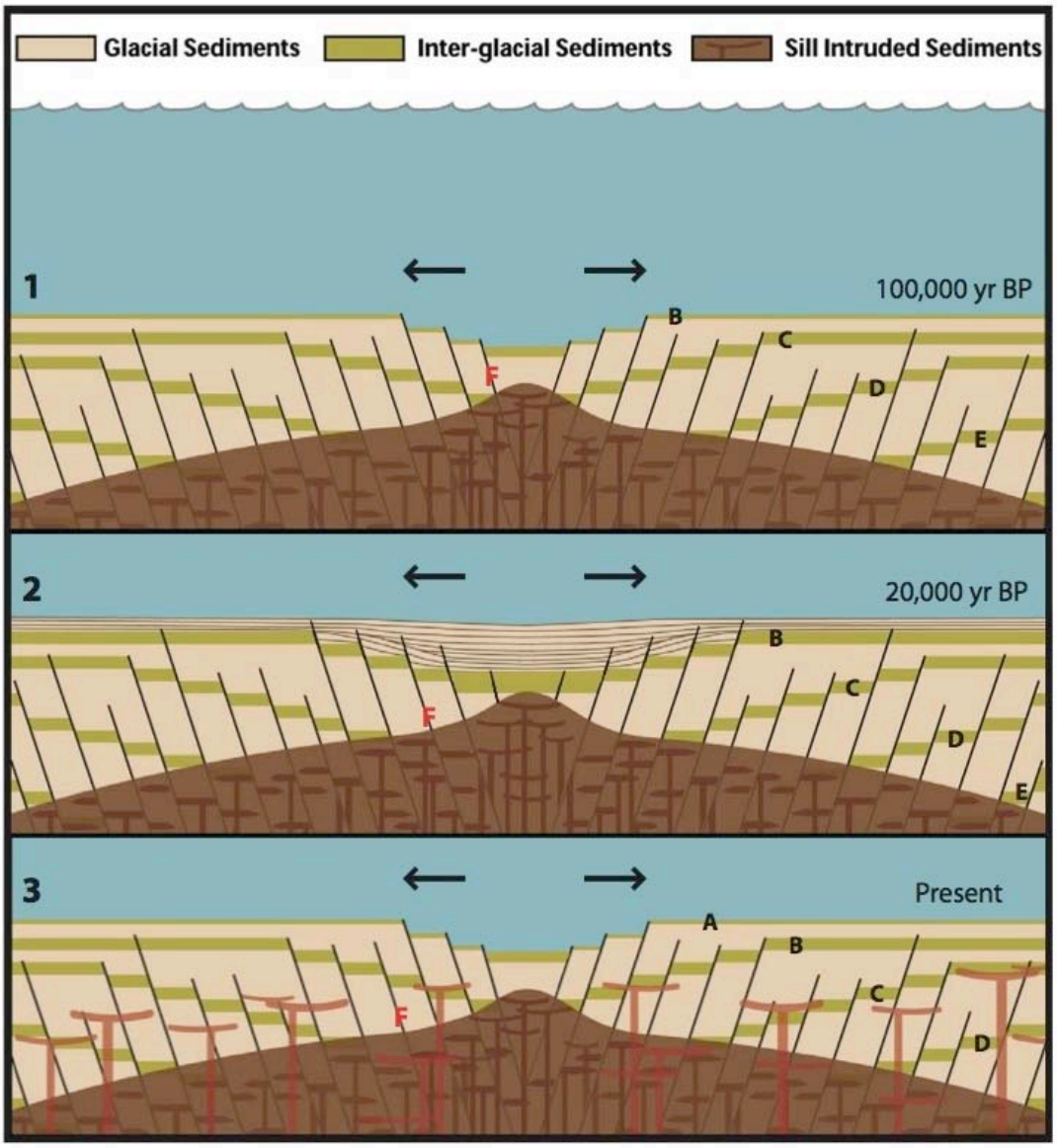
Glacial Sediments
Inter-glacial Sediments
Sill Intruded Sediments
1
100,000 yr BP
B
C
D
E
F
2
20,000 yr BP
B
C
D
E
F
3
Present
A
B
C
D
F

Figure 2-7. Detailed bathymetric map of Carmen Basin (located in Figure 1) and a seismic transit of Carmen axis. Panel A: Location of the axial trough (black arrow represents 3D view angle in Figure 7B) and bathymetrically inferred pathways for turbidity currents, including Mayo and Fuerte fan channels. Colored multibeam bathymetry has 50 m isobaths; dashed isobaths are interpolated using conventional sounding lines. Labeled contours are in hundreds of meters (10 = 1000 m). B.C.S. = channel from the Baja California Sur margin. Panel B: MCS Profile 3 (located above) superimposed on a 3D multibeam bathymetry image. Viewing angle is to the southwest and bathymetry and seismic image have ~4x vertical exaggeration. White line represents a 2008 ROV JASON dive path, with red boxes indicating location of rock samples. The picture inset is of pillow basalts collected at a recent spreading-axis eruption site; scale bar in this image is in centimeters. Cooked, diatomaceous muds were sampled along the northwest rift wall that cuts a transparent reflector unit. Note alternating transparent and high-amplitude reflector packages below rift walls and adjacent basin floor.

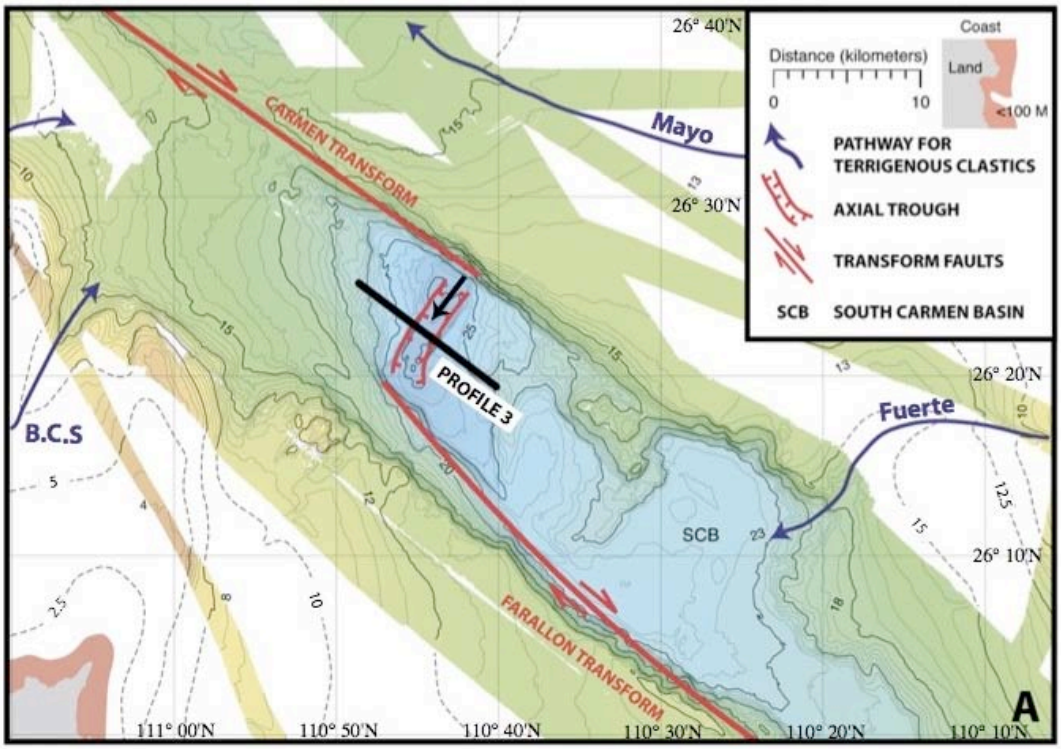
26° 40'N
26° 30'N
26° 20'N
26° 10'N
111° 00'N
110° 50'N
110° 40'N
110° 30'N
110° 20'N
110° 10'N
CARMEN TRANSFORM
FARALLON TRANSFORM
Mayo
Fuerte
B.C.S
SCB
PROFILE 3
Coast
Distance (kilometers)
Land
0
10
<100 M
PATHWAY FOR TERRIGENOUS CLASTICS
AXIAL TROUGH
TRANSFORM FAULTS
SCB SOUTH CARMEN BASIN
A

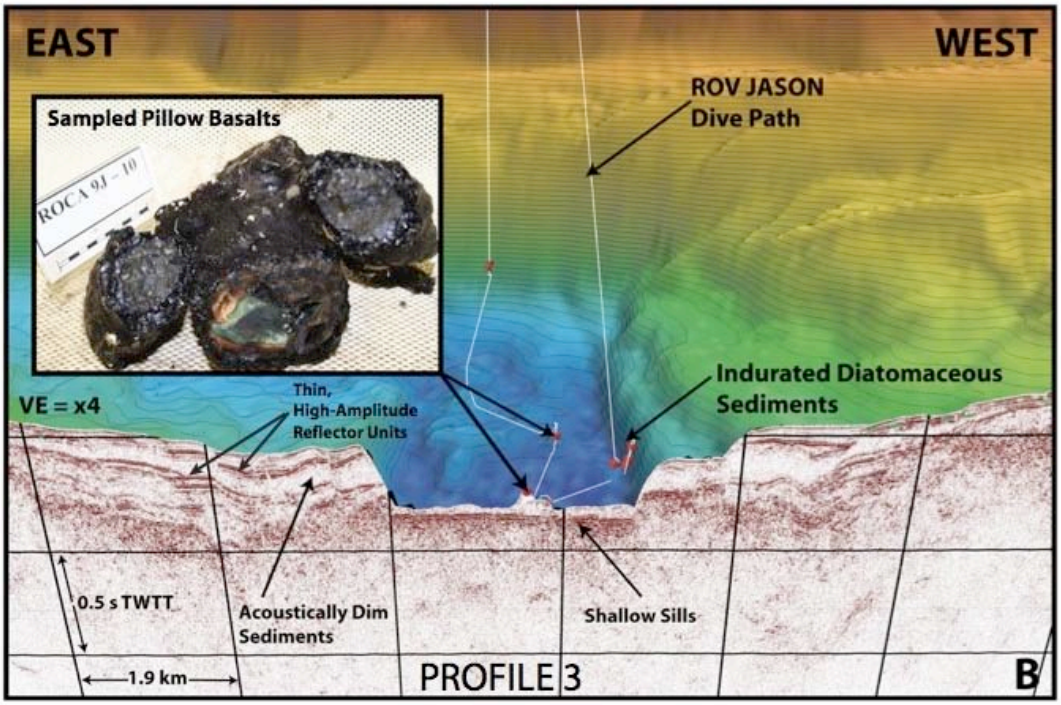
EAST
WEST
Sampled Pillow Basalts
ROCA 91 - 10
ROV JASON
Dive Path
VE = x4
Thin,
High-Amplitude
Reflector Units
Indurated Diatomaceous
Sediments
0.5 s TWTT
1.9 km
Acoustically Dim
Sediments
Shallow Sills
PROFILE 3
B

Figure 2-8. The turbidite-accumulating North Pescadero transform valley near its intersection with the axial rift valley of the North Pescadero spreading axis (located in Figure 1, inset). The multibeam bathymetric map (50 m contour interval) locates the profile shown above it, and shows the intersection of the two valleys. It is oriented so that horizontal lines are parallel to the local 305° vector of Baja California - North America plate motion, as estimated from geodetic data (Plattner et al., 2007); note that the bathymetrically located trace of the transform fault zone near its spreading center intersection is ~13° oblique to relative plate motion, accounting for creation of a deep transtensional valley in this location. (But note also that the bathymetric expression of the fault zone across the flat valley floor is slight, and en echelon stepping of less oblique fault zones may be involved.) On the MCS profile, five units with only low-amplitude internal reflectors have been highlighted in pale green. The thickness of each unit (and of the more reflective intervening layers) changes systematically across the active strike-slip fault zone, evidence for both steady uplift of young oceanic crust on the southwest side of the transform, and for turbidity current deposition of the valley fill.

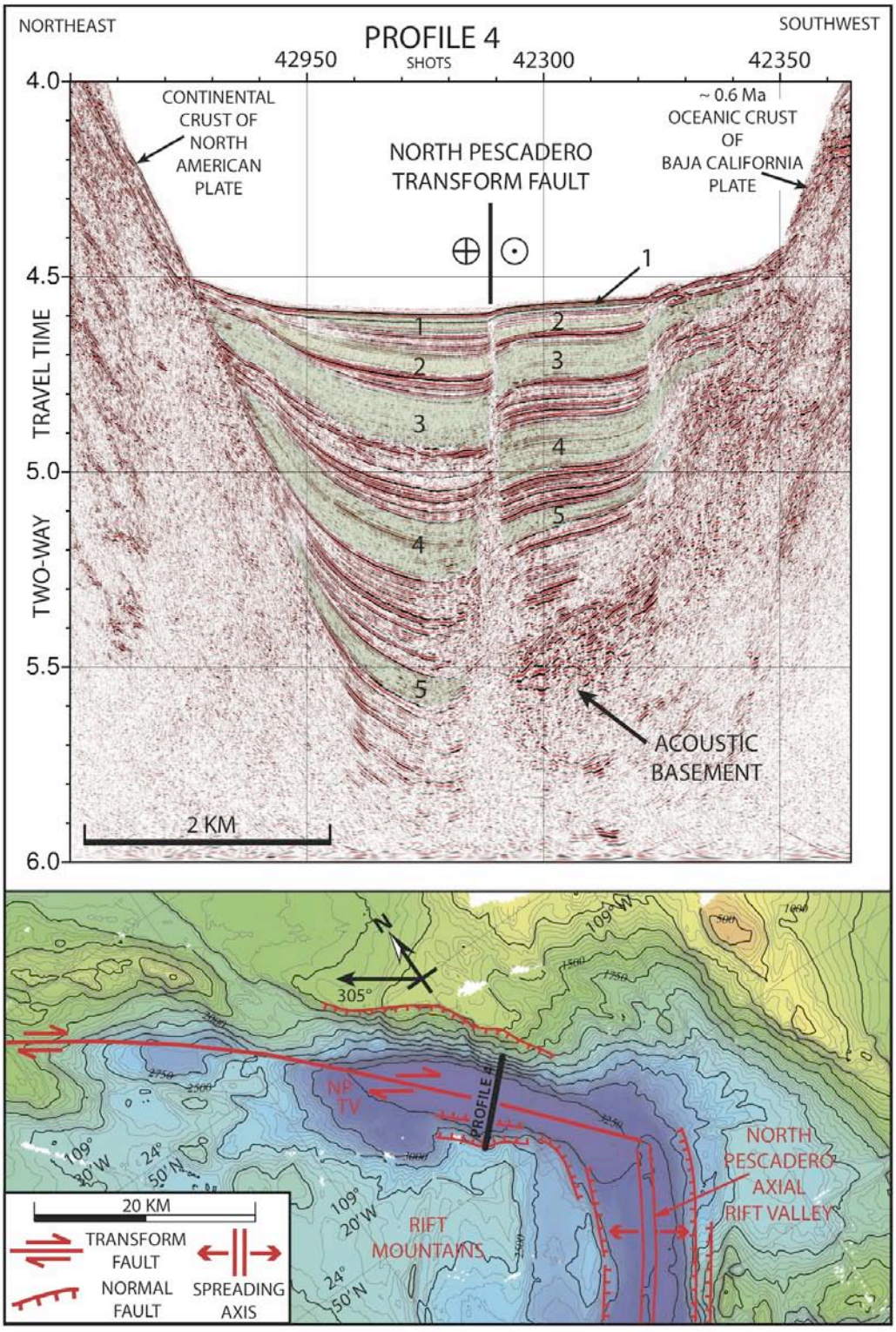
NORTHEAST
PROFILE 4
SOUTHWEST
42950
SHOTS
42300
42350
4.0
4.5
5.0
5.5
6.0
TRAVEL TIME
TWO-WAY
CONTINENTAL CRUST OF NORTH AMERICAN PLATE
NORTH PESCADERO TRANSFORM FAULT
~ 0.6 Ma OCEANIC CRUST OF BAJA CALIFORNIA PLATE
1
2
3
4
5
ACOUSTIC BASEMENT
2 KM
N
305°
109° W
24° 50' N
NP TV
PROFILE 4
NORTH PESCADERO AXIAL RIFT VALLEY
RIFT MOUNTAINS
109° 30' W
109° 20' W
24° 50' N
20 KM
TRANSFORM FAULT
NORMAL FAULT
SPREADING AXIS

Chapter 3

Geological and Hydrological Effects of Young Intrusive Magmatism in the Central and Southern Gulf of California

3.1 ABSTRACT

Multi-channel seismic (MCS) reflection profiles collected across the central and southern Gulf of California display saucer-shaped igneous sills and associated overburden deformations, fluid migration pathways, and possible feeder networks; many sills 1-2 km in diameter have a characteristic concave-upwards profile. These shallow, bowl-like sills are most common as off-axis intrusions into unconsolidated hemipelagic muds flooring the Guaymas, Carmen, and Farallon Basins, but some can also be identified in sediment ponded in at least one of the narrow rift valleys that mark the principal, axial, sites of magmatic crustal accretion within these young, actively growing oceanic basins. Clusters of similar sills also occur within the sediment cover of subsided continental crust at the basins' rifted and shearing (transform) margins, where they may mask the geologic boundaries between oceanic and continental crust. In both off-axis oceanic and supra-continental settings, some sills are very young, uplifting the present seafloor and disrupting turbidite deposition patterns, causing onlap of the youngest strata and providing relative ages of intrusions, associated deformation, and sedimentation. Integration of multibeam bathymetry and a dense grid of 3.5 kHz profiles over young concave-up sills imaged on a single MCS profile suggests that off-axis sills have circular to elliptical three-dimensional (3D) structures. Plotting concave-upwards sill width against emplacement depth

reveals an overall linear trend (deeper = wider sill) and two distinct trends based on geographic location. Modeling results suggest emplacement depth as a main control on sill structure and that development of asymmetrical stress fields above the sill once uplift of the overburden occurs may be responsible for the upturned sill edges. MCS profiles also reveal sub-vertical, cross-cutting reflectors below the sills that differ from seismic artifacts and sideswipes; they do not resemble the unique diffraction “smiles” caused by over-migration and are found only underlying areas of intrusions. Some of these steeply inclined, high-amplitude reflectors can be traced directly below a sill and probably represent the inclined tips of older sills, feeding the overlying younger sills. Narrow vertical disturbances ('chimneys' or 'pipes') observed over large off-axis sills on several MCS profiles are probably hydro-fractured pathways that funnel super-heated fluids away from the magma-sediment contact zone, and some have formed pockmarks where they reach the seafloor. Within the heavily faulted axial troughs, fluids have used fault zones for low-resistant conduits to the seafloor. MCS profiles collected over young sills that lack visible fluid pathway to the seafloor (i.e., pipes or faults) show extensive evidence for concentrated hydrocarbons and trapping and leakage features.

3.2 INTRODUCTION

Formation of sediment-sill complexes, intercalations of igneous sills and sedimentary rocks, is a typical result of injection of magma via dike or pipe

conduits into the base of a section of weak unconsolidated sediment. As explained by Einsele (1982), when a buoyant sheet or column of rising melt has a magmatic pressure, generated by the lithostatic load at the magma source, that exceeds the lithostatic pressure of surrounding sediment by enough to overcome the sediment's (very low) tensile strength, it will leave its vertical conduit and spread out and freeze as a quasi-horizontal sheet, i.e., a sill. In the simplest situation, later magma injections from the same source, perhaps with higher magmatic pressure because of addition of sills to their overburden, may rise through fractures in preexisting sills and spread out above them, but not directly above them, because especially in marine environments the process of magma injection causes expulsion of pore-water and lithification of sediments above (and below) cooling sills, significantly increasing their tensile strength and resistance to subsequent lateral spreading of magma (Einsele, 1982). That is why layers of sedimentary rocks are preserved in the sill complexes.

Intrusion of igneous sills into unconsolidated marine sediments is an important process, and the subject of much current research. As well as lithifying sediments sill intrusion, as discussed below, drive and/or cap hydrothermal systems in the seabed, cause mineralization and ore formation, and if the intruded sediment has a suitable organic component, generate thermogenic hydrocarbons. Where sills are thick enough, their intrusion deforms the overlying seabed, and may modify basin bathymetry in ways that affect sedimentation patterns. It is a common process, especially at rifting continental margins, which

are typified in the early stages of continental rupture by broad belts of syn-rift volcanism and rapid accumulation of syn-rift sediments in rift basins. Now-inactive example of such sites in rifted continental crust, notably along the margin of northwest Europe where a complex magma-rich rift system was created by the orthogonal Late Cretaceous to Early Eocene separation of Greenland, have become classic locations for pioneering field studies (Smallwood and Maresh, 2002; Thomson and Hutton, 2004; Hansen and Cartwright, 2006). These studies have allowed interpretation of the geometries, emplacement processes, and geological consequences of sill intrusion into unconsolidated marine sediments, by the use of 3D multichannel seismic reflection profiling (3D MCS). Application of this technique, complemented by recent studies of onshore outcrops of erosionally dissected sill complexes in this same region (Hansen et al., 2011), and at more ancient continental margin sites (Chevallier and Woodford, 1998; Polteau et. al., 2008) has revealed a far richer pattern of clustered sill intrusions than that envisaged by Einsele (1982), with repeated magma injection into still molten sills having caused magma break-out along inclined fissures that lead to satellite sills. In this chapter I apply the results of these 3D field programs, and of the theoretical (Malthe-Sorenssen, 2004; Menand, 2007; Goulty and Schofield, 2008) and modeling (Kavanagh et al., 2006; Mathieu et al., 2008; Galland et al., 2008) studies they have spawned to interpret high-resolution 2D MCS and acoustic profiles of young sills emplaced in the sediment cover of submerged continental crust at the recently rifted and still magmatically active margins of the

Gulf of California and along some of the Gulfs long sheared and still-shearing (transform) margins.

Most of this chapter, however, concerns interpretation of seismically imaged sills recently emplaced in the sediment fills of the central and southern Gulf's young (Plio-Pleistocene) oceanic basins, focusing predominantly on sills emplaced off-axis than on those being intruded at the narrow neovolcanic zones along the basin's axes where the sediment-sill "basement" of this crust is being accreted. Nascent volcanically active oceanic basins of this type become the principal locales for rapid deposition of syn-rift and post-rift sediments at Atlantic-type margins as rupture of continental lithosphere nears completion, and plate-boundary volcanism becomes focused at spreading centers at the feet of continental slopes. Sill intrusion at such locations was probably a principal magmatic process during the development of most of the rifted and sheared margins of the Atlantic. But along even the youngest parts of these margins the boundary between rifted continental crust and newly accreted (i.e., oceanic) crust is commonly buried by several kilometers of obscuring post-rift sediment (Klitgord et al., 1988), preventing high-resolution imaging of the results of sediment-magma interactions during the birth of an oceanic basin, before the spreading axis has migrated so far away from the margin that its shallow volcanism is no longer smothered by rapid terrigenous sedimentation. In many MCS studies of rifted continental margins even the boundary between oceanic and continental

crust is difficult to define, and is commonly placed within a broad “transition zone”, floored by ill-defined “transitional crust”.

There are currently several young rifted, and still rifting, continental margins that are adjacent to nascent oceanic basins containing near-shore spreading centers, that might be suitable, accessible, magmatically active field areas for studying sill emplacement in sediments overlying oceanic as well as adjacent continental crust, thereby helping clarify processes that affected most ancient rifted and sheared margins. In some cases, though, thick near-surface layers of mobile evaporite mask the structures, stratigraphy and results of shallow magmatism e.g. along the orthogonally opening Red Sea basin. Some young oceanic basins near the mouths of major river systems have received such large sediment influxes that no sill intrusions are known to have risen within 1-2 km of the surface, and the nature of crystalline basement is poorly known; this is the situation at the northern end of the obliquely opening Gulf of California rift, where in the past ~5 Myr the Colorado River has built a ~10 km-thick subaerial delta in the Salton Trough (Fuis et al., 1984), and a submarine delta of comparable thickness beneath the shallow waters of the northernmost part of the Gulf (Phillips, 1964; Dorsey, 2010). The presence of small, young, silicic volcanoes, both onshore and offshore (e.g. Robinson and Elders, 1976), shows that rapid accumulation of Colorado River sediment did not completely suppress upper crustal volcanism, but deep drilling onshore, even within 5 km of these eruptive centers, has encountered no shallow sills (e.g., none shallower than

2880 m in the Salton Trough borehole described by Herzig and Elders, 1988), and high-resolution MCS profiles that image the upper 1 km of crust at the northernmost submarine spreading center in the Gulf show no sills within the recorded section (Persaud et al., 2003). That is why this study was limited to the central and southern Gulf, where shallow sills and their surrounding sediments had already been sampled by drill-cores (Curray, Moore et al., 1982), and there was already evidence (mainly from Guaymas Basin) of secondary effects of shallow intrusions, such as high and extremely variable conductive heat flow (Lawver et al., 1975), hydrothermal systems that are precipitating metalliferous mineral deposits (Lonsdale et al., 1980), discharges of thermogenic petroleum and methane (Lonsdale, 1985), and local seafloor uplifts (Lonsdale and Lawver, 1980), both at spreading axes and off-axis. The only evidence for extensive, structure-masking evaporites comes from MCS profiles across submerged continental crust at a rifted margin of Guaymas Basin (Miller et al., 2009), a region avoided by our high-resolution MCS survey.

3.3 GEOLOGICAL SETTING

The Gulf of California occupies most of a broad 1750km-long rift zone created since the Middle Miocene by the oblique separation of the Baja California microplate from the North America plate and links the northern tip of the East Pacific Rise (EPR) to the southern end of the San Andreas Fault System (SAFS (Figure 1, subset; Curray et al., 1979). Most of the Gulf's floor is stretched, rifted

and sheared continental crust, mostly covered with syn-rift volcanics and a thickening cover of sediment. Since entry of Pacific waters at 7-6 Ma (Oskin and Stock, 2003), when rifting of granitic crust opened a deep seaway at the mouth of the Gulf, the sediment accumulated on continental crust in the central and southern parts of the Gulf rift has mainly been deltaic at the mouths of major rivers draining the Mexican mainland, marine turbidite deposits in channeled fans, and blankets of marine hemipelagic muds elsewhere (Figure 1). During the Pliocene, not long after submergence of the Gulf floor, transitions from rifting to spreading began, as short spreading centers linked by long transform fault zones developed in what had by this time become the principal boundary zone (at these latitudes) between the Pacific and North American plates. In the central and southern parts of the Gulf these spreading centers have accreted the oceanic crust of Guaymas, Carmen, Farallon Pescadero, and Alarcon Basins; their strips of newly accreted crust differ in width (Figure 2) because the rifting–to-spreading transition was not synchronous along the entire plate boundary zone. Except for Alarcon Basin, the widening strips of newly accreted crust are still entirely, or almost entirely, surrounded by shallower continental crust, and the upper "oceanic crust" in these enclosed sediment-trapping basins is quite different from the basaltic flows and dikes of most open-ocean spreading centers: it is a thicker sediment-sill complex of intruded magma and sediment, as discussed above in the introduction. Alarcon Basin has broad passages by which sediment entering the basin, e.g., in turbidity currents, can escape southwards to deeper oceanic

crust of the East Pacific Rise flanks (Figure 2; Lonsdale and Kluesner, 2010) and has developed a typical oceanic rise with eruptive fissural volcanism at its crest (Castillo et al., 2003). For those basins with a sediment-sill oceanic crust, the typical landform of the spreading center is a regenerating axial rift valley, or axial trough, that contains a mainly or in some cases (e.g., in Guaymas Basin) entirely intrusive neovolcanic zone in its 3-4 km-wide floor. These axial troughs contain turbidite ponds of reworked hemipelagic muds, and our MCS survey provided strong evidence that during glacial times of enhanced supply of terrigenous sediment several of these troughs were overfilled with turbidites, and almost obliterated as bathymetric features (Kluesner et al., submitted).

Multibeam bathymetry (Figure 1) shows that all five of the oceanic basins in the central and southern Gulf have volcanic seamounts, evidence of off-axis eruptions, that poke through the sediment cover of newly accreted crust (Figure 3). In Alarcon Basin these include chains of 1-1.5 km-high cratered tholeiitic seamounts with many smaller satellite cones, similar to those erupted at near-axis sites on the open-ocean East Pacific Rise (Castillo et al., 2003) Pescadero Basin has a 1 km-high off-axis volcanic ridge apparently formed by coalesced volcanoes, a similar volcanic ridge and many tiny (100-200 m-high) volcanic cones have been built outside the axial trough of Carmen basin, and in Guaymas Basin a larger volcano, again with several satellite cones, has grown above sea-level to form Isla Tortuga (Batiza, 1978). Only three small (2-4 km-diameter, 250-500 m-high) volcanoes rise above the thickly sedimented crust of

Farallon Basin (Figure 3). Many other volcanoes that are inferred from their uneroded morphology to have erupted subaqueously, and therefore since the 7-6 Ma marine incursion, have been mapped on the submerged continental crust that surrounds the oceanic basins; some of the larger examples are indicated on Figure 3. Eruptive volcanism persisted on large parts of the oceanic and continental floor of the central and southern Gulf even after most magmatic activity was concentrated at its spreading centers. Our MCS survey of sill intrusions strongly reinforces this conclusion.

3.4 GEOPHYSICAL DATA

In September 2006, ~2500 km of high-resolution MCS reflection profiles were collected throughout central and southern Gulf of California, with a few additional profiles further north across Guaymas and Carmen Basins (Figure 1). Our survey vessel was CICESE's *FRANCISCO DE ULLOA* firing a single small (45+105 cubic inches) G.I. gun. Using Scripps Institution of Oceanography's high-resolution 48-channel, 12.5 m-group spacing streamer we collected approximately 8-fold seismic reflection data. A shooting interval of 12 seconds was used while traveling at an average of 6 knots using a sampling interval of 1.00 ms. The average record length was 6 seconds Two-Way Travel Time (TWTT), and the estimated dominant frequency was approximately 80 Hz. Using a mean velocity of 1600 m/s (Einsele and Niemitz, 1982) at a depth of 2,000 m

results in a vertical resolution of approximately 5 m and a post-migrated horizontal resolution (Fresnel Zone radius) of approximately 100 m.

The second MCS dataset used in this study was collected in 1978 during the DSDP Leg 64 survey cruise across Guaymas Basin aboard the *R/V THOMAS WASHINGTON* (Figure 1). Multi-fold seismic reflection data was collected using an Exxon 24-channel research streamer with nonlinear hydrophone spacing (150 and 300 ft sections with "tapered" phone spacing) in combination with an array of 3 Bolt airguns (20, 120, and 40 cubic inches) firing every 15 seconds at an average ship speed of 6 kts. Sampling intervals were frequently switched between 1.5 and 2.0 ms, and the average record length was 6 seconds TWTT. After data collection, a number of preprocessing steps accomplished at Scripps in 1978 were necessary to get the data into a workable, industry standard format. During this step, shots/blank zones were created due to the loss of 16 shots (4 min) every 3 hours because of 7-track tape changing on-board the ship. This resulted in systematically spaced data "gaps" on the seismic sections. For this study, data was broken into different hydrophone spacing groups before initial processing and was concatenated back together before stacking and post-stack processing. Additionally, 3.5 kHz profiles were simultaneously collected with the MCS data and are presented in their original analog form.

During a research-dredging cruise (www.geoform2009.com) in October of 2009, 3.5 kHz profiles were collected during dredging transits throughout the

southern and central Gulf (Figures 1 and 10). In combination with dredge sampling, a dense 3.5 kHz survey was conducted west of Farallon Basin over previously identified sill intrusions and uplift mounds (Figure 1). 3.5 kHz profiles were displayed using Knudsen's Post-Survey software and gains were adjusted based on acquisition parameters and sediment type. All subbottom depths were calculated using a sonic velocity of 1500 m/s.

Data processing on both MCS data sets was preformed using Seismic Unix and SIOSEIS, and included bandpass filtering, dip filtering, semblance velocity analysis, predictive deconvolution, normal move-out correction, partial prestack migration (dip move-out), stacking, post-stack migration with a variable velocity model, water column muting, and time-varied gain. Post-processing software packages SMT Kingdom and IVS Fledermaus were used to aid in integration, interpretation, and visualization of MCS profiles, 3.5 kHz profiles, and multibeam bathymetry.

On MCS profiles an average velocity of 1600 m/s was used to convert TWTT to meters of sediment thickness. This number is based on physical property and acoustic loss tests conducted on core samples during DSDP drilling Leg 64 in Guaymas Basin (Shipboard Scientific Party, 1982; Einsele and Niemitz, 1982) in combination with calculated interval velocities from 2006 MCS data. A few sill thickness were calculated assuming a velocity of 5550 m/s; however, sill thicknesses are not fully constrained due to difficulty in clearly identifying the base of sills using seismic reflection imaging (there is a large amount of

attenuation at the top sediment-sill interface that limits the ability to clearly image the base of thick sills) (Skogly, 1998; Hansen and Cartwright, 2006). Estimating sill thickness is further complicated if the imaged sill is thinner than half the dominant wavelength, making the seismic responses from the top and base sill contacts indistinguishable from each other (Hansen et al., 2004). Hansen and Cartwright (2006) stated that it is possible to resolve the top and base of objects imaged through seismic reflection if the thickness is greater than or equal to half the wavelength. Using the 2006 Ulloa 48-channel streamer data, which shows a dominant frequency of 80 Hz, and using an estimated sill velocity of 5550 m/s at 2,000 m depth, the absolute minimum sill thickness that can be clearly imaged is approximately 18 m. Thick, high-amplitude reflections interpreted as magmatic sills could also represent a series of interconnected thin sills separated by thin, cooked sedimentary sequences, producing a high-amplitude, stacked reflection sequence, possibly causing an overestimate of sill thickness (Hansen et al., 2004). Furthermore, smaller impedance contrasts within the imaged intrusions could be products of 'incoherent noise' caused by ringing associated with imaging features of high acoustic impedance (Trude, 2004).

3.5 RESULTS

3.5.1 Seismic Characteristics of Magmatic Sills

Sills are easily identified in our MCS profiles as high-amplitude, positive-polarity reflection anomalies that end abruptly and both concordant and discordant with the surrounding reflectors (Figure 4). The high impedance contrast between igneous sills and host sediments is due to the considerable difference in acoustic properties, with sills having high compressional velocities and densities relative to the surrounding sediments, resulting in high amplitude reflections (Smallwood and Maresh, 2002; Hansen, 2006). Additional characteristics of sill intrusions that aid in interpreting seismic reflection data include cross-cutting internal reflections, associated overburden deformation structures, upturned edges, and a poorly illuminated “shadow zone” below (Figure 3; Planke et al., 2000; Thomson and Hutton, 2004; Hansen et al., 2006, Rocci et al., 2007). Additionally, high-amplitude reflections interpreted as sills show sharp increases in stacking velocities in semblance analysis plots, indicating a sharp increase in density and/or velocity. Furthermore, Sheriff (1975) showed that concave-upwards reflections can act as a curved mirror by focusing seismic energy, further increasing the amplitude of interpreted bowl-shaped igneous intrusions.

While shallow sills are identifiable as amplitude anomalies on seismic reflection images, reflections directly below thick, shallow sills are poorly illuminated due to the large attenuation of energy caused by the high reflection coefficients of igneous rocks. This results in a loss of higher frequencies and a sudden reduction of vertical and horizontal resolution below the sills, limiting the

ability to clearly illuminate and discern sub-sill structures and lithological units (Smallwood and Maresh, 2002). This low-amplitude region below thick intrusions can be referred to as a “shadow zone” (Figure 4). Despite this limitation, a few of our high-resolution MCS profiles imaged steeply inclined, cross-cutting, high-amplitude reflectors just off to the side and below of a few saucer-shaped intrusions with some leading up to the bottom of identified sills (Figures 4 and 5). These features differ from seismic artifacts and sideswipes since they do not resemble the easily identifiable diffractions caused by seismic migration processing and are only found neighboring areas of intrusions, with no nearby out-of-plan point reflections that would produce steeply inclined, cross-cutting sideswipes (Lee et al., 2006). Furthermore, diffraction “smiles” caused by over-migration are generally lower in amplitude and are much less continuous than genuine reflections (Hansen et al., 2004). Detailed velocity analysis was preformed (every 50-100 common-depth-points) in order to accurately correct for normal move-out, reduce migration artifacts, and to produce the best possible image of the upturned sill edges and host-rock deformations. Through analysis of multibeam, 3.5 kHz mapped elliptical mounds, and underlying high-amplitude reflectors identified as concave-upwards sills, I deduce that multiple sills have a 3D saucer-like geometry. In summary, sills identified from the 2D seismic profiles as 3D saucer-shaped intrusions is based on (1) their concave-upward profiles, (2) the overlying circular and elliptical plans of domal uplifts on the present multibeam-mapped seafloor and a dense 3.5 kHz survey, (3) their striking

resemblance to doleritic saucer-shaped sills imaged with 3D seismic reflection along the North Atlantic Margins, the Norwegian Sea, and other rifted margins (Cartwright and Huuse, 2005; Hansen and Cartwright 2006), and (4) similarities with field-mapped saucer-shaped dolerite sills in western Karoo, South Africa (Chevallier and Woodford, 1999; Polteau et al., 2008).

3.5.2 Magmatic Sills and Deformation

Subject to the supply of magmatism and sediment load, magma will either inject into the sediments or extrude onto the seafloor. As a general trend of axial magmatism northward along the Gulf, magma is extruded at a spreading ridge in Alarcon Basin located in the mouth of the Gulf, emplaced below the axial trough floor in South Pescadero Basin, Farallon Basin, and Guaymas Basin, and deeply intruded in the northern Basins, which are flooded with Colorado River sediments. Two exceptions to this northerly trend of deeper sill emplacement is the axial troughs of North Pescadero and Carmen Basins, where extrusive magmatism has been sampled and mapped as local bathymetric highs and patches of high reflectivity, indicating a steep surface or hard rock. MCS profile C across Carmen Basin shows that the axial floor is composed of very shallow sills, possible flows, and pillow lavas (Figure 6), the later was recently sampled (2008) using the *ROV JASON* onboard the *R/V Atlantis*. Due to the diversion of clastic-rich turbidites away from the uplifted transform boundaries, magma is able to rise up through the relatively thin sedimentary cover, extruding onto the seafloor in

the form of pillow lavas (Kluesner et al., submitted). Imaged shallow sills below the rift shoulders of Carmen axis display complex structures, most of which appear to crosscut each other and lack the broad continuous individual reflections characteristic of off-axis sill intrusions. Additionally, this shallow, chaotic sediment-sill complex can be seen kilometers away from Carmen axis, below the floors of Carmen Basin and North Pescadero Basin, and on MCS profiles near sampled off-axis seamounts as seen in western Farallon Basin (Figures 5 and 7). One explanation for shallow chaotic sill structure with little deformation of the overburden, as proposed by Einsele (1982), is that smaller shallow intrusions are able to rapidly expel the surrounding pore-waters away and through the seafloor fast enough to prevent deformation of the overburden.

Unlike Carmen Basin, MCS profiles and mutlibeam bathymetry across Farallon and Guaymas Basins show that large amounts of sediment flood the axial troughs and off-axis flanks (especially the southwest flank), affecting the depth and structure of intrusive magmatism. The sediment input is mainly riverine runoff from the Rio Yaqui, Rio Mayo, and Rio Fuerte, as well as pelagic rain from the highly productive surface waters (Figure 2; Van Andel, 1964; Lonsdale, 1989). Multiple off-axis intrusions over oceanic crust form concave-up reflections on MCS profiles that cross-cut stratigraphy and commonly uplift the overlying sedimentary section. MCS profile E (Figure 8) along the western flank of Farallon Basin displays an approximately 1.3 km wide stack of high-amplitude reflectors (Sill O), which is exceptionally thick (> 400 m), probably representing an

interconnected network of sills and beds of indurated sediments that developed through successive intrusive events (Figure 8; Hansen et al., 2004; Menand, 2007). A large mound-shaped feature immediately above Sill O appears to be uplifted, showing a maximum offset of 45 m, gradually widening up-section. It is possible to clearly trace sedimentary reflectors across the mound-like feature, supporting the interpretation of Hansen and Cartwright (2006, 2007) that dome-like structures above magmatic sills are commonly sedimentary displacement mounds and not small volcanic centers, as was previously suggested by Thomson (2005). In contrast to Hansen and Cartwright (2006), Thomson (2007) argued that three criteria must be met in order to confirm that the mound-like structures are indeed sedimentary-forced folds as opposed to volcanic centers; (I) clear evidence of folding sediments, (II) no thickening across the mound structure, and (III) no evidence for syn-intrusive eruptions, such as lava flows. Above Sill O the seismic record displays traceable folded reflectors, no major thickening across the mound, and no evidence for syn-intrusive eruptions (there is a lack of very high-amplitude reflections on sides of the mound). Although MCS profile E only provides a two-dimensional image of Sill O and associated overburden deformation, the mound is interpreted as a sedimentary forced fold above a complex saucer-shaped sill. There is also clear evidence of faulting above the sill complex and decrease in sedimentary reflector amplitudes directly above Sill O, indicating sediment alteration (Figure 8). The disagreement between Thompson (2005, 2007) and Hansen and Cartwright (2006b, 2007) was

most likely due to the low resolution of the seismic data and absence of clear internal reflections. As the high-resolution (~4.4 times the resolution of the 3D volume in the North Atlantic; Hansen and Cartwright, 2006b) profile E shows (Figure 8), the mound-like feature directly above Sill O is clearly a sedimentary forced fold structure.

Assuming uplift mounds were displaced during sill emplacement, younger sediments onlapping the uplift allow us to identify the paleo-seabed at the time of intrusion (Figure 8). Acting as a local bathymetric high, uplift mounds disrupt turbidite deposition patterns, creating onlap of the youngest sediments; thus, onlapped mound structures above saucer-shaped sill intrusions can be assigned a relative age to surrounding intrusions and structures. With tightly constrained sedimentation rates and sources, it would be possible to date sill intrusions and associated uplift features. Trude et al. (2003) proposed such dating techniques and showed that it was possible to date sill intrusions if the first onlapped sedimentary reflection could be tied to a nearby biostratigraphic horizon identified from borehole data, thereby providing a precise age of intrusion and uplift. Lack of drilling and biostratigraphically-dated horizons in the vicinity of mapped saucer-shaped sills prevents us from making such an accurate correlation in this study.

Other nearby uplifts above saucer-shaped intrusions (over oceanic crust in west Farallon Basin) show chaotic internal reflections, producing a seismically “blank” section directly above the sill, limiting our ability to trace reflectors across the mound (Figure 9). As discussed later in this chapter, the chaotic zones

directly overlying the sills are probably caused by rapid expulsions of super-heated pore fluids, leading to fluidization of sediments and forming zones of highly disrupted, fractured, mixed rock strata (Bell and Butcher, 2002). Trapped gas in the sedimentary section could also account for low internal reflector amplitudes. High concentrations of gas in sediments can cause acoustic blanking and the attenuation of seismic energy, inhibiting or dampening the impendence response of reflections below and commonly producing acoustically turbid responses (Judd and Hovland, 2007; Løseth et al., 2008). Additionally, drilling results from DSDP Leg 64 revealed that turbidites directly above and below magmatic intrusions were severally indurated/altered and included remobilization of silica, formation of dolomite, and recrystalization of clay minerals, all of which would affect the impedance contrast of existing host strata (Einsele, et al., 1980).

Young, saucer-shaped intrusions also intrude into the blanketed sediments covering extended continental crust. Figure 10 (Profile G) shows a large, ~2 km wide, > 280 m thick, sill (Sill E) with sharply upturned tips buried beneath approximately 340 m of sediment. Sill E is located southwest of Farallon Transform near a major Western Farallon basin boundary fault scarp (Figure 1), and is emplaced in young sediments blanketing extended continental crust. The base of the sill is somewhat flat, with a small peak near its center separating two distinct bowl-shaped depressions. This could represent the junction of two smaller, saucer-like intrusions, since two distinct folded uplifts are visible directly above the features, broadening up-section and merging together into one large

dome-like mound. The sill edges are relatively thin and sharply upturned, clearly cross-cutting stratal reflections and terminating just above (~80 m) the sill base. The uplift has been mapped with multibeam bathymetry and is approximately circular in shape, measuring ~2 km in diameter and appearing as a local bathymetric high (Figure 11). Additionally, a dense 3.5 kHz survey over the multibeam-mapped mounds conducted in 2009 revealed a cluster of uplift mounds above probable sill intrusions (Figures 11 and 12). The 3.5 kHz profiles (Figure 12) show clear evidence of sediment deformation above large concave-upwards sill imaged on MCS Profile G (Figure 10). Furthermore, elliptical-to-circular bathymetric features can be seen over many of the buried uplift mounds imaged on the 3.5 kHz and MCS profile G and the approximate location and diameter is shown on Figure 11. The enclosed contour feature nearest Farallon Transform appears as an out-of-plane sill reflection on the nearby MCS profile. On the 3.5 kHz profiles a high-amplitude reflection (Horizon A) can be traced around the imaged mounds and correlates to the time of sill emplacement and deformation for all imaged uplift mounds in the region (Figure 11). Sediments younger than Horizon A onlap the uplifted mounds with different deposition patterns observed on the northwest and southeast sides of the mounds (Figure 12). Southeast of the mounds sediments gently onlap, while on the northwest side sediments dive down towards the base of the mound. This depositional pattern may be a result of strong current flow on the northwest side of the mound, preventing deposition against the side of the mound. The youngest sedimentary

layers onlap the mounds on both sides and appear not to have been affected by current flow, a recent change on current patterns and/or strength. Similar erosional scours are found at the base of multiple fault scarps and seamounts in western Farallon Basin and further south (Figure 2).

On MCS Profile A we have imaged an additional sill-sediment complex overlying extended continental crust northeast of the Farallon transform, at the southern margin of Carmen Basin (Figure 4). Convex upwards Sill K is approximately 1.2 km wide and at least 90 m thick, displaying a broad bowl shape with gently upturned edges, flattening out and terminating into the seabed parallel strata (Figure 4). Directly above the sill, a large uplift mound displays a seismically blank internal structure (Figure 4) and is onlapped by channeled turbidite sediments from the Rio Fuerte (Figure 2). Southwest of Sill K is a shallower sill complex and a large, deeper intrusion (Sill L) that has a large uplift mound directly above it. The width of the mound probably reflects the approximate width of the deeper sill; yet, the northeast side of the sill is shadowed by the overlying, younger sills that attenuate seismic energy, preventing the seismic system from clearly imaging impedance contrasts below. Tracing onlapping reflectors indicates that both Sills K and L were emplaced during the same episode of intrusive magmatism.

Using a submersible, Lonsdale and Lawver, (1980) described mound-like features in Guaymas Basin, where they observed large, intrarift hills in the northern and southern troughs with no resolvable internal structure, faulted and

folded sides, and turbidites perched on the small flat summits. They concluded that the mounds were created by thick intrusions into soft sediments and that the features were folded uplifts of the axial floor sediments. Multi-channel seismic reflection profiles collected during DSDP Leg 64 survey cruise across the northern trough of Guaymas Basin imaged one of the described mounds and similarly displayed a blank internal structure (Figure 13). Directly below the seismically blank zone inside the mound, there is a large, high-amplitude, concave-upwards reflection approximately the width of the sediment mound (Figure 13). This high-amplitude feature, although in low-resolution due to poor data quality, looks very similar to other saucer-shaped sills and associated uplifts described in this study, suggesting this mound may have been uplifted by a saucer-shaped sill intrusion. 3.5 kHz sub-bottom profiles collected simultaneously with MCS data show the mound feature and younger on-lapping sediments on the sides. Penetration of the 3.5 kHz sonar through the mound is limited, probably due to the presence of gas, carbonate cementation, cooking of sediments, and hydrothermal deposits, all of which could cause the mounds to rapidly attenuate the 3.5 kHz energy and appear as highly reflective features on multibeam-derived backscatter plots. Very similar acoustic response can be seen on the dense 3.5 kHz survey over uplift mounds and sills west of Farallon Transform, intruded over extended continental crust (Figure 12).

Widespread geophysical evidence of young sill intrusion through both off-axis oceanic crust and extended continental crust suggests that melt delivery is

not confined to the axial troughs and off-axis basins. These young intrusions are evident on multiple high-resolution MCS profiles collected across oceanic basin floors (Figures 5, 14, 15, and 16) extended continental crust (Figure 10) and near transform boundaries (Figure 4), suggesting that melt in the central Gulf of California is able to intrude upwards through both highly faulted and thinned continental crust and off-axis oceanic crust, injecting into overlying young, unconsolidated sediments. As described earlier, attenuation of seismic energy at the sediment-sill interface results in an acoustic shadow zone below. Identification of the boundary zone between continental and oceanic crust in the central Gulf of California using seismic reflection profiling is not trivial due to the lack of clear, sharp structural evidence of the continental-oceanic crustal transition.

Multiple crossings of the continental-oceanic boundary were made at the western flank of Farallon Basin with the high-resolution MCS (Figure 1). Multibeam bathymetry shows major continental crust fault scarps bounding the western part of the basin, with the seafloor gently sloping towards the axial trough until about 2,000 m depth (see 2,000 m contour, Figure 1). MCS Profile M collected near the Farallon Transform reveals faulted, back-tilted crust, interpreted as continental crust, stepping down from the major bounding fault scarp (Figure 14). The back-tilted crust has subsequently been blanketed by a thick section of turbidites that have filled in and covered the highly faulted basement, resulting in a relatively smooth basin floor. Located above the faulted

and back-tilted basement and sediments are a few high-amplitude, abruptly ending reflections interpreted as magmatic sills.

Profile N (Figure 15) located west of Profile M transects the center of western Farallon Basin and displays similar basin structure except that high-amplitude reflections interpreted as sills are more extensive and the lower section of the sediment cover is acoustically dim. Low-amplitudes are most likely due to gas concentrations within the sediments. As discussed later on in this chapter, the gas is probably a product of extensive sill intrusion into the carbon-rich sediments. During intrusion and gas generation, the gas most likely migrates upslope, concentrating in sediments below a trapping horizon. The combination of relatively shallow magmatic sills and gas-rich sediments massively attenuates the seismic energy, acoustically masking the basement structure below. This same pattern (magmatic sills above basement and gas-rich sediments) can also be seen on Profile O (Figure 16) located west of Profiles M and N (Figure 1). On Profiles N and O (Figures 15 and 16) just past the break in slope on the seafloor, the emplacement depth of magmatic sills rapidly shoals towards the seafloor and sill structure is much more complex, forming a dense and extensive shallow sill horizon. The grayed bars and black zig-zag lines on Figures 14, 15 and 16 represent our best interpretation of the continental-oceanic boundary and zone of uncertainty. This zone of uncertainty is due to the presence of extensive, intrusive magmatism over rifted continental crust and/or oceanic crust, as shown on Figures 14, 15, and 16. Off axis intrusions, if large enough, may also

complicate or mask the magnetic signal from the crust below if the younger intrusions were emplaced during a time with different polarity. Recently, Rocchi et al. (2007) showed this effect offshore of Senegal, where Miocene saucer-shaped sills were mapped via integration of seismic, magnetic, and gravity profiles. Despite these complications, Figure 3, best represents the continental-oceanic boundary in western Farallon Basin. Much of the structural interpretations on Figure 3 are based on previous studies made by P. Lonsdale primarily using multibeam bathymetry and magnetic profiling (Lonsdale and Kluesner, 2010). Piñero (2008) also interpreted the continental-oceanic boundary across western Farallon Basin using the 2006 MCS dataset, however these profiles were processed using different techniques, yielding clear differences in acoustic basement structure.

3.5.3 Sills Feeding Sills?

Inclined features imaged below saucer-shaped sills probably represent highly transgressive margins of older sills acting as feeder conduits for the overlying younger sills, which are intruding into the porous, young host sediments (Figures 4 and 5). The sub-vertical, high-amplitude reflections cut up through stratigraphy, terminating near the base of younger shallow sills forming a “stair-step” growth pattern. Presumably, younger sills tend to intrude above older sills because the magma can intrude into soft, young sediments more easily than sediments that have been cooked, compacted, and indurated by older intrusions

(Einsele, et al., 1980). Assuming deeper older sills feed younger overlying sills, seismically mapped structures within the sill complexes can provide insight into flow direction and branching patterns away from the magma source (Thomson, 2007; Thomson and Hutton, 2004; Hansen et al., 2004). Because current seismic reflection techniques are unsuited for imaging near-vertical features, dikes are not imaged below the sills (Hansen et al., 2004). Near-vertical dikes, which vertically transport magma, feed the majority of sills, thus one can assume that there are as many feeder dikes as sills in the region, although some of the feeder dikes may simply be inclined wings of older sills with inclined tips.

3.5.4 Buried Lava Flows?

In addition to high-amplitude reflections interpreted as sills, a few MCS profiles image extensive, concordant high-amplitude reflections that are interpreted as lava flows. MCS Profile B that crosses near West Farallon Seamount (Figures 5 and 6) imaged a shallow, laterally extensive high-amplitude reflection that exhibits minimal-to-no overburden deformation. Unlike the smooth reflection of identified sill intrusions, the feature has a jagged upper reflection and is concordant with sedimentary reflections imaged directly below. Since lava flows only deform sediments below, sediments deposited after eruption would drape the flows, producing a concordant sedimentary sequence above that shows no magmatism-related deformation. Due to its nearby proximity, this flow is likely derived from Western Farrallon Seamount. It also appears that the flow is

younger than nearby Sill H, since it onlaps, or terminates, against Sill H's associated deformation mound (Figure 5). Additionally, a profile across the east flank of North Pescadero Basin reveals a large crater and semi-layered high-amplitude reflections interpreted as lava flows that are onlaped by sediments that have most likely been truncated due to current erosion (Figure 17). ROV samples collected in the crater and around the crater rim were all basaltic flows (where reflections identified as flows on Figure 17 appear to outcrop), supporting our interpretation of nearby subbottom reflections.

3.5.5 Sill Geometry and Emplacement Depth

Various authors have hypothesized that formation of saucer-shaped sill geometry is controlled by magma pressure, viscosity, flexural response of the overburden, and emplacement depth (Galland et al., 2006; Menand, 2007; Goulty and Schofield, 2008; Mathieu et al., 2008). Additionally, recent modeling studies have suggested that anisotropic stress fields form around sill tips during emplacement due to overburden uplift, and that emplacement depth and sill length control the geometry of sills (Malthe-Sorenssen et al., 2004). When a sill's length surpasses its emplacement depth, its shape and the stress field caused by the overburden become asymmetrical. As a result, the edges of the sill branch upwards, relieving the pressure inside the sill as it propagates above the depth of neutral buoyancy. This logic suggests that if a sill intrudes too shallow or too deep, then it will not take on the saucer-shaped geometry. If the sill is emplaced

too shallow, then it will not produce the proper long-range stress fields, whereas if the intrusion is too deep, then the sills are typically not long enough to start curving upwards. This is sill width-to-depth relationship is observed in this study: very shallow sills do not take on the broad saucer-shape, but appear as smaller, complex structures (Figure 7), whereas deep sills are much broader, commonly exhibiting inclined transgressive tips (Figure 10).

All imaged concave-upwards sills have been mapped and their locations, widths, and emplacement depths are plotted on Figure 18. Widths on Figure 18 represent minimum values, as the MCS profile could have crossed any part of each sill (minus known central crossing of Sill E). For example, if the typically 3D geometry of each sill were circular or elliptical, as is assumed in this study, a MCS profile crossing the edge of a large sill would reveal a much smaller sill. This might also account for why multiple concave-upwards sills show a broad bowl shape with no flat inner sill. If the MCS profile crossed the edge of a sill it would image the upward turned sill edged, appearing as a continuous concave-upwards sill. Additionally, the high-resolution of the MCS profiles allows easy identification of onlap onto deformation mounds (paleosurface) and thus, the emplacement depth for each sill (Figures 4, 5, 8, 9, and 10). Sill thicknesses are not included in Figure 18 due to the large attenuation of seismic energy at the top sediment sill interface, resulting in an inability to accurately image the base of most sills.

Plotting imaged sill widths against emplacement depths (Figure 18) reveals a general linear relationship, which agrees with previous field studies (Polteau et al., 2008), modeling results (Malthe-Sørenssen et al., 2004), and experimental results (Galland et al., 2007). In addition to the general linear trend on Figure 18, two sets of points have been identified that can be separated by slope and geographical location; one set includes concave upwards sills located in North Pescadero and western Farallon Basins ($R^2 = 0.75321$), and the other includes sills from Guaymas Basin and east of Farallon Transform near the Fuerte Delta ($R^2 = 0.8778$). Currently, North Pescadero and Western Farallon Basins have very limited terrrigenous input, whereas Guaymas Basin is flooded with terrigenous turbidites (especially during glacial periods) (Kluesner et al., submitted), and sills east of Farallon Transform were emplaced into a fan of turigenous turbidites overlying continental crust. These geographical clusters of sill width vs. emplacement depth suggest that sediment type may play an important role in determining the depth at which magma reaches neutral buoyancy and begins to spread laterally, eventually deforming the overburden and resulting in upturned sill edges. Alternatively, the depth of concave-upwards sills could be influenced by the ratio of magma supply to sedimentation rate. Sedimentation is much faster in basins along the upper trend-line ($R^2 = 0.8778$) compared to basins along the lower trend-line ($R^2 = 0.75321$), possibly indicating a simple sediment loading to sill depth relationship. Thick, stacked sill complexes found in western Farallon Basin fall along the upper trend-line (red circles, Figure

18) indicating that thick, stacked sills, likely interbedded with sediments, do not deform the overburden as easily as other sills imaged across western Farallon Basin. Additionally, the large concave-upwards reflection imaged below the Great Northern Hill in the Northern Trough, Guaymas Basin is very large (> 2.7 km wide), elongated, shallow, and was excluded from Figure 18. This is primarily due to the different conditions in which Sill U was intruded compared to other sills mapped below basin floors and over continental crust, including (i) concentrated tension and extensive normal faulting along the spreading axis, (ii) intense focused magmatism along an elongated central point, (iii) sediment composition of very low-density hemipelagic turbidites with very thin sandy beds (Kluesner et al., submitted), and (iv) increased hydrothermal activity within the spreading axis and extensive fluid-flow along extensional faults. Combination of these factors appears to produce complex magmatism within the axis composed of widespread diking, plug-like intrusions, and large, elongated sills with upturned wings that produce uplifted deformation mounds that have been mapped with multibeam bathymetry (Figures 13 and 19) and seismic reflection profiles (Figures 13 and 20).

Displacements and compressive stresses above Sill E (Figure 10) were modeled using the modeling program Poly3D (Thomas, 1993), which is based on the governing equations of linear elasticity. Sill E was used as the example sill because of good multibeam (Figure 11), 3.5 kHz (Figure 12), and MCS coverage (Figure 10) that enabled the calculation of approximate sill diameter, minimum

thickness, and emplacement depth. Using the 3D boundary element-based numerical modeling program, the object of interest (e.g., a sill) is made up of a group of polygons (called "elements") that are each able to undergo some form of displacement, whether opening or sliding. They are essentially "dislocations". Numerous elements are used to construct an object so that certain parts of a feature open or slide more than others (this is necessary because sills and dikes open more at their centers than at their edges, and faults slip more near their centers than their tip-lines). The model was run assuming a Poisson's ratio of 0.33 and a Young's modulus of 10 GPa (approximating sea floor sediments). It is a half-space model (i.e., the sea floor was treated as a free surface-- no water pressure was included in the model). The modeled sill (Sill E) is approximately 2 km wide and is emplaced at a burial depth of about 340 m below the sea floor (Figure 21A). Using observational planes, the model shows the full dilatational thickness of the sill (280 m, Figure 21B) and the associated displacements (at the sea floor, Figure 21C) and stresses around the sill. Maximum displacement occurs approximately 230 m above the center of the sill (Figure 22D). Using a sonic velocity of 1600 m/s and establishing a datum across the sill imaged on MCS profile G (Figure 10), uplift over the sill is ~ 70 m. This suggests that either significant room is made for the sill during initial sill emplacement through pore-fluid expulsion as suggested by Einsele et al. (1980), or there has been substantial compaction of sediments above the sill. Another possibility is that Sill E is composed of interbedded sills and cooked sediments, resulting in much less

overburden displacement. The distribution of compressive stress (S3) magnitude on a vertical observation plane across the center of the sill shows zones of tension (warm colors) above the tips of the sill and zones of compression (cool colors) at the seabed above the tips and directly above the sill (Figure 22E). Distribution of maximum compressive stress (S3) magnitude at the seabed shows zones of tension (warm colors) above the center of the sill and a ring of compression at the surface above the sill tip zone (cool colors, Figure 22E). Distribution of maximum tensile stress (S1) magnitude on the seabed above the sill shows a zone of tension (warm colors) above the center of the sill (Figure 22F).

In reality, stresses will never actually attain the values that result from the model because the strength of the material (whether tensile strength or compressive strength) will dictate how big the stresses can realistically get in the intruded materials. Fracturing (either tensile cracking or shear fracturing) or inelastic processes (ductile deformation near the sill margins) during progressive sill opening will eventually reduce the stresses. This is a necessary outcome of elastic models, which predict stress singularities (i.e., infinite stress) along crack tips. An underlying assumption of elastic models is that this is not physically possible in reality and that deformation reduces these stresses to manageable levels by cracking of the material.

The 3D modeling results (Figures 21 and 22) in combination with observed sill width verses emplacement depths (Figure 18) suggests that sill geometry in

the Gulf of California is largely controlled by emplacement depth and displacement and deformation of the overburden. Initially, magma rises to a level of neutral buoyancy through diking or inclined tips of sills (Figure 23A) and begins to inject laterally into the host strata, cooking surrounding sediments and forming a contact aureole (Figure 23B). As the sill grows a chilled margin forms around the sill and the sill thickens near its center or feeding point (Figure 23C). At first, the sill drives off pore-fluids from the water-rich sediments, making room as it intrudes, resulting in minimal displacement of the overburden and a relatively symmetrical stress field (Figure 23B). If the sill continues to grow (i.e. there is enough magma pressure) the chilled sill margin will thicken, hindering further heating and pore-fluid expulsion of the surrounding sediments (Figure 23C). Since the sill can no longer successfully make room for itself via pore-fluid expulsion, it will begin to displace sediments in the direction of least resistance, resulting in uplift of the overburden and the development of an asymmetrical stress field (Figure 23C). As modeling results demonstrate, once this asymmetrical stress field is established, zones of tension form above and slightly off to the side of the sill tips (Figure 22E). At this point, intruding magma takes the path of least resistance, preferentially intruding upwards into the zones of tension rather than continuing to intrude laterally (Figure 23C). Magma will continue to intrude upwards until capped by zones of compression overlying the zones of tension (Figure 22E) at which point it will take the path of least resistance and began to spread laterally into the host strata (Figure 23D). Spreading will

continue until the new concordant sill thickens to a point at which it displaces the overburden, starting the cycle again (Figure 23E). If magma pressure stops then the sill complex is subsequently buried by young sediments, which onlap the local bathymetric high (Figure 23F). This pattern of sill intrusion creates a “stair-step” structure in which younger sills are fed by and intrude above older sills. Since shallower sills have less overburden pressure relative to deeper, older sills, they begin to displace the overburden at a smaller width and thickness, as is observed in this study (Figure 18). As sill emplacement depth approaches the seabed, the stress field becomes easily deformed at very short widths and thin thicknesses, resulting in a complex sill-sediment structure composed of cross-cutting, winged sills and intensely deformed overburden (Figure 7).

In addition to revealing sill geometry, multiple MCS profiles collected across the axial troughs and basin floors of the central Gulf of California reveal broad asymmetry in acoustic basement structure. Profile P (Figure 24) across Farallon axial trough reveals the structure of the axial rift and rift shoulders. One striking pattern is the depth of the sill horizon below the rift shoulders (Figure 24). On the northwest side of the axis sills have been emplaced within approximately a hundred meters of the seafloor, whereas below the southeast rift shoulder sills are buried beneath hundreds of meters of sediment. Looking at multibeam bathymetry (Figure 1) Farallon Basin looks fairly symmetrical; however MCS profile P shows that sub-seafloor structure is highly asymmetrical. This same pattern can be seen across the northern trough of Guaymas Basin, suggesting

that emplacement depth asymmetry on the basin flanks is caused by differences in sediment supply/loading. An imbalance in sediment supply to the basin floors would result in differences of lithostatic stress and subsequently differences in the depth of sill emplacement. This suggests that sills on the northwestern side of Farallon Basin rise to a much higher depth before reaching neutral buoyancy, whereas sills on the southeastern side emplace at a much deeper depth due to the thick overlying pile of sediment. Furthermore, as discussed in Chapter 2, these sediment pathways have changed through time because of relief-creating tectonic events such as changes in the relative plate motion, and steady, systematic changes like the migration of spreading-center/transform intersections along shearing continental margins.

3.5.6 Sill-Driven Hydrothermal Fluid-Flow

A major conclusion from sites 477, 478, and 481 drilled in Guaymas Basin during DSDP Leg 64 (Figure 1) was that there were 2 separate hydrothermal systems present in the spreading axis, a shallow short-lived one caused by dewatering after sill intrusion, and a much more important deep-seated one, caused (as at typical EPR risecrests) by emplacement and cooling of axial plutons, with that system being capped in part by shallow sills (Kastner, 1982). This study focuses on the first system that is driven by shallow magmatic intrusion and although the shallow intrusions don't account for significant hydrothermal activity in the axial troughs (and act as cap rocks, forcing horizontal

flow away from the sill), they appear to play a more significant role in off-axis hydrothermal fluid-flow.

Most large sill intrusions imaged in this study have an acoustically quiet and/or chaotic zone directly above the sill top (Figures 4, 5, 9, 10, and 13). Drilling results from DSDP Leg 64 in Guaymas Basin (Sites 477, 478, 481; Figure 1) showed that magmatic sills are directly overlain by indurated, homogenized sediment, implying significant expulsion and up-streaming of heated pore waters, which disrupt bedded turbidites and pelagic sediments (Einsele et al., 1980). Bell and Butcher, (2002) suggested that the uppermost and lowermost portions of sills and adjacent sediments imaged in the North Faroe-Shetland Basin most likely have reduced sonic velocities due to the presence of gas cavities and fractures formed during crystallization and cooling. Even in low concentrations gas can cause a large attenuation of seismic energy and a rapid reduction in seismic wave velocity, seen as low stacking velocities in semblance analysis and low amplitudes on seismic images (Shankar et al., 2006; Chand et al., 2008). In this study, stacking velocities picked within the blanking zones are low in velocity, suggesting the presence of gas. However, as mentioned above, drilling results from DSDP Leg 64 showed that sediments surrounding the sills were greatly indurated, which increases the density and sonic velocity of the host rock. Thus, low stacking velocities and low amplitudes recorded above sills in this study are most likely a product of homogenized sediments and the presence of gas, both of which cause low impedance contrasts, with gas reducing the sonic velocity

(Figures 5, 9 and 13). This alteration is most likely caused by rapid pore fluid expulsion during sill emplacement, resulting in fluidization of sediments within the contact aureole and the formation of a lithologically homogeneous zone above the sill that on MCS profiles appears chaotic and seismically transparent on MCS profiles (Figure 9).

Pathways for fluid and gas expulsion, such as 'pipes' or 'chimneys,' are evident on conventional 2D seismic reflection profiles as seismically blank or chaotic near-vertical zones that cut through surrounding stratigraphy, most of which extend up to or near the seafloor (Heggland 1998; Chand et al., 2008). Recent 3D seismic reflection studies in areas of concentrated fluid-flow (Parnell and Schwab, 2003; Cartwright and Huuse, 2005) have interpreted these structures as cylindrical ‘pipes’,typically circular to sub-circular in planform, in which the continuity of reflections is disrupted, with some 'pipes' reaching vertical extents greater than 1 km (Løseth et al., 2001). Similar features imaged in this study are visible branching and migrating upwards, away from sills and through associated uplift mounds. MCS profile H (Figures 13 and 25), collected across the basin floor west of the Northern Trough, Guaymas Basin, revealed near-vertical zones of seismic disturbance that extend from the seabed down to high-amplitude reflections interpreted as sills. A 3.5 kHz profile collected simultaneously with MCS profile H reveals that the vertical zones of disturbance imaged on MCS profile H line up with pockmarks on the seabed and underlying vertical acoustically blank zones (Figure 25). Both lithology and entrained fluids

affect seismic response, so these sub-vertical zones of disrupted reflectors may be conduits for expulsion of gas and hydrothermal fluids away from the heated sill-sediment interface (Figure 26D; Parnell and Schwab, 2003). The cross-cutting pattern of the sub-vertical pipes indicates that fluid and steam pressure generated by sill heating is able to overcome the tensile strength and lithostatic load of the overlying sediments, essentially “blasting” through the overburden via fluid channeling and matrix deformation (Figure 26D), forming pockmarks (Figure 20) and hydrothermal mounds on the seafloor (Jamtveit et al., 2004; Hansen, 2006). For these hydrothermal systems to be sustained, fluid recharge must occur around the sill until it has cooled (Figure 26D). However, the near-vertical ‘pipes’ most likely act as fluid conduits long after sill cooling. As the ‘pipe’ and underlying sill get rafted away from the spreading axis and subsequently buried with turbidites, compaction of the carbon-rich sediments will promote biogenic methane production and dewatering of sediments. In this scenario, the “pipes” likely act as fluid conduits long after sill cooling. Recently, a high resolution side-scan and seafloor imagery survey across Northern Guaymas Basin (Lizarralde et al., 2010) discovered that concentrated zones of precipitates and biological activity (clams, tubeworms, and bacterial mats) occur on the seafloor above several seismically imaged pipes, including those imaged on profile H (Figure 25). Lizarralde et al. (2010) concluded that water samples rich in thermogenic methane (3 to 6,800 times the background measurement) collected above the highly reflective patches of seafloor indicate that chemosynthetic communities

are supported by young off-axis sill intrusion into carbon-rich sediments. This study suggests that the 'plumbing' of these off-axis chemosynthetic communities is probably composed of near-vertical cylindrical 'pipes' that formed through hydrofracturing and fluidization of sediments, many of which extend down hundreds of meters, terminating directly above large, abruptly ending reflections interpreted as off-axis sill intrusions.

In areas of extensive faulting, such as the axial troughs located at spreading centers, heated fluids and gases preferentially migrate along these zones of least resistance (Figure 27), rather than form pipe-like blowout structures imaged off-axis below the basin floor (Einsele, 1980; Planke et al., 2005). Lonsdale et al. (1980) discovered and sampled extensive terraces and ledges of high-temperature (~280° C) hydrothermal deposits along the NW fault scarp in the Northern Trough of Guaymas Basin and on uplifted sediment mounds on the axial floor (Figure 19). They concluded that hydrothermal deposits form along extensional normal faults, where heated fluids channel and migrate along fault planes (Figure 27B), precipitating out onto the seafloor as the heated fluids mix with cold bottom water. Drilling results confirmed (Kastner, 1982) that vertical discharge hydrothermal fluids from intrusion of axial magma chambers occur through faults until they encountered sills, at which fluids flow horizontally until reaching a fault or other sub-vertical pathway towards the seafloor. Fluid-flow structures imaged in multiple smaller basins along the southwest margin of the Gulf suggest that pore-fluid venting is widespread over crust not intruded with

young sills, indicating fluid-flow driven by sediment compaction and decay of carbon-rich sediments or by a deeper heating source. Profile M across the Southern Trough, Guaymas Basin reveals extensive faulting along the trough walls and extensive evidence of fluid-flow and channeling along fault planes (Figure 27). Multiple reflections cut by faults on Profile M (Figure 27) show increased amplitudes near the fault trace, indicating concentrations of gas or alteration of sediments. Evidence for fluid-flow along fault planes and formation of fluid-flow 'pipes' can be found in smaller continental rifted basins in the southwest portion of the Gulf of California (Figure 28) and is not limited to the larger, intensively magmatic oceanic basins.

High amplitudes associated with multiple imaged sub-vertical seismic pipes are probably a result of trapped gas, hydrothermal deposits, and/or carbonate cementation within the conduits (Figures 25 and 26A). Multiple studies have identified and shown that fluid conduits similar in shape, structure, and size have internal compositions ranging from reworked sedimentary material (Svensen et al., 2006) to carbonate precipitate (Svensen et al., 2003), hydrothermal breccias (Jamtveit et al., 2004), and magmatic rocks (Hansen, 2006c). In the Gulf of California, carbonate cementation within the seismically mapped pipes is likely, since outcrops of talc and other carbonates have been observed on the ledges of pockmarks, sediment mounds, and along fault walls in Guaymas Basin (Figure 19; Lonsdale et al., 1980; Lizarralde et al., 2010). Stacked high-amplitude reflections within some of the imaged pipes (Figures

25,and 26A) could be a result of successive deposition of carbonate and hydrothermal precipitates through time, with constant burial of the deposits by rapidly accumulating sediments, which then consecutively ‘blast’ through the overburden. However, down-warped reflections below multiple ‘pipes’ suggest that lower velocity materials (i.e. hydrocarbons) eventually get trapped under a sealing horizon (Figure 21D). Trapping could result from precipitation within the pipe or rapid blanketing of sediments. Since the sonic velocity of the material within the ‘pipe’ is slower than the surrounding sediments it takes longer for the reflected frequencies to travel back to the hydrophones. If there are continuous reflectors across the feature and if the sound delay within the ‘pipe’ is large enough (compared to surrounding sediments) and not accounted for in velocity analysis (normal move-out correction) then reflections below the lower velocity horizon will appear pulled-down due to the overlying low-velocity material (Figures 9, 25, and 29). This is a classic exploration industry sign of gas concentrations and recently was clearly shown during a time-lapse seismic reflection study, in which Statoil and its Sleipner partners injected 2.3 million tons of CO_2 into a saline aquifer in the North Sea at a depth of 1012 m below sea level, 200 m below a shale reservoir top (Figure 26B; Eiken et al., 2008). A repeated seismic reflection survey in 1999 revealed stacked, abruptly ending, high-amplitude reflections directly above the injection point (Figure 26C). Below the reservoir top, reflections gradually down-warp compared to the 1994 survey and just above the injection point, the stacked high-amplitude reflections are

heavily down-warped (Figure 26C), indicating an overlying large concentrated zone of low-velocity material, known to be a CO_2 plume. Based on similar acoustic characteristics observed in this study and known venting of hydrocarbons (Lonsdale et al., 1980; Lizarralde et al., 2010), concentrated gas pockets or plumes, most likely partially composed of or capped with precipitates, hydrothermal breccias, and/or reworked sedimentary material, are interpreted to be responsible for reflector pull-downs observed above multiple sill intrusions (Figures 9, 26A, and 29) and other non-magmatic fluid-flow pathways (Figure 28). Below multiple mound-shaped high-amplitude features imaged on seismic reflection profiles reflections appear to warp upwards, indicating a sharp increase in velocity directly above the pulled-up reflectors (Figure 28).

A large, high-amplitude, ‘eye’-shaped feature along an extensional fault trace in Figure 27B is most likely a hydrothermal deposit that precipitated on the paleo-seabed next to the fault-wall and was subsequently buried by younger sediments. The location of this mound-like feature next to a fault trace matches the model proposed by Einsele et al. (1980) and fluid-flow migration described by Lonsdale et al. (1980) and Kastner (1982). Einsele et al. (1980) suggested that hydrothermal precipitates deposited at the base of the fault scarps get buried as sediments rapidly fill in the spreading troughs. The deposits are further buried under the basin floors as the crust is rafted away from the spreading axis. The feature observed in Figure 27B is buried by an upper acoustically transparent unit identified as hemipelagic turbidites deposited during the current interglacial

period (Kluesner et al., submitted), indicating the ‘eye’-shaped feature was formed sometime during the last glacial period. A high-amplitude stack of down-warped reflectors below and off to the side of the mound suggests that this was, and most likely still is, a zone of concentrated fluid flow (Figure 22B). Reflections below the ‘eye’-shaped feature are weak in amplitude, likely due to higher frequencies being attenuated by the overlying vent-like structure and are not drastically warped-down, indicating a limited concentration of gas. Alternatively, reflections below the interpreted vent could be weak in amplitude due to channelization and hydrofracturing of sediments along the fault trace, resulting in a homogenized sedimentary section and low impedance contrasts when imaged with seismic reflection profiling. A similar ‘eye’-shaped structure was imaged on a 3.5 kHz profile recently collected between Farallon Transform and Isla Carmen (Figure 30). The profile shows widespread evidence of fluid-flow and high gas concentration in the form of a bottom simulating reflector (BSR), gas curtains, vertical blanking zones, mounds, and an eye-shaped structure with a blank internal acoustic response (Figure 30). If the ‘eye’-shaped structure was a result of gas it would most likely have attenuated most of the acoustic energy, creating a ‘gas-curtain’ as is seen below the surrounding gas horizons. The imaging of sediments below the feature suggests that the internal composition of the feature is composed of homogenized sediments or precipitates, similar to the ‘eye’-shaped feature imaged on profile M (Figure 27B.) Additionally, the ‘eye’-shaped features imaged in this study share similar seismic/acoustic characteristics to that

of previously mapped ‘eye’ structures throughout volcanic basins in the Atlantic, which have been interpreted (Rocchi et al., 2007; Hansen et al., 2008) and found to be hydrothermal vents (Jamtveit et al., 2004; Planke et al., 2005). Based on the structural similarity with previously seismically mapped features from other regions outside the Gulf of California, submersible-sampled hydrothermal deposits within Guaymas Basin (Lonsdale et al., 1980), and the similarities with the model proposed by Einsele (1980) and Figure 27B, ‘eye’-shaped structures imaged on seismic reflection and 3.5 kHz profiles are interpreted as hydrothermal vent deposits, all of which have been subsequently buried by younger sediments.

3.5.7 Hydrocarbon Generation, Trapping, and Leakage

Previous studies in Guaymas Basin using deep-tow and up-looking sonars detected multiple acoustic targets in the water column in Guaymas Basin (Merewether et al., 1985; Lonsdale and Becker, 1985). In these studies, targets appeared as large mid-water anomalies, and the authors interpreted them as buoyant hydrocarbon plumes originating from seeps along faults or truncated outcrops (such as those observed along the Guaymas Transform; Merewether et al., 1985). One imaged plume (Plume A; Lonsdale and Becker, 1985) over the Southern Trough of Guaymas Basin was located directly above a small mound-like feature imaged on the sub-bottom profiler, interpreted as the surface trace of uplift over an axial dike swarm (Lonsdale and Becker, 1985). The location of the deep-tow vehicle track across this feature approximately matches that of the

Ulloa MCS profile M (Figure 27A). Profile M imaged the same mound-like feature, revealing that the structure is rooted more than 250 m below the seafloor, forming a dike-like uplift structure. The uplift most likely is acting as a leaky trap for hydrocarbons and other hydrothermal fluids due to the high permeability of the sediments and the presence of multiple faults that prevent a good seal, similar to that described by Lee et al. (2006) in the South Yellow Sea Basin.

Industry commonly uses interpretation of seismic reflection anomalies to identify hydrocarbons and gas below the seafloor; above the seafloor it is possible to identify evidence of hydrocarbon and gas leakage as bathymetric features such as mounds, mud volcanoes, bioherms, and pockmarks, or as acoustic plumes when observed in the water column. Some characteristic indicators of hydrocarbons and gas imaged sub-seafloor seismic reflection profiles are bright spots, dim spots, flat spots, and phase reversals (Litenberg, 2005; Andreassen et al., 2007; Løseth et al., 2008). Bright spots are the most common and easily identifiable anomaly in seismic reflection profiles; they are typically defined as localized increases in positive or negative amplitude along a reflection (Løseth et al., 2008). Throughout the central Gulf of California multiple localized high-amplitude reflections imaged on seismic profiles are interpreted as hydrocarbon bright spots, most of which are found in shallow sediments above identified sill intrusions and associated sediment deformation (Figures 9, 25, 27, and 29). MCS profile F (Figure 9) imaged a series of bright spots above a sill intrusion and deformation mound. Below the stacked high-amplitude reflections

(above the seismically dim and chaotic zone) reflections are warped-down, indicating gas concentration within the stacked brights. Near the seafloor a bright spot displays a waveform opposite the seabed, indicating negative polarity and the presence of gas/hydrocarbons. Also, this bright spot (Figure 9) mimics the seafloor (BSR) and appears to go through a phase reversal at the end nearest the stacked brights below. Near profile F, on Figure 29, there are bright spots with clear negative polarity near the seafloor, overlying positive polarity high-amplitude reflections interpreted as magmatic sills. Below these bright spots, reflections are down-warped and dimmed, relative to the surrounding sediments, indicating bright spots above are concentrated zones of gas/hydrocarbons. Other bright spots imaged through the central Gulf of California are commonly present along the edges of fault traces (Figures 27A and 28), supporting our interpretation that hydrocarbons and other fluids travel upwards along the fault trace and migrate laterally when reaching layers of high-porosity and/or a sealing horizon. As proposed earlier, hydrocarbons and other buoyant fluids travel along the path of least resistance, migrating towards the seafloor. However, when capped by a sealing horizon, fluids will spread laterally up-dip towards the seabed, creating concentrated zones of hydrocarbons/gas that appear as bright spots when imaged on seismic reflection profiles (Figures 27A and 28). In summary, when sills intrude and heat the surrounding sediments in Guaymas Basin and throughout the Gulf of California they convert immature organic sediments to thermogenic hydrocarbons, which is then scavenged by heated,

upstreaming pore fluids that migrate upwards towards the seafloor along zones of weakness (faults and fractured fluid 'pipes'), eventually expelling from the seafloor saturated with a broad range of hydrocarbons (Lonsdale et a., 1980; Simoneit et al., 1988; Lizarralde et al., 2010).

The overall time-temperature conversion of organic-rich sediments to hydrocarbons in Guaymas Basin takes place over a short geological timescale (< 5,000 yr) due to the constant intrusion of sills, which rapidly cook the surrounding strata (Didyk et al., 1989). Due to the short time-temperature conversion, shallow generation, and ease of expulsion/leakage, accumulations of large concentration of hydrocarbons within the Gulf of California is unlikely until the rifted margins and adjacent oceanic crust is no longer extensively magmatic and buried by prograding slope and shelf sediments. The present distribution of hydrocarbons and gases in the Gulf of California are of vital importance to certain biological communities (Lizarralde et al., 2010) and the ventilation of hydrocarbons from the seafloor may be a significant source of methane to the ocean and atmosphere (Judd et al., 2002; Svensen et al., 2004, 2007). The wide distribution of young sills and associated fluid-flow structures in the central Gulf of California shows that sill-induced hydrothermal venting is not confined to spreading centers, but occurs over vast areas. Our results suggest that widespread intrusive magmatism and fluid-flow should be considered when modeling or studying other heavily sedimented rifted margins and spreading centers.

3.6 COMPARISON WITH MAGMA INTRUSION AROUND OTHER TURBIDITE-SMOTHERED SPREADING CENTERS

While there are multiple old, deeply buried rifted margins that have been heavily studied using geophysical tools (deep seismic refraction, seismic reflection), there are very few modern examples of the rift-to-drift transition. The obvious modern examples are the Red Sea Rift and the Gulf of California; however, the inherent geology in which each rift formed is significantly different—the Gulf of California formed on a formerly convergent margin and ruptured along a hot, weak volcanic arc, is highly oblique, and is flooded with sediments, whereas the Red Sea Rift formed due to regional plate stresses that exploited lithospheric weakening caused by the Afar plume, is orthogonal, and has relatively low sedimentation rates. Other than the Red Sea Rift, there are very few modern analogues to the Gulf of California, though Middle Valley, located on the northern end of the Juan de Fuca ridge, and Bransfield Strait provide interesting comparison sites.

Although the Middle Valley is located on a well established spreading center (northern Juan de Fuca ridge) it has a very similar structure to axial spreading centers in the central Gulf of California. Middle Valley is a heavily sedimented rift valley that formed through simultaneous spreading center volcanism, extensional faulting, and sedimentation (Rohr and Schmidt, 1994).

The spreading center has been flooded with Pleistocene turbidites (up to 3.0 km thick) derived from the nearby western U.S. continental margin that has suppressed extrusive volcanism (Davis and Lister, 1977). Single and multichannel seismic reflection profiling across Middle Valley (Rohr and Schmidt, 1994) imaged a thick section of sediments underlain with high-amplitude reflectors interpreted as the top of a sediment-sill complex, with some high-amplitude reflectors found just below mound-like structure on the seafloor. Drilling results from ODP Legs 139 (Davis et al., 1992) and 169 (Frouquet et al., 1998) revealed that the high-amplitude reflections were indeed magmatic sills, some of which are concave upwards on seismic reflection profiles and uplift and deform the seafloor (Mottl et al., 1994). In fact, drilling of one uplift mound (Bent Hill) discovered a thick sill below the center of the mound and a thinner, shallower sill below the edge of the mound (Mottl et al., 1994). Based on the seismic reflection image (Rohr and Schmidt, 1994) and the thickness of the two drilled sills, it is likely that the two sills are actually one large, concave upwards sill that has relatively thin inclined ‘wings’. Additionally, drilling results found extensive evidence of sill-driven fluid-flow and hydrothermal deposits (Mottl et. al., 1994).

Between the northern margin of the Antarctic Peninsula and South Shetland Islands sits the Brainsfield Strait, a young active rift basin that is currently transitioning from rifting to incipient seafloor spreading (Prieto et al., 1998). It is a back-arc basin formed through complex interactions between plate and microplate convergence and plate divergence (Prieto et al., 1998).

Multichannel seismic reflection profiling across the rift basin revealed that the rift is opening northeast to southwest, and that extensive axial rift volcanism (mostly intrusive) gives way to more fissural-like eruptive features to the southwest (Barker and Austin, 1998). Detailed analysis of high-amplitude reflections within the sediments of the axial rift reveals extensive evidence of magmatic intrusion and even concave-upwards sills (Figure 31; Barker and Austin, 1994). Additional studies have shown that sediment supply to Bransfield Strait is highly asymmetrical, with most of the sediment input coming from the passive Antarctic Peninsula margin (Galindo-Zaldivar et al., 2004).

Comparison of Middle Valley and Bransfield Strait with our results from the central Gulf of California suggests that widespread, thick sediment-sill complexes, saucer-shaped sills, and sill-driven hydrothermal systems are common to heavily sedimented volcanic rifts and oceanic spreading centers. In addition, our results suggest that further high-resolution and 3D seismic reflection analysis of these settings should help clarify how these processes influence each other and provide valuable information about the rift-to-drift transition.

3.7 CONCLUSIONS

1. On multiple MCS profiles collected throughout the central Gulf of California, high-amplitude, abruptly ending, positive reflections (that are both concordant and discordant with the surrounding reflectors) are interpreted as magmatic sills intruded into unconsolidated sediments.

Multiple large sills (1-2 km in diameter) are interpreted as 3D saucer-shaped intrusions based on (I) their concave-upward profiles, (II) the overlying circular and elliptical plans of domal uplifts of the present multibeam-mapped seafloor, (III) their striking resemblance to saucer-shaped sills imaged with 3D seismics along the North Atlantic Margins, and (IV) similarities with field-mapped saucer-shaped sills.

2. In partial disagreement with Einsele (1980), results from this study show multiple sills do indeed uplift and deform the seafloor, as the removal of water from neighboring sediments fails to create sufficient space for large sill intrusions. As a result, the overburden is uplifted and deformed. The expulsion of pore-waters may create enough room for smaller intrusions, as most shallow small sills imaged in this study have minimal overburden deformation.

3. Circular mound-like features that occur directly overlying concave-upwards intrusions are interpreted as sedimentary forced folds. Low internal amplitudes and complex structure within some of the mounds may be the result of gas concentrations and rapid expulsion of super-heated pore fluids, which leads to fluidization and mixing of sediments, forming zones of highly fractured, mixed rock. Uplift mounds above sill intrusions disrupt turbidite deposition patterns, creating onlap of the youngest sediments,

enabling the assignment of relative ages to surrounding intrusions, fluid-flow structures, and sedimentary features. More accurate dating of sills would be possible with tightly constrained sedimentation rates or by tying biostratigraphic horizons to the onlapped reflectors.

4. Sediment uplifts in the axial floors in Guaymas, Carmen, and Farralon Basins are probably caused by a variety of igneous intrusions influenced by (I) concentrated tension and extensive normal faulting along the spreading axis, (II) intense focused magmatism along an elongated central point, (III) sediment composition that is composed of very low-density hemipelagic turbidites with very thin sandy beds, and (IV) increased hydrothermal activity within the spreading axis and extensive fluid-flow along extensional faults. Combination of these factors appears to produce complex magmatism within the axis composed of widespread diking, plug-like intrusions, and large, elongated sills with upturned wings that produce uplifted deformation mounds

5. Inclined, cross-cutting, high-amplitude reflectors imaged below and off to the side of indentified magmatic sills are most likely the inclined tips of deeper, older sills that act as feeders to younger, overlying sills. Additionally, continuous, layered high-amplitude reflections near seamounts and a crater are interpreted as lava flows. Sediment reflections

above identified flows appear to be unaltered unlike sediment reflections above sill intrusions.

6. Seismically disturbed, sub-vertical zones directly above sills are interpreted as pipe-like conduits for hydrothermal fluids, hydrocarbons, and gases, commonly connecting to hydrothermal mounds and pockmarks on the seafloor. Rapid build-up in fluid pressure during sill emplacement into off-axis unfaulted sediments most likely results in hydrofracturing of the overlying sediments and development of fluid-flow conduits (pipes). Stacked bright spots and pull-down of reflections below suggest that multiple fluid-flow conduits have trapped concentrated zones of gas, possibly due to the buildup of hydrothermal precipitates or blanketing of sediments (trapping horizon). Additionally, high-amplitude 'eye'-shaped structures imaged on MCS profiles and 3.5 kHz acoustic profiles are interpreted as buried hydrothermal vents, in agreement with the model proposed by Einsele (1982). Widespread evidence of bright spots, dim spots, and phase reversals suggest that intrusion-driven hydrocarbon generation occurs throughout the oceanic basins and bordering rifted margins in the central Gulf of California.

7. Widespread geophysical evidence of magmatic intrusions into the shallow crust suggests melt is being delivered not just to oceanic

spreading centers, but to a much broader area of oceanic and continental crust. The influence of sedimentation rate on magmatism is evident on MCS profiles crossing the Northern Trough of Guaymas Basin and Farallon axial Trough, where the top sill horizon depth appears to be partially controlled by the sediment load. Results from this study suggest that oceanic basins smothered with sediment have widespread intrusive magmatism and as the spreading centers migrate away from the continental rifted margins through time, sedimentation rates slow, resulting in reduced sediment loading at the axial trough and development of the classic ridge structure found at the center of Alarcon Basin in the mouth of the Gulf.

8. Comparison with other modern heavily sedimented spreading centers (Middle Valley and Bransfield Straight) suggests that widespread sediment-sill complexes, saucer-shaped sills, and sill-driven hydrothermal systems may be a common to the transition to volcanic continental rifting to oceanic seafloor spreading.

3.8 ACKNOWLEDGMENTS

Thanks are given the captain and crew of the Mexican research vessel *FRANCISCO DE ULLOA*, and Scripps geophysical engineer Lee Ellett, for their skill and perseverance while conducting the high-resolution seismic survey. Dr.

Barry Eakins helped prepare the bathymetric maps that guided the survey, and are used in study. Figures were prepared using Generic Mapping Tools (GMT) and IVS Fledermaus software packages. Funding was by grants from the U.S. NSF (OCE-0203348, OCE-0646563) and its Mexican partner CONACYT.

This chapter, in part, is currently being prepared for submission for publication of the material. Kluesner, J., Lonsdale, P. The dissertation author was the primary investigator and author of this paper.

3.9 REFERENCES

Andreassen, K., Nilssen, E., and Degaard., M., 2007, Analysis of shallow gas and fluid migration within the Plio-Pleistocene sedimentary succession of the SW Barents Sea continental margin using 3D seismic data. Geo-Mar Lett., 27, p. 155-171.

Barker, D. H. N., and Austin, J. A., 1994, Crustal diapirism in Bransfield Strait, West Antarctica: Evidence for distributed extension in marginal basin formation, Geology, v. 22, p. 657–660.

Barker D. H. N., and Austin, J. A ,1998, Rift propagation, detachment faulting and associated magmatism in Bransfield Strait, Antarctic Peninsula. J. Geophys. Res., v. 103**,** p. 24017–24043.

Batiza, R., 1978, Geology, petrology and geochemistry of Isla Tortuga, a recently formed tholeiitic island in the Gulf of California. Geol. Soc. Am. Bull. v. 89, p. 1309–1324.

Bell, B. and Butcher, H., 2002, On the emplacement of sill complexes: evidence from the Faroe-Shetland Basin. In: The North Atlantic Igneous Province: Stratigraphy, Tectonic, Volcanic and Magmatic Processes (D.W. Jolley and B.R. Bell, eds), Geol. Soc. London Spec. Publ., v. 197, p. 307–329.

Castillo, P.R., Hawkins, J.W., Lonsdale, P.F., Hilton, D.R., Shaw, A.M., and Glascock, M.D., 2002, Petrology of Alarcon Rise lavas, Gulf of California: nascent intracontinental ocean crust: Journal of Geophysical Research, v. 107 p. 2222-2237.

Cartwright, J., and Huuse, M., 2005. 3D seismic technology: the geologic 'Hubble'. Basin Research, v. 17, p. 1-20.

Chand, S., Rise, L., Ottesen, D., Dolan, M., Bellec, V., and Bøe, R., Pockmark-like depressions near the Goliat hydrocarbon field, Barents Sea: morphology and genesis. Marine and Petroleum Geology, doi:10.1016/f.marpetgeo.2008.09.002.

Chevallier, L. & Woodford, A., 1999, Morpho-tectonics and mechanism of emplacement of the dolerite ring and sills of the western Karoo, South Africa. S. Afr. J. Geol., v. 102, p. 43–52.

Curray, J., et al., 1979, Leg 64 seeks evidence on development of Basins. Geotimes, v. 24, 7, p. 18-20.

Davis, E. E., and C. Lister, 1977, Tectonic structures on the Juan de Fuca Ridge, Geol. Soc. Am. Bull., v. 88, p. 346–363.

Davis, E.E., Mottl, M.J., Fisher, A.T., et al., 1992, Proc. ODP, Init. Repts., v. 139: College Station, TX (Ocean Drilling Program), p. 5–7.

Didyk, B., Bernd, R., and Simoneit, T., 1989, Hydrothermal oil of Guaymas Basin and implications for petroleum formation mechanisms, Nature, v. 342, p. 65-69.

Dorsey, R., 2010, Sedimentation and crustal recycling along an active oblique-rift margin: Salton Trough and northern Gulf of California: Geology, v. 38, p. 443-446.

Douglas, R., Gonzalez-Yajimovich, O., Ledesma-Vazquez, J., and Stainess-Urias, F., 2007, Climate forcing, primary production and the distribution of Holocene biogenic sediments in the Gulf of California: Quaternary Science Review, v. 26 p. 15–129.

Eiken, O., Brevik, I., Arts, R., Lindeberg, E., Fagervik, K., 2000, Seismic monitoring of CO2 injected into a marine acquifer. Society of Exploration Geophysi-cists Annual Meeting.

Einsele, G., Curray, J. M., Moore, D. M., Aguayo, E., Aubry, M. P., Fornari, D., Guerrero, J., Kastner, M., Kelts, K., Lyle, M., Matoba, Y., Molina-Cruz, A., Niemitz, J., Rueda, J., Saunders, A., Schrader, H., Simoneit, B. & Vacquier, V., 1980, Intrusion of basaltic sills into highly porous sediments, and resulting hydrothermal activity. Nature, v. 283, p. 441- 445.

Einsele G., Niemitz J.W., 1982, Budget of postrifting sediments in the Gulf of California and calculation of the denudation rate in neighboring land areas. In: Curray JR, Moore DG et al. (eds) Init Rep Deep Sea Drilling Progr 64, part 2. U.S. Government Printing Office, Washington, p. 571–592.

Einsele, G., 1982, Mechanism of sill intrusion into soft sediment and expulsion of pore water, in Curray, J.R., Moore, D.G., et al., Initial reports of the Deep Sea Drilling Project, Volume 64, Part 2: Washington, D.C., U.S. Government Printing Office, p. 1169-1176.

Fouquet, Y., Zierenberg, R.A., Miller, D.J., et al., 1998, Introduction, Proc. ODP, Init. Repts., v. 169: College Station, TX (Ocean Drilling Program), p. 7–16.

Fuis, G.S., Mooney W.D., Healy, J.H., McMechan G.A., and Lutter, W.J., 1984, A seismic refraction survey of the Imperial Valley region, California, Journal of Geophysical Research,v. 89, p. 1165-1169.

Galland, O., Cobbold, P., Hallot, E., de Bremond d'Ars, J., and Delavaud, G., 2006, Use of vegetable oil and silica powder for scale modelling of magmatic intrusion in a deforming brittle crust. Earth and Planetary Science Letters, v. 243, p. 786-804.

Galindo-Zaldívar, J., Jabaloy, A., Maldonado, A. & Sanz de Galdeano, C. 1996, Continental fragmentation along the South Scotia Ridge transcurrent plate boundary (Antarctic Peninsula). Tectonophysics, v. 259, p. 275–301

Goulty, N., and Schofield, N., 2008, Implications of simple flexure theory for the formation of saucer-shaped sills. Journal of Structural Geology, v. 30, p. 812-817.

Hansen, D. M., Cartwright, J. & Thomas, D., 2004, 3D seismic analysis of the geometry of igneous sills and sill junction relationships. In: 3D Seismic Technology: Application to the Exploration of Sedimentary Basins (Ed. by R.J Davies, J. Cartwright, S.A. Stewart, J.R. Underhill & M. Lappin), Geol. Soc. London, Mem., v. 29, p. 199–208.

Hansen, D. M., Cartwright, J.A., and Thomas, D., 2006a, 3D seismic analysis of the geometry of igneous sill junction relationships, Geological Soc., London, v. 29, p. 199-208.

Hansen, D. M., Cartwright, J., 2006b, The three-dimensional geometry and growth of forced folds above saucer-shaped igneous sills. J. Struct. Geol. v. 28, p. 1520-1535.

Hansen, D. M., 2006c, The morphology of intrusion-related vent structures and their implications for constraining the timing of intrusive events along the NE Atlantic margin. J. Geol. Soc. London, v. 163, p. 789–800.

Hansen, D. M., and Cartwright, J., 2007, Reply to comment by K. Thomson on “The three-dimensional geometry and growth of forced folds above

saucer-shaped igneous sills" by Hansen and Cartwright, Journal of Structural Geology, 29, p. 741-744.

Hansen, D. M., Redfern, J., Federici, F., Biase, D., Bertozzi, G., 2008, Miocene igneous activity in the Northern Subbasin, offshore Senegal, NW Africa, Marine and Petroleum Geology, 25, p. 1-15.

Hansen, J., Jerram, D. A., McCaffrey, K., and Passey, S. R., 2011, Early Cenozoic saucer-shaped sills of the Faroe Islands: an example of intrusive styles in basaltic lava piles, Journal of the Geological Society, v. 168 (1), p. 159-178.

Heggland, R., 1998, Gas seepage as an indicator of deeper prospective reservoirs. A study based on exploration 3D seismic data. Marine and Petroleum Geology, v. 15, p.1-9.

Herzig, C.T., and Elders, W.A., 1988, Nature and significance of igneous rocks cored in the State 2-14 research borehole: Salton Sea Scientific Drilling Project, California, J.Geophys.Res., v.93, p. 13069- 3080.

Jamtveit, B., Svensen, H., Podladchikov, Y. Y. and Planke, S., 2004, Hydrothermal vent complexes associated with sill intrusions in sedimentary basins. In: Physical Geology of High-Level Magmatic Systems (C. Breitkreutz and N. Petford, eds), Geol. Soc. London Spec. Publ., v. 234, p. 229–232.

Judd A., and Hovland, M., 2007, Seabed Fluid Flow, Cambridge University Press, 475 p.

Judd, A., Hovland, M., Dimitrov, L., Garcia, S., and Jukes, V., 2002, The geological methane budget at continental margins and its influence on climate change. Geofluids, v. 2, p. 109-126.

Kastner, M., 1982, Evidence for two distinct hydrothermal systems in the Guaymas Basin, DSDP Init. Repts, v. 64 ,in: J.R. Curray, D.G. Moore, Editors et al., US Govt. Print. Office, Washington. p. 1143–1157.

Kavanagh, J. L., Menand T., and Sparks, R. S. J., 2006, An experimental I nvestigation of sill formation and propagation in layered elastic media. Earth and Planetary Science Letters, v. 245**,** p. 799–813.

Klitgord, K., Hutchinson, D., and Schouten, H., 1988, U.S. Atlantic continental margin: Structural and tectonic framework, in Sheriden, R. E., and Grow, J. A., eds, The Atlantic continental margin: U.S.: Boulder Colorado, GSA, Geology of North America, Vol. I-2, pp. 19-55.

Kluesner, J., and Lonsdale, P., 2008, Young saucer-shaped sills within rapidly accumulated sediments of the central Gulf of California: Eos Trans, AGU, 89 (53), Fall Meet. Suppl., Abstract T11A-1847.

Kluesner, J., Lonsdale, P., Kirtland, S., and González, A., submitted, Influence of Glacial-Interglacial Cyclicity on Sedimentation and Axial Rift Structure at the Southern Trough, Geosphere.

Lawver, L. A., Williams, D., and Von Herzen, R.P., 1975, A major geothermal anomaly in the Gulf of California. Nature, v. 257, p. 23–28.

Lee, G., Kwon, Y., Yoon., C., Kim., H., and Yoo, H., 2006, Igneous complexes in the eastern Northern South Yellow Sea Basin and their implications for hydrocarbon systems. Marine and Petroleum Geology, v. 23, p. 631-645.

Lizarralde, D., Axen, G., Brown, H., Fletcher, J., Gonzalez-Fernandez, A., Harding, A., Holbrook, S., Kent, G., Paramo, P., Sutherland, F., and Umhoefer, P., 2007. Variation in styles of rifting in the Gulf of California. Nature, v. 448, p. 466-469.

Lizarralde D., Soule, A., Seewald., J., and Proskurowski, G., 2010. Carbon release by off-axis magmatism in a young sedimented centre: Nature Geoscience, v. 4, p. 50-54. doi:10.1038/NGEO1006.

Lonsdale P., Bischoff, J., Burns, V., Kastner, M., and Sweeney, R., 1980, A high-temperature hydrothermal deposit on the seabed at a Gulf of California spreading center. Earth and Planetary Science Letters, v. 49, p. 8-20.

Lonsdale P., and Becker, K., 1985, Hydrothermal plumes, hot springs, and conductive heat flow in the Southern Trough of Guaymas Basin, Earth and Planetary Science Letters, v. 73, p. 211-225.

Lonsdale P., 1985, A transform continental margin rich in hydrocarbons, Gulf of California, AAPG v. 69, p. 1160–1180.

Lonsdale, P., 1989, Geology and tectonic history of the Gulf of California, in The Eastern Pacific Ocean and Hawaii, edited by Winterer, E. L., Hussong, D. M. & Decker, R. W., The Geology of North America N, Geological Society of America, p. 499-521.

Lonsdale, P., and Kluesner J., 2010, Routing of terrigenous clastics to oceanic basins in the Southern Gulf of California, inherited from features of the pre-spreading protogulf. Fall Meet. Suppl., Abstract T33C-2265.

Lonsdale, P., and Lawver, L.A., 1980, Immature plate boundary zones studied with a submersible in the Gulf of California. Geol. Soc. Am. Bull., v. 91, p. 555–569.

Løseth, H., Gading, M., and Wensaas, L., 2008, Hydrocarbon leakage interpreted on seismic data. Marine and Petroleum Geology, v. 27, 7, p. 1304-1319. doi:10.1016/j.marpetgeo.2008.09.008.

Løseth, H., Wensaas, L., Arntsen, B., Hanken, N., Basire C., and Graue, K., 2001, 1000 M Long Gas Blow-Out Pipes Extended abstract, EAGE, Amsterdam.

Malthe-Sørenssen, A., Planke, S., Svensen, H. and Jamtveit, B, 2004, Formation of saucer-shaped sills. In: Physical Geology of High-Level Magmatic

Systems (C. Breitkreutz and N. Petford, eds), Geol. Soc. London Spec. Publ., v. 234, p. 215–227.

Mathieu, L., van Wyk de Vries, B., Holohan, E., and Troll, V., 2008, Dykes, cups, saucers and sills: Analogue experiments on magma intrusion into brittle rocks. Earth and Planetary Letters, v. 271, p. 1-13.

Menand, T., 2007, The mechanics and dynamics of sills in layered elastic rocks and their implications for the growth of laccoliths and other igneous complexes. Earth and Planetary Letters, v. 267, p. 93-99.

Merewether, R., Olsson, M., Lonsdale, P., 1985, Acoustically detected hydrocarbon plumes rising from 2-km depths in Guaymas Basin, Gulf of California, Journal of Geophysical Research, v. 90, p. 3075-3085.

Miller, N. C., Lizarralde, D., Harding, A. J., and Kent, G., 2009, Constraints on early Gulf of California rifting from seismic images across the eastern margin of Guaymas Basin, AGU Fall Meeting, Abstract T31A-1783.

Mosher, D., and Simpkin, P., 1999, Environmental marine geosciences 1. Status and trends of marine high-resolution seismic reflection profiling: data acquisition. Geoscience Canada, v. 26, p. 174-188.

Mottl, M.J., Wheat, C.G., and Boulègue, J., 1994, Timing of ore deposition and sill intrusion at Site 856: evidence from stratigraphy, alteration, and sediment pore-water composition. In Mottl, M.J., Davis, E.E., Fisher, A.T., and Slack, J.F. (Eds.), Proc. ODP, Sci. Results, v. 139: College Station, TX (Ocean Drilling Program), p. 679–693.

Oskin M., Stock J.M., 2003, Pacific–North America plate motion and opening of the Upper Delfín basin, northern Gulf of California: Geological Society of America Bulletin, v. 115, p. 1173–1190, doi: 10.1130/B25154.1.

Parnell J., and Schwab A., 2003, Seismic evidence for the distribution and migration of fluids in sedimentary basins. Geofluids v. 3, p. 213–217.

Persaud, P., Stock, J.M., Steckler, M.S., Martin-Barajas, A., Diebold, J.B., González-Fernández, A. & Mountain, G.S., 2003, Active deformation and shallow structure of the Wagner, Consag and Delfín Basins, Northern Gulf of California: Mexico, J. Geophys. Res., v. 108 (B7), p. 2355-2377.

Phillips R.P., 1964, Seismic refraction studies in the Gulf of California, Amer. Assn. Petroleum Geologists Memoir 3, (van Andel, T., and Shor, G.G. ,eds.), p. 90-121.

Pinero, D., 2008, Sismica de Reflexion y Fechamiento ^{40}AR-^{39}Ar del Basemento Continental en el Margen Oeste de la Cuenca Farallon (Sur del Golfo de California, Mexico, M. Sc., 159 p.

Planke, S, Symonds, P., Alvestad, E., and Skogseid, J., 2000, Seismic volcanostratigraphy of large-volume basaltic extrusive complexes on rifted margins. Journal of Geophysical Research, v. 105, 19, p. 335-19,351.

Planke, S., Rasmussen, T., Rey, S.S. and Myklebust, R., 2005, Seismic characteristics and distribution of volcanic intrusions and hydrothermal vent complexes in the Vøring and Møre basins. In: Petroleum Geology North-West Europe and Global Perspectives – Proceedings of the 6th Petroleum Geology Conference (S. Planke, T. Rasmussen, S.S. Rey and R. Myklebust, eds), p. 833–844.

Prieto, M.J., Canals, M., Ercilla, G., and De Batist, M., 1998, Structure and geodynamic evolution of the Central Bransfield basin (NW Antarctica) from seismic reflection data: Marine Geology, v. 149 p. 17-38.

Polteau S., Ferré E.C., Planke S., Neumann E.-R., Chevallier L., 2008, How are saucer-shaped sills emplaced? Constraints from the Golden Valley Sill, South Africa: Journal of Geophysical Research, v. 113, B12104, doi: 10.1029/2008JB005620.

Robinson, P.T. Elders W.A., and Muffler, L.J.P., 1976, Quaternary volcanism in the Salton Sea geothermal field, Imperial Valley, California, Geol. Soc. Am. Bull., v.87, pp.347-360.

Rocchi, S., Mazzotti, A., Marroni, M., Pandolfi, L., Costantini, P., Giuseppe, B., Biase, D.d., Federici F., and Lo, P.G., 2007, Detection of Miocene saucer-shaped sills (offshore Senegal) via integrated interpretation of seismic, magnetic and gravity data, Terra Nova, v. 19, p. 232–239.

Rohr, K.M.M., and Schmidt, U., 1994, Seismic structure of Middle Valley near Sites 855–858, Leg 139, Juan de Fuca Ridge. In Mottl, M.J., Davis, E.E., Fisher, A.T., and Slack, J.F. (Eds.), Proc. ODP, Sci. Results, v. 139: College Station, TX (Ocean Drilling Program), p. 3–17.

Shankar, U., Thakur, N., and Ashalatha, B., 2006, Fluid flow related features as an indicator of potential gas hydrate zone: western continental margin of India, Marine Geophysical Research, v. 27, p. 217-224.

Sheriff, R.E., 1975, Factors affecting seismic amplitudes. Geophysical Prospecting, v. 23, p. 125–138.

Simoneit, B., Kawka, O., and Brault, M., 1988, Origin of gases and condensates in the Guaymas Basin hydrothermal system (Gulf of California). Chemical Geology, v. 71, p.169-182.

Simoneit, B., Lonsdale, P., Edmond, M., and Shanks, W., 1990, Deep-water hydrocarbon seeps in Guaymas Basin, Gulf of California, Applied Geochemistry, v. 5, p. 41-49.

Skogly, O., 1998, Seismic characterisation of and emplacement of intrusives in Voring Basin. M.Sc. Thesis, University of Oslo, Norway.

Smallwood, J.R. & Maresh, J., 2002, The properties, morphology and distribution of igneous sills: modelling, borehole data and 3D seismic from the Faroe-

Shetland area. In: The North Atlantic Igneous Province: Stratigraphy, tectonic, volcanic and magmatic processes (Ed. by D.W Jolley & B.R. Bell), Geol. Soc. London. Spec. Publ., v. 197, p. 271–306.

Svensen, H., Planke, S., Jamtveit, B., and Pederson, T., 2003, Seep carbonate formation controlled by hydrothermal vent complexes: a case study from the Voring Basin, the Norwegian Sea. Geo-Mar Lett., v. 23, p. 351-358.

Svensen, H., Planke, S., Malthe-Sørensen, A., Jamtveit, B., Myklebust, R., Eiden, T.R. & Rey, S.S. 2004, Release of methane from a volcanic basin as a mechanism for initial Eocene global warming. Nature, v. 429, p. 542–544.

Svensen, H., Jamtveit, B., Planke, S. and Chevallier, L., 2006, Structure and evolution of hydrothermal vent complexes in the Karoo Basin, South Africa. J. Geol. Soc. London, v. 163, p. 671–682.

Svensen, H., Planke, S., Chevallier, L., Malthe-Sorenssen, A., Corfu, F., and Jamtveit, B., 2007, Hydrothermal venting of greenhouse gases triggering Early Jurassic global warming, Earth Planet. Sci. Lett. v. 256, p. 554–566.

Thomas, A. L., 1993, Poly3d: a three-dimensional, polygonal element, displacement discontinuity boundary element computer program with applications to fractures, faults, and cavities in the Earth's crust: Master thesis, Stanford University, Stanford, California, U.S.A., p. 69.

Thomson, K. & Hutton, D., 2004, Geometry and growth of sill complexes: insights using 3D seismic from the North Rockall Trough. Bull. Volcanol., v. 66, p. 364–375.

Thomson, K., 2005, Volcanic features of the North Rockall Trough: application of visualization techniques on 3D seismic reflection data, Bull Volcanol, v. 67, p. 116-128.

Thomson, K., 2007, Comment on “The three-dimensional geometry and growth of forced folds above saucer-shaped igneous sills” by Hansen and Cartwright, Journal of Structural Geology, v. 29, p. 736-740.

Trude, K.J., 2004, Kinematic indicators for shallow level igneous intrusions from 3D seismic data: evidence of flow direction and feeder location. In: 3D Seismic Technology: Application to the Exploration of Sedimentary Basins (Ed. by R.J. Davies, J. Cartwright, S.A. Stewart, J.R. Underhill & M. Lappin), Geol. Soc. London, Mem., v. 29, p. 209–217.

Trude, K.J., Cartwright, J.A., Davies, R.J. & Smallwood, J.R., 2003, A new technique for dating igneous sills. Geology, v. 31, p. 813–816.

Van Andel T., 1964, Recent marine sediments of Gulf of California, *in* Van Andel T.,Shor G.G., eds., Marine geology of the Gulf of California: American Association of Petroleum Geologists Memoir 3, p. 216–310.

Ziolkowski, A., Hanssen, P., Gatliff, R., Jakubowicz, H., Dobson, A., Hampson, G., Li, X. & Liu, E., 2003, Use of low frequencies for subbasalt imaging, Geophys. Prosp., v. 51(3), p. 169–182.

Figure 3-1. Topography of central and southern Gulf of Caifornia. Bathymetry is from multibeam surveys, supplemented in shallow water by contour interpolation of archival soundings; subaerial relief from satellite altimetry. Red circles locate DSDP Leg 64 drilling sites which encountered magmatic sill intrusions. Labeled contours are in hundreds of meters (10 = 1000 m). Colored lines represent location of MCS profiles collected on multiple cruises (see legend). Inset. Pattern of the plate boundary throughout the Gulf, with spreading centers labeled: W-Wagner, UD = Upper Delfin, LD = Lower Delfin, G = Guaymas, C = Carmen, F = Farallon, NP = North Pescadero, SP = South Pescadero, A = Alarcon, EPR = East Pacific Rise. Land is dark grey, newly accreted crust light grey; dashed red box locates area of main map.

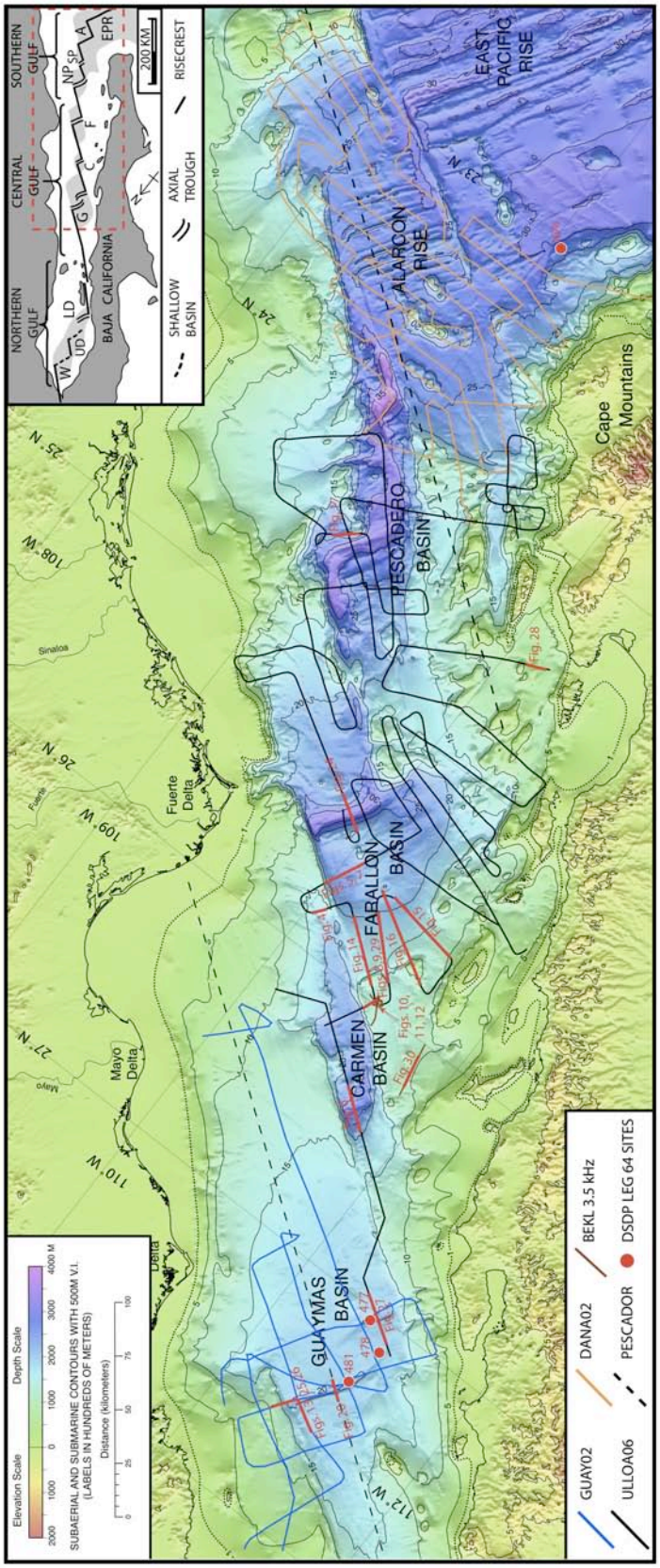
NORTHERN GULF
CENTRAL GULF
SOUTHERN GULF
BAJA CALIFORNIA
LD
UD
W
G
F
NP
SP
A
EPR
200 KM
SHALLOW BASIN
AXIAL TROUGH
RISECREST
GUAYMAS BASIN
CARMEN BASIN
FARALLON BASIN
PESCADERO BASIN
ALARCON RISE
EAST PACIFIC RISE
Cape Mountains
Mayo Delta
Fuerte Delta
Sinaloa
Elevation Scale
Depth Scale
SUBAERIAL AND SUBMARINE CONTOURS WITH 500M V.I.
(LABELS IN HUNDREDS OF METERS)
Distance (kilometers)
GUAY02
DANA02
BEKL 3.5 kHz
ULLOA06
PESCADOR
DSDP LEG 64 SITES

Figure 3-2. Map of sedimentary features in the central and southern Gulf of California. Interpretations made based primarily on MCS profiles and multibeam bathymetry. Labeled contours are in hundreds of meters (10 = 1000 m). Note: currently only a few sedimentary pathways deliver sediments from arid Baja California, with runoff from the Cape Mountains providing a significant amount to western Alarcon Basin. Large amounts of rainfall over the deeply incised Sierra Madre Occidental plateau is responsible for development of large deltas, deep-sea fans, and provides the majority of terrigenous clastics to the oceanic basins. CP = Conception Peninsula. EFS = East Farallon Seamount. WF = West Farallon.

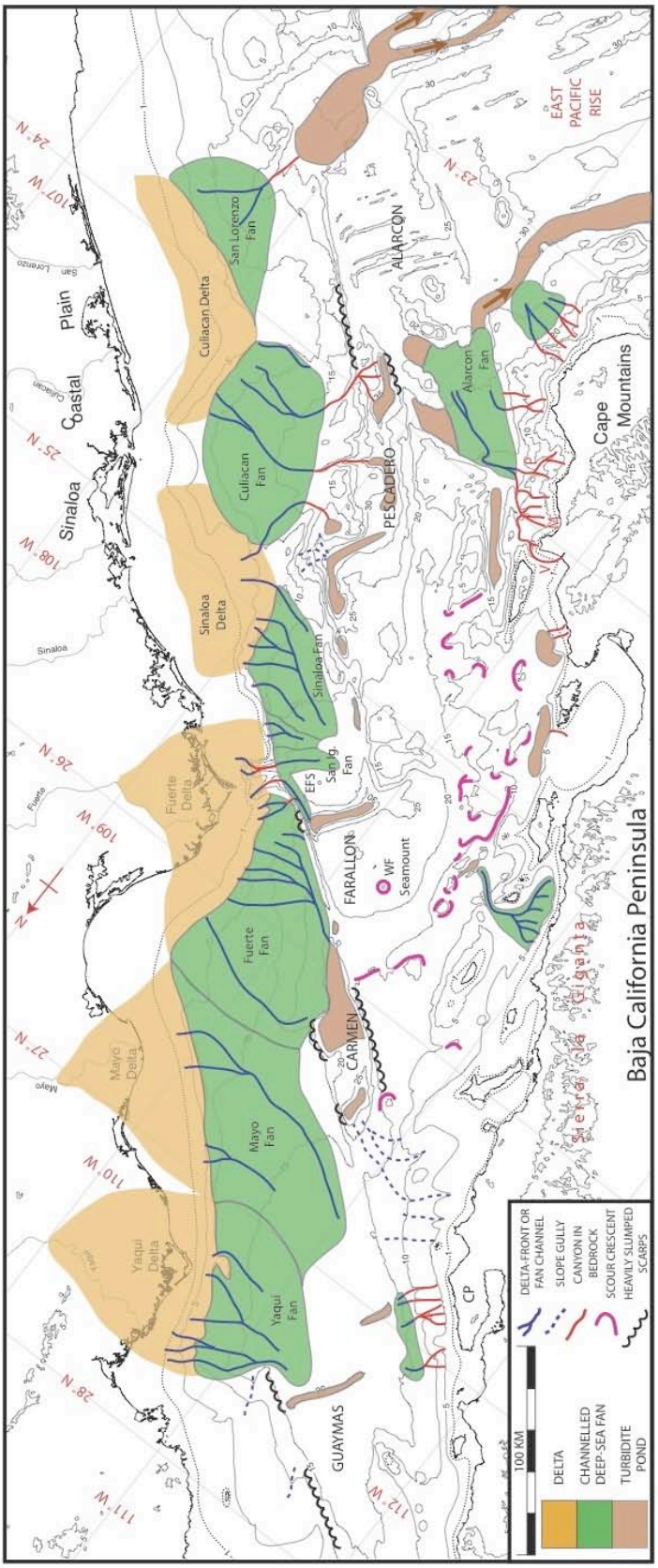
Baja California Peninsula
Coastal Plain
Sinaloa
Cape Mountains
Sierra La Giganta
EAST PACIFIC RISE
ALARCON
PESCADERO
FARALLON
CARMEN
GUAYMAS
CP
WF Seamount
EFS
San Lorenzo Fan
Culiacan Delta
Culiacan Fan
Alarcon Fan
Sinaloa Delta
Sinaloa Fan
San Lorenzo
Culiacan
Sinaloa
Fuerte Delta
Fuerte Fan
Fuerte
Mayo Delta
Mayo Fan
Mayo
Yaqui Delta
Yaqui Fan
24° N
25° N
26° N
27° N
28° N
107° W
108° W
109° W
110° W
111° W
112° W
23° N
DELTA-FRONT OR FAN CHANNEL
SLOPE GULLY
CANYON IN BEDROCK
SCOUR CRESCENT
HEAVILY SLUMPED SCARPS
100 KM
DELTA
CHANNELLED DEEP-SEA FAN
TURBIDITE POND

Figure 3-3. Structural interpretation map of the central and southern Gulf of California (modified from Lonsdale and Kluesner, 2010). The interpretive structural map and uses results from dense but uneven grids of magnetic profiles and single-channel seismic profiles that are not located in Figure 1, and from mostly analyzed and partly dated igneous rock samples recently collected by dredge and ROV from more than 600 sites on the Gulf floor. Note the location of the continental-oceanic boundary in western Farallon Basin based on Figures 26, 27, and 28, and light blue zones that outline areas of young sill intrusion through thinned continental crust.

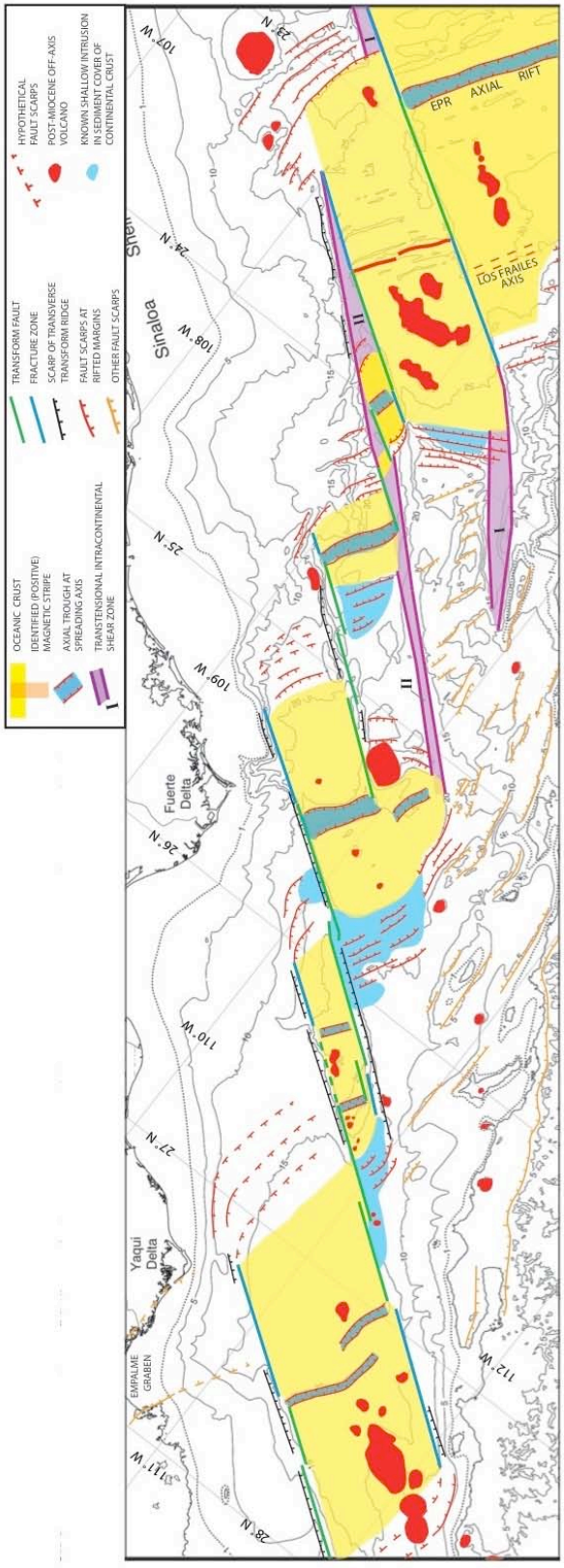
OCEANIC CRUST
IDENTIFIED (POSITIVE) MAGNETIC STRIPE
AXIAL TROUGH AT SPREADING AXIS
TRANSTENSIONAL INTRACONTINENTAL SHEAR ZONE
TRANSFORM FAULT
FRACTURE ZONE
SCARP OF TRANSVERSE TRANSFORM RIDGE
FAULT SCARPS AT RIFTED MARGINS
OTHER FAULT SCARPS
HYPOTHETICAL FAULT SCARPS
POST-MIOCENE OFF-AXIS VOLCANO
KNOWN SHALLOW INTRUSION IN SEDIMENT COVER OF CONTINENTAL CRUST
EPR AXIAL RIFT
LOS FRAILES AXIS
Sinaloa
Fuerte Delta
Yaqui Delta
EMPALME GRABEN
23°N
24°N
25°N
26°N
27°N
28°N
107°W
108°W
109°W
110°W
112°W
117°W

Figure 3-4. MCS profile A. Seismic profile (located on Figure 1) across the channeled Fuerte fan near Farallon Transform. Seismic image displays evidence of young magmatic sills emplaced into sediments overlying continental crust. Seismic characteristics of magmatic sills are highlighted using black arrows and include: high-amplitudes, positive polarity, abrupt terminations, cross-cut stratigraphy, sediment deformation, and seismic shadowing. Additionally, concave upwards sills (K and L) are labeled. Dashed blue line represents interpretation of extent of Sill L, which has been shadowed by younger sills above..

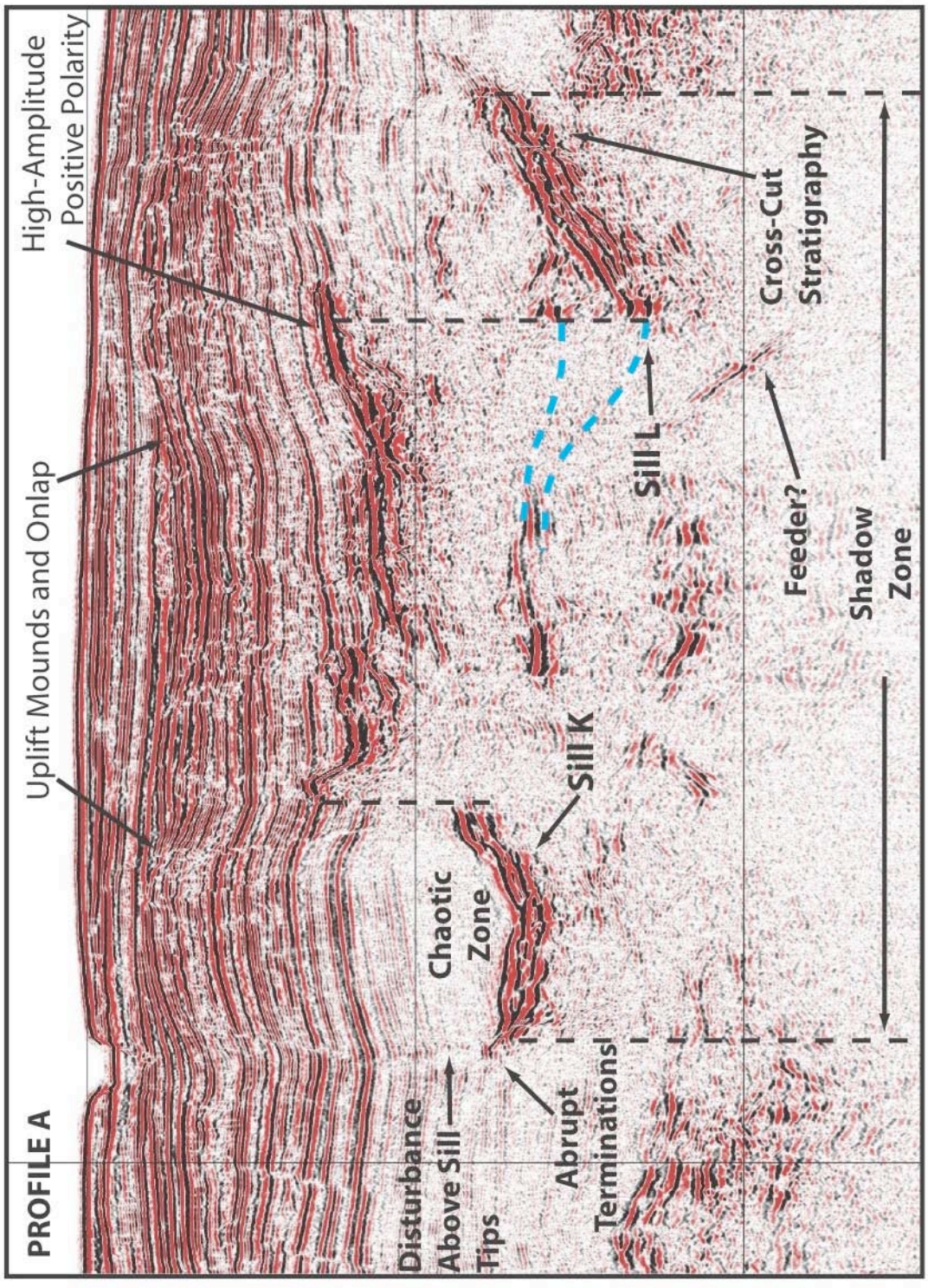
PROFILE A
High-Amplitude Positive Polarity
Uplift Mounds and Onlap
Disturbance Above Sill Tips
Chaotic Zone
Sill K
Abrupt Terminations
Sill L
Feeder?
Cross-Cut Stratigraphy
Shadow Zone

Figure 3-5. MCS profile B. Seismic profile across western Farallon Basin, crossing Farallon Transform. Profile B illuminates off-axis magmatic intrusions, including concave-upwards sills (I and H), associated deformation, and probable lava flows. Inclined, cross-cutting reflectors bellow and off to the side of interpreted sills are identified as possible feeders. Dashed black boxes highlight 3 zoomed in sections displayed above the seafloor. NE = Northeast, SW = Southwest, VE = Vertical Exaggeration.

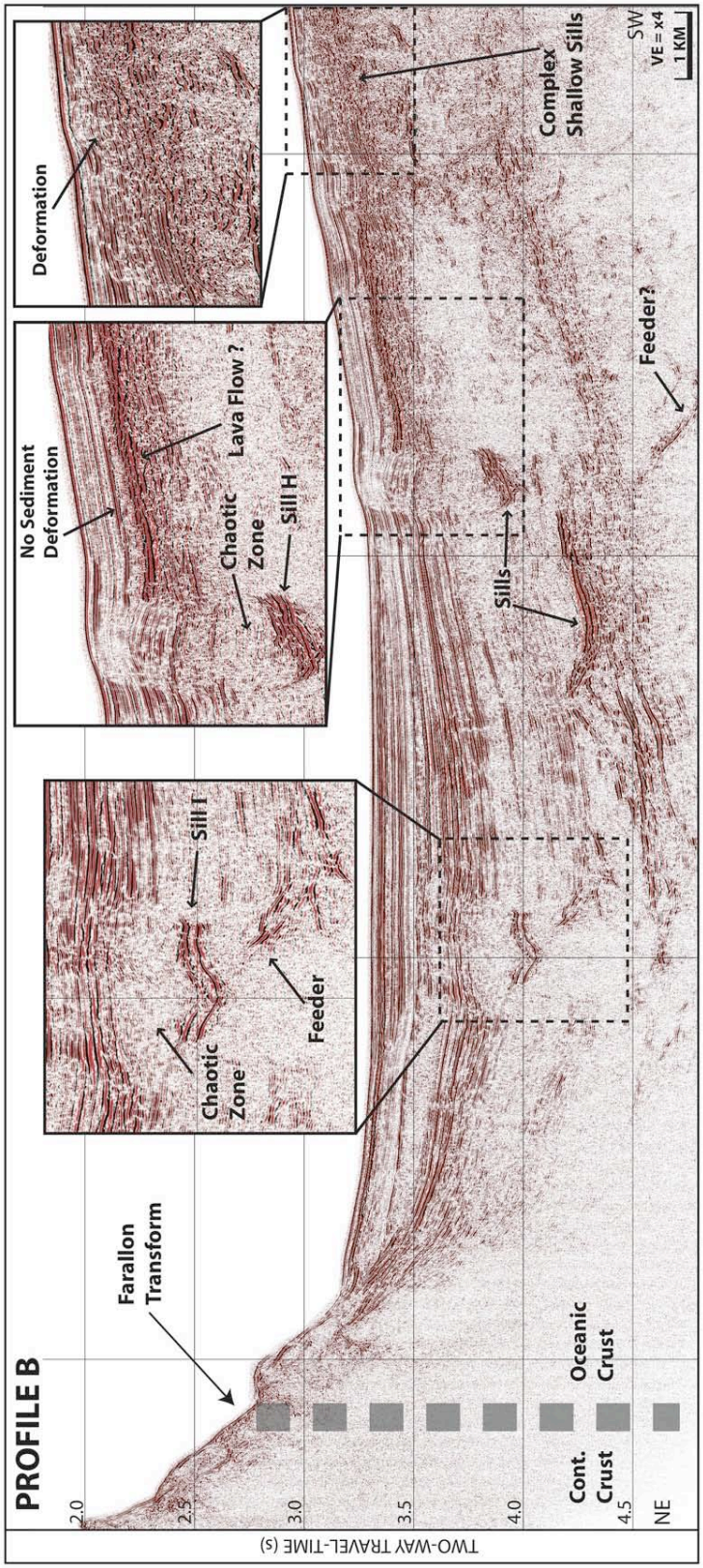
PROFILE B
Farallon Transform
Oceanic Crust
Cont. Crust
NE
SW
VE = x4
1 KM
TWO-WAY TRAVEL-TIME (s)
2.0
2.5
3.0
3.5
4.0
4.5
Deformation
No Sediment Deformation
Lava Flow ?
Chaotic Zone
Sill H
Sills
Complex Shallow Sills
Feeder?
Sill I
Chaotic Zone
Feeder

Figure 3-6. MCS profile C. Seismic profile (located on Figure 1) superimposed on a 3D multibeam bathymetry image. Viewing angle is to the southwest and bathymetry and seismic image have ~4x vertical exaggeration. White line represents a 2008 *ROV JASON* dive path, with red boxes indicating location of rock samples. The picture inset is of pillow basalts collected at a recent spreading-axis eruption site; scale bar in this image is in centimeters. Cooked, diatomaceous muds were sampled along the northwest rift wall that cuts a transparent reflector unit. Note shallow high-amplitude reflections interpreted as sills below the axial floor and rift shoulders. VE = Vertical Exaggeration.

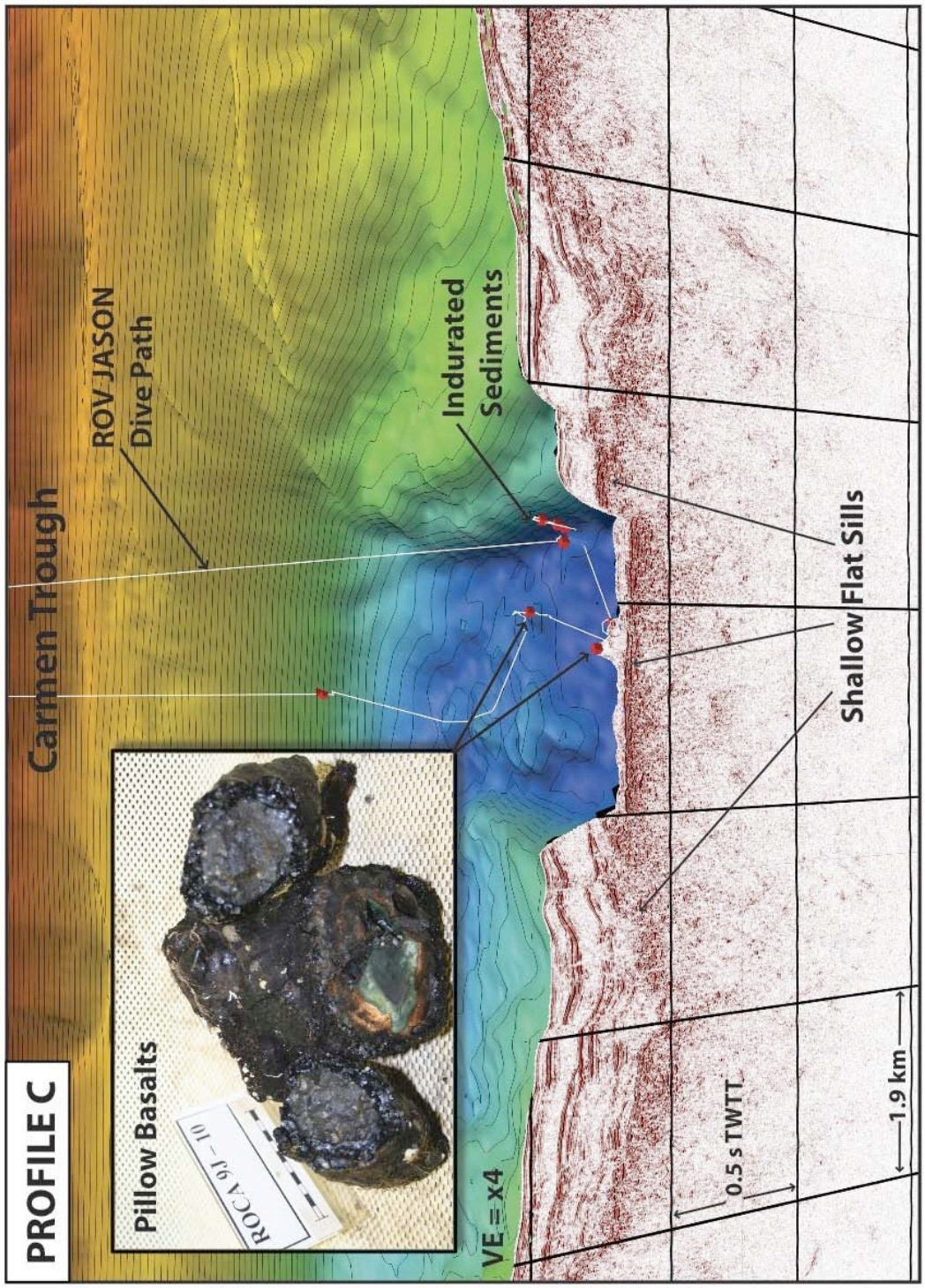
PROFILE C
Carmen Trough
ROV JASON
Dive Path
Indurated
Sediments
Pillow Basalts
ROCA 91 – 10
VE = x4
Shallow Flat Sills
0.5 s TWTT
1.9 km

Figure 3-7. MCS profile D. Seismic section (located on Figure 1) superimposed on 3D bathymetric data near West Farallon Seamount. Viewing angle is to the southeast and bathymetry and seismic image have ~4x vertical exaggeration. White line represents a 2008 *ROV JASON* dive path, with red boxes indicating location of rock samples. Samples including thoeletic basalts at the base and fractionated dacitic rocks at the summit. Note possible lava flow and complex shallow reflections located at the base of West Farallon Seamount, interpreted as sill intrusions. Y-axis on seismic profile is in seconds TWTT.

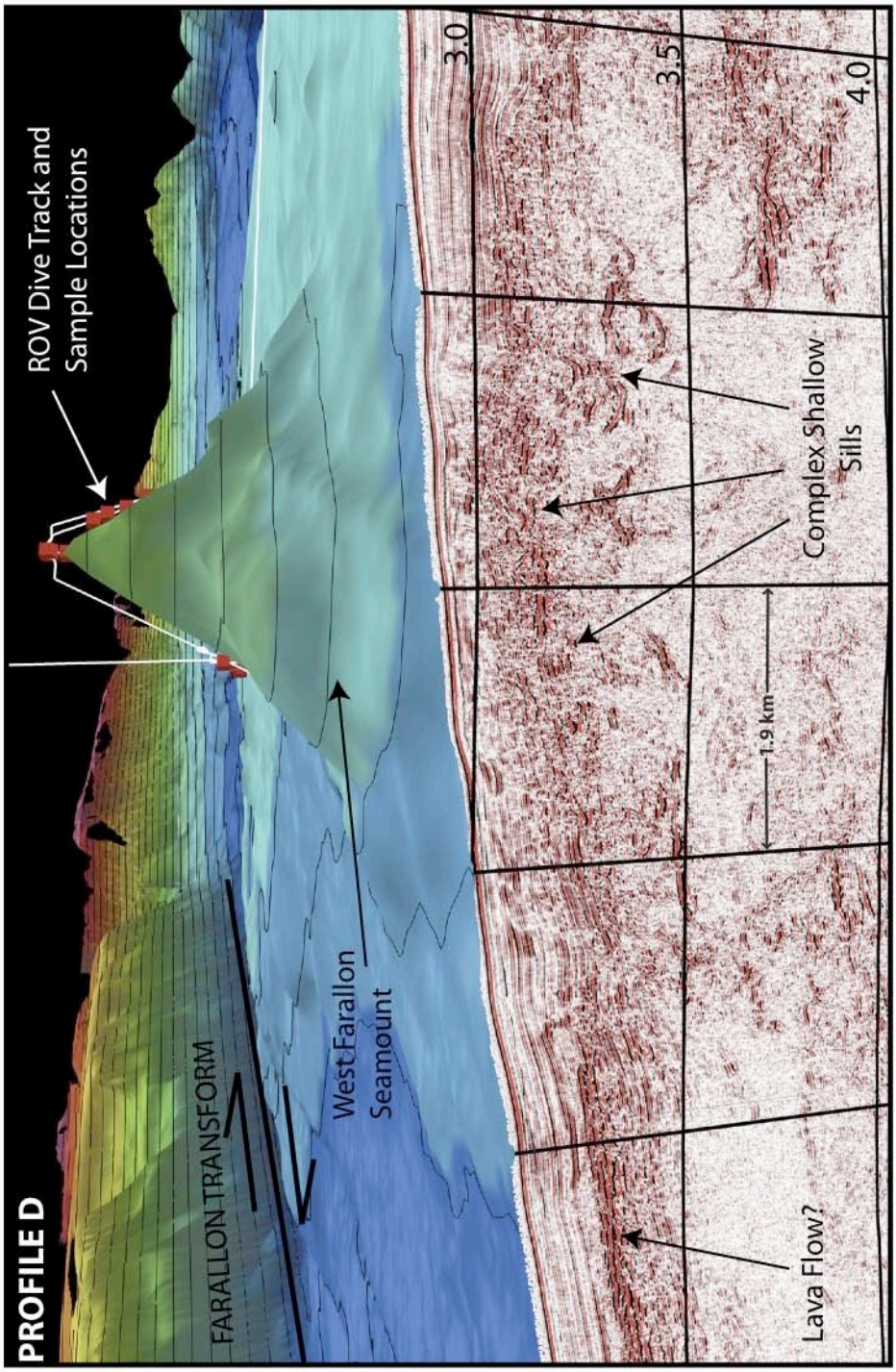
PROFILE D
ROV Dive Track and Sample Locations
FARALLON TRANSFORM
West Farallon Seamount
3.0
3.5
4.0
1.9 km
Complex Shallow Sills
Lava Flow?

Figure 3-8. MCS profile E. Seismic profile (located on Figure 1) collected across western Farallon Basin. Profile shows stacked high-amplitude section of reflectors and mound-like structure above interpreted as a large concave-upwards sill and associated sedimentary forced fold. Black lines above the sill highlight evidence of normal faulting and reflectors can be traced across the structural feature. Note evidence of sediment alteration or fluid-flow (decreased amplitudes) above the sill and onlap of younger sediments.

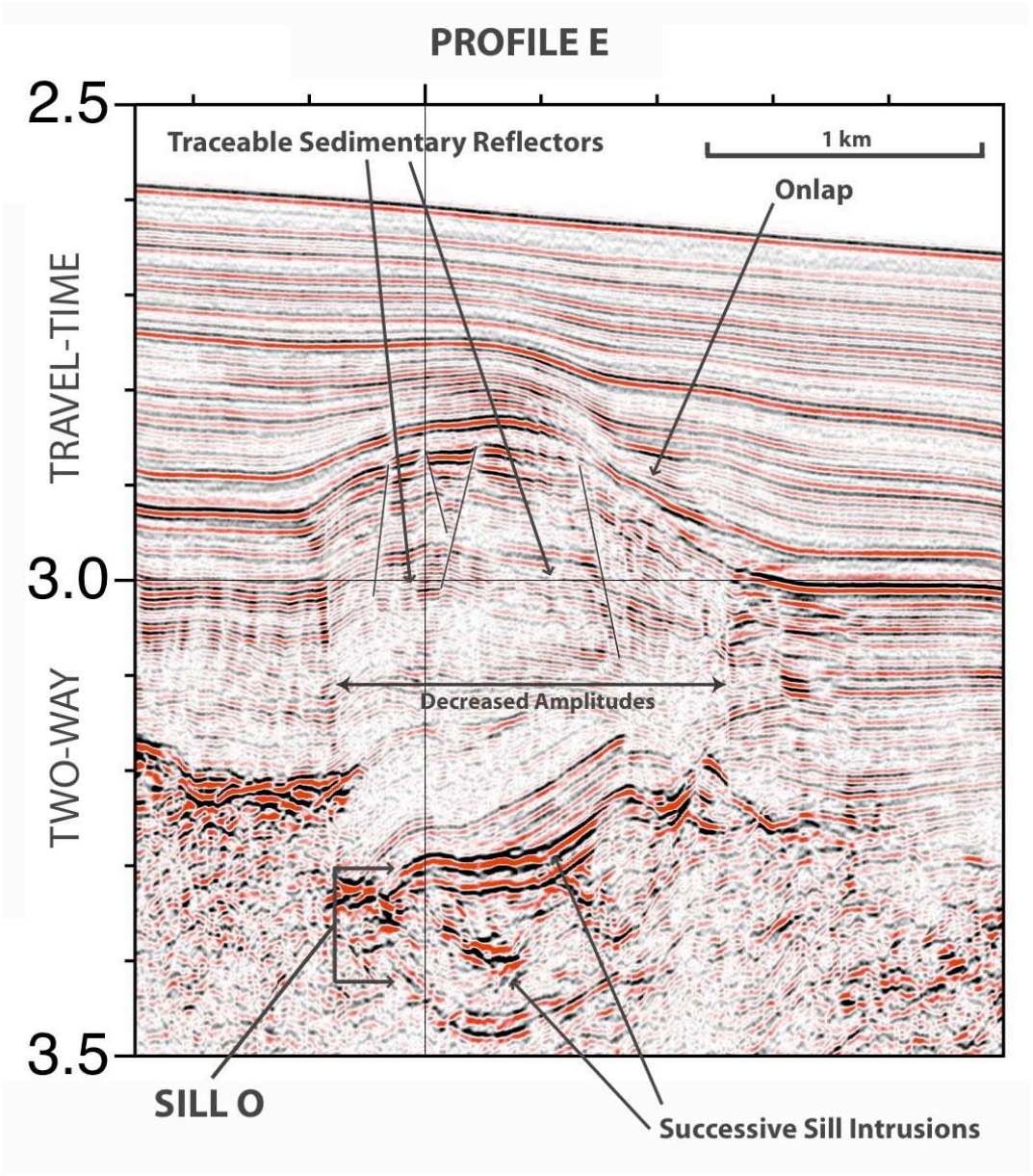
PROFILE E
2.5
3.0
3.5
TRAVEL-TIME
TWO-WAY
Traceable Sedimentary Reflectors
1 km
Onlap
Decreased Amplitudes
SILL O
Successive Sill Intrusions

Figure 3-9. MCS profile F. Seismic image (located on Figure 1) collected nearby profile E across western Farallon Basin. Profile shows evidence of a large sill intrusion, deformation mound with chaotic internal structure, and concentrated gas/hydrocarbons. Dashed black box highlights section of profile shown in zoomed-in image above. Zoomed-in image shows wiggle traces (in blue) and high-amplitude, clear negative polarity reflections (in yellow) indicating the presence of low-velocity material (i.e. gas/hydrocarbons). Note other evidence of gas/hydrocarbon concentrations: velocity pull-down, phase reversal, stacked brights, and a shallow bottom simulating reflector.

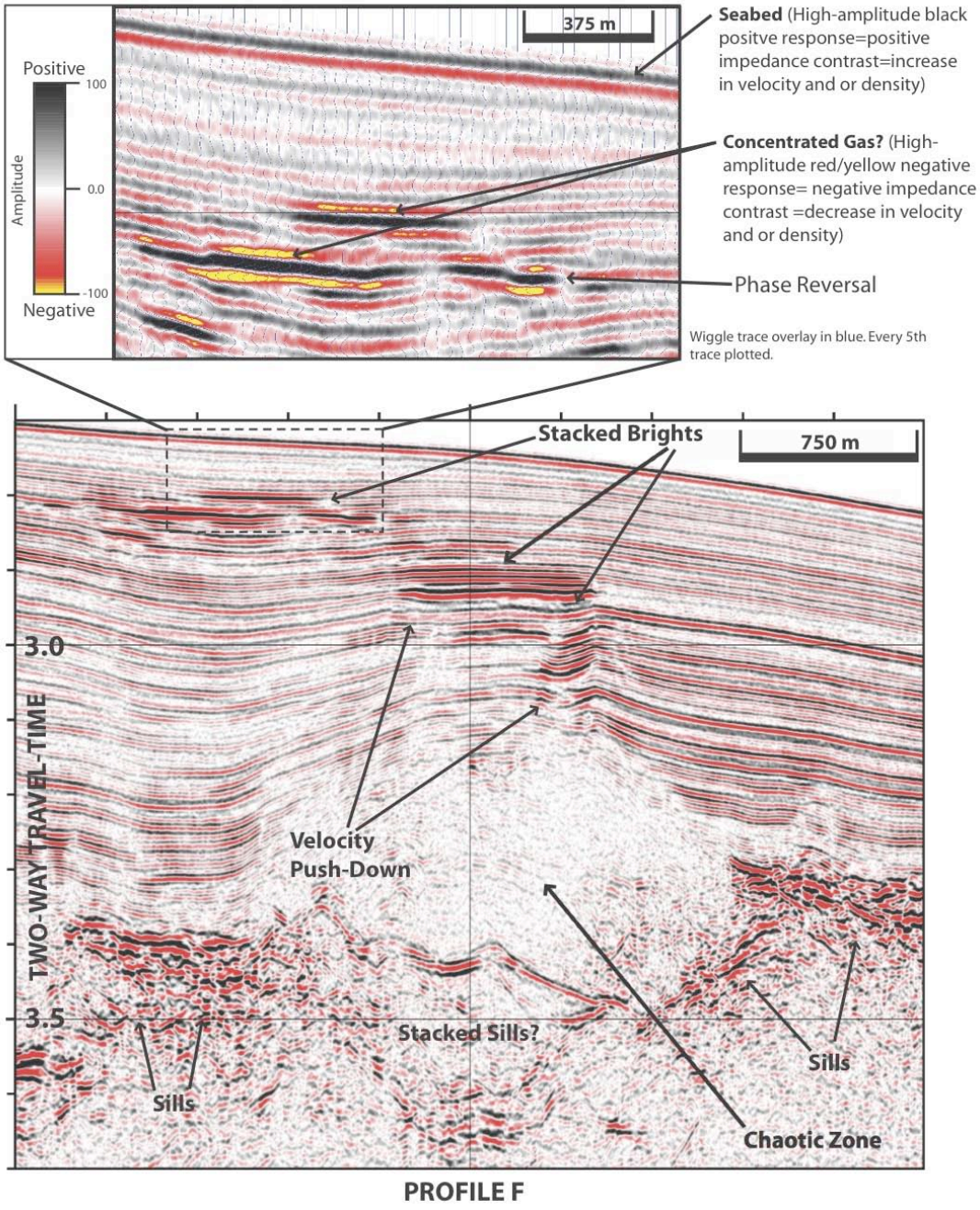
375 m
Positive
100
Amplitude
0.0
-100
Negative
Seabed (High-amplitude black positve response=positive impedance contrast=increase in velocity and or density)
Concentrated Gas? (High-amplitude red/yellow negative response= negative impedance contrast =decrease in velocity and or density)
Phase Reversal
Wiggle trace overlay in blue. Every 5th trace plotted.
Stacked Brights
750 m
3.0
TWO-WAY TRAVEL-TIME
Velocity Push-Down
3.5
Stacked Sills?
Sills
Sills
Chaotic Zone

PROFILE F

Figure 3-10. MCS profile G. Seismic profile (located on Figures 1 and 10) collected near Farallon Transform, west of south Carmen Basin. Profile G is superimposed on a 3D multibeam bathymetry image, crossing a mound-like feature, located directly over a large, concave upwards structure interpreted as a saucer-shaped magmatic sill (Sill E). Dashed black box outlines zoomed in area shown next to the 3D image. Dashed green line represents a datum across the sedimentary uplift mound and the dashed blue line represents the actual horizon, indicating at least 70 m of uplift. Note the upturned “wings” of the sill and how the overlying mound is circular-to-elliptical in shape, suggesting the presence of a circular-to-elliptical shaped sill below. VE = Vertical Exaggeration.

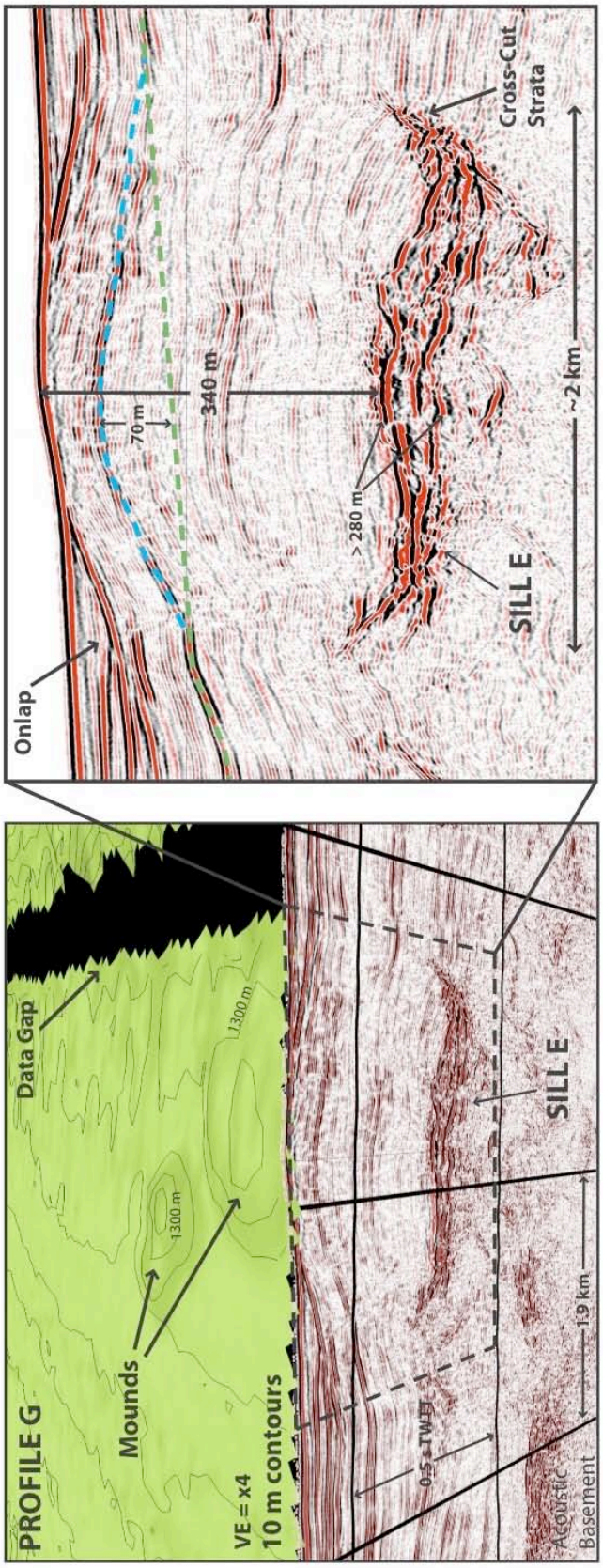
PROFILE G
Mounds
Data Gap
1300 m
1300 m
VE = x4
10 m contours
0.5 s TWTT
1.9 km
Acoustic Basement
SILL E
Onlap
70 m
340 m
> 280 m
Cross-Cut Strata
SILL E
~2 km

Figure 3-11. Bathymetric map of 3.5 kHz survey near Farallon Transform scarp. Dashed red circles outline multiple mound-like features (mounds A to I) imaged on the bathymetric map. The outlines of mounds with limited seafloor relief are based on evidence imaged on MCS profile G (Figure 9) and 3.5 kHz profiles (see Figure 11). Thick black arrows indicate 3D viewing direction on Figures 9 and 11.

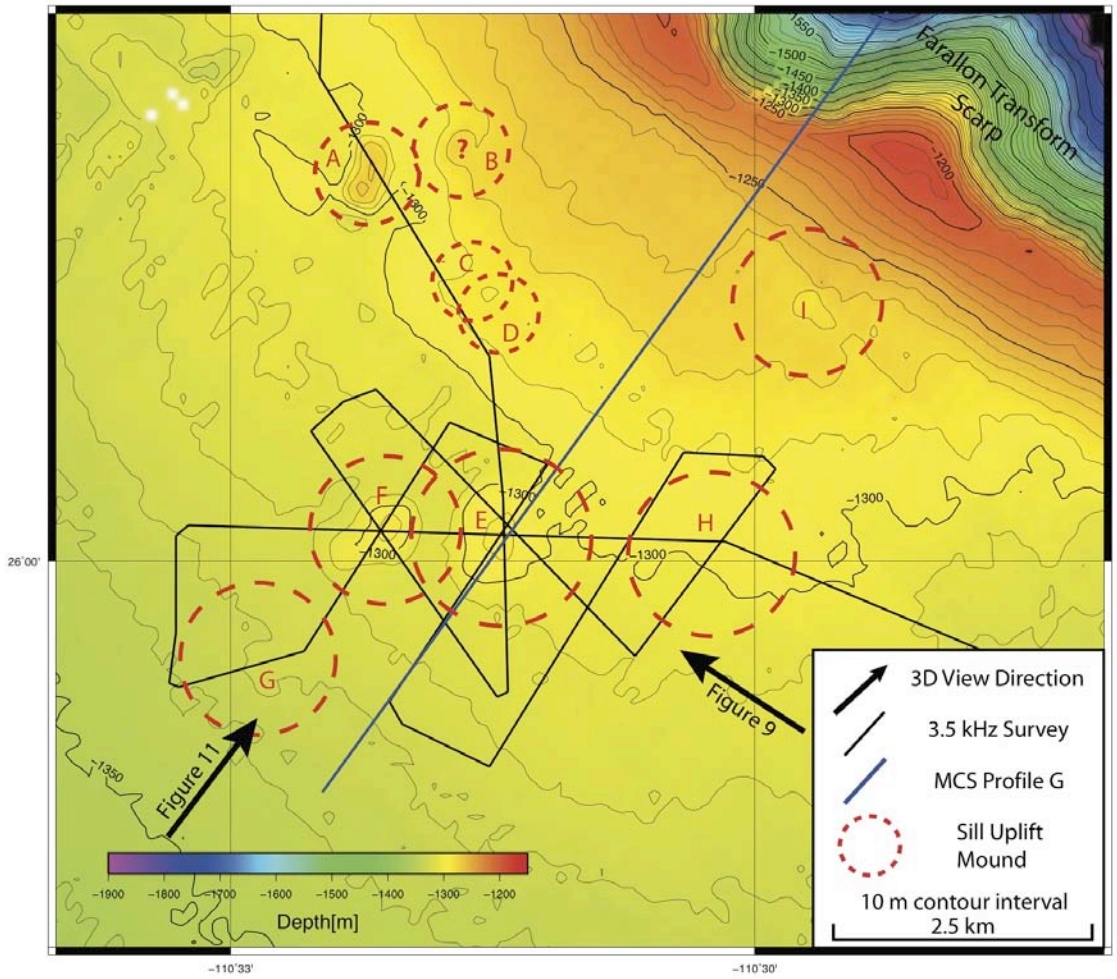
Farallon Transform
Scarp
A
B
C
D
E
F
G
H
I
Figure 11
Figure 9
3D View Direction
3.5 kHz Survey
MCS Profile G
Sill Uplift
Mound
10 m contour interval
2.5 km
Depth[m]
−1900 −1800 −1700 −1600 −1500 −1400 −1300 −1200
26°00'
−110°33'
−110°30'

Figure 3-12. 3D grid of the BEKL 3.5 kHz survey. 3.5 kHz profiles cross multiple mound-like features, most of which display acoustically blank internal structures. Mound E, imaged on MCS profile G (Figure 9) has four 3.5 kHz crossings, each showing a strong acoustic basement just below the seafloor. On profile G (Figure 9) this correlated to the upper sedimentary reflections and suggests the blank acoustic response on 3.5 kHz profiles is due to alteration of sediment and/or concentrations of gas. Each colored line represents the ‘deformation horizon’ imaged on each profile. Note how this horizon, imaged on all profiles, correlates to the timing of the formation of the mounds, with younger sediments onlapping this horizon.

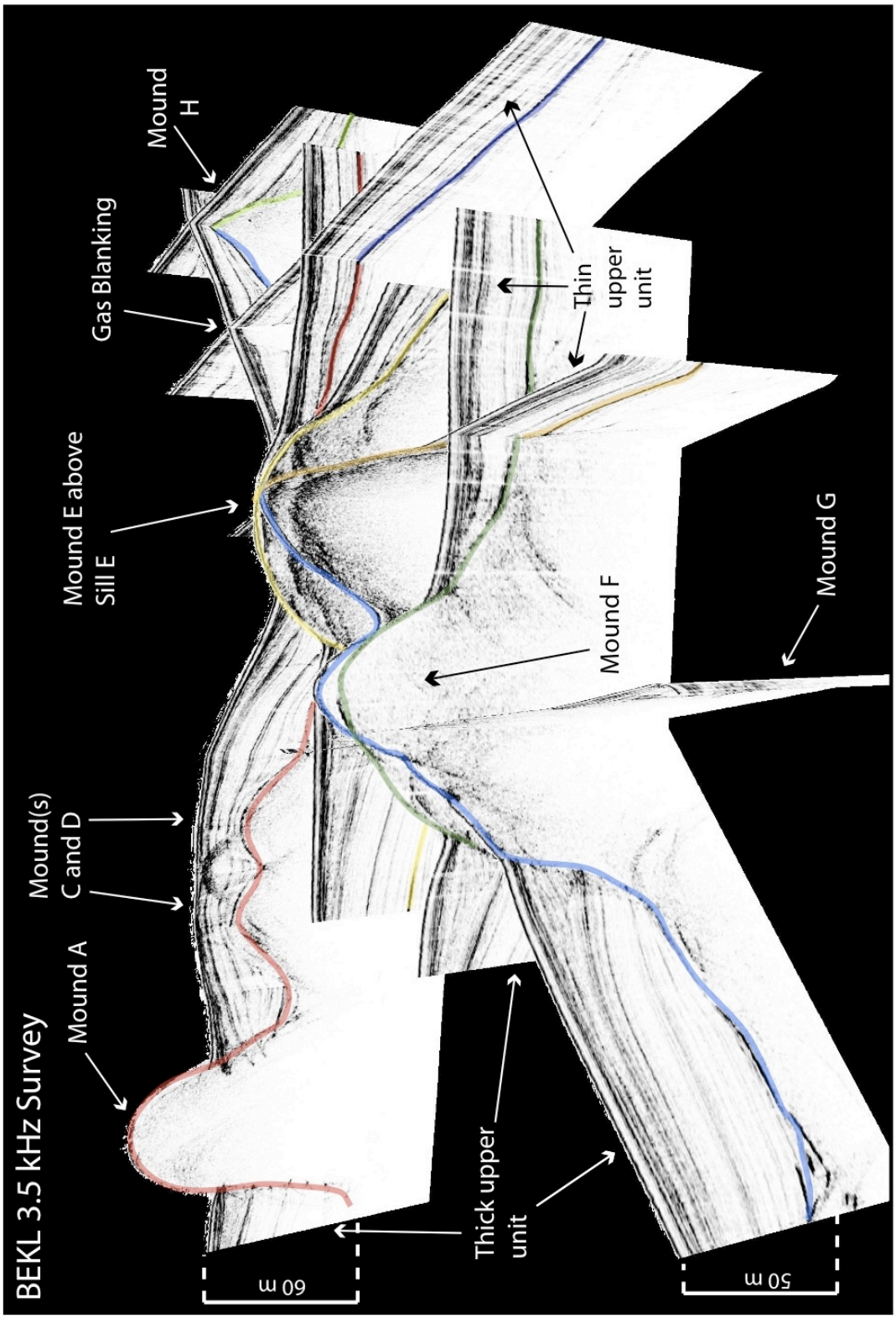
BEKL 3.5 kHz Survey
Mound A
Mound(s) C and D
Mound E above Sill E
Gas Blanking
Mound H
Thin upper unit
Mound F
Mound G
Thick upper unit
60 m
50 m

Figure 3-13. MCS profiles H and I. Seismic sections superimposed with 3D bathymetry near the junction of the Northern Trough of Guaymas Basin and Guaymas Transform. Location of profile shown in Figure 1. Near the crossing of profiles H and I is a large axial uplift mound previously named the Great North Hill (Lonsdale et al., 1980). On Profile I the mound has a relatively blank internal structure, with a strong concave upwards reflection directly below. Dashed black box on profile H outlines the zoomed in portion shown on Figure 20.

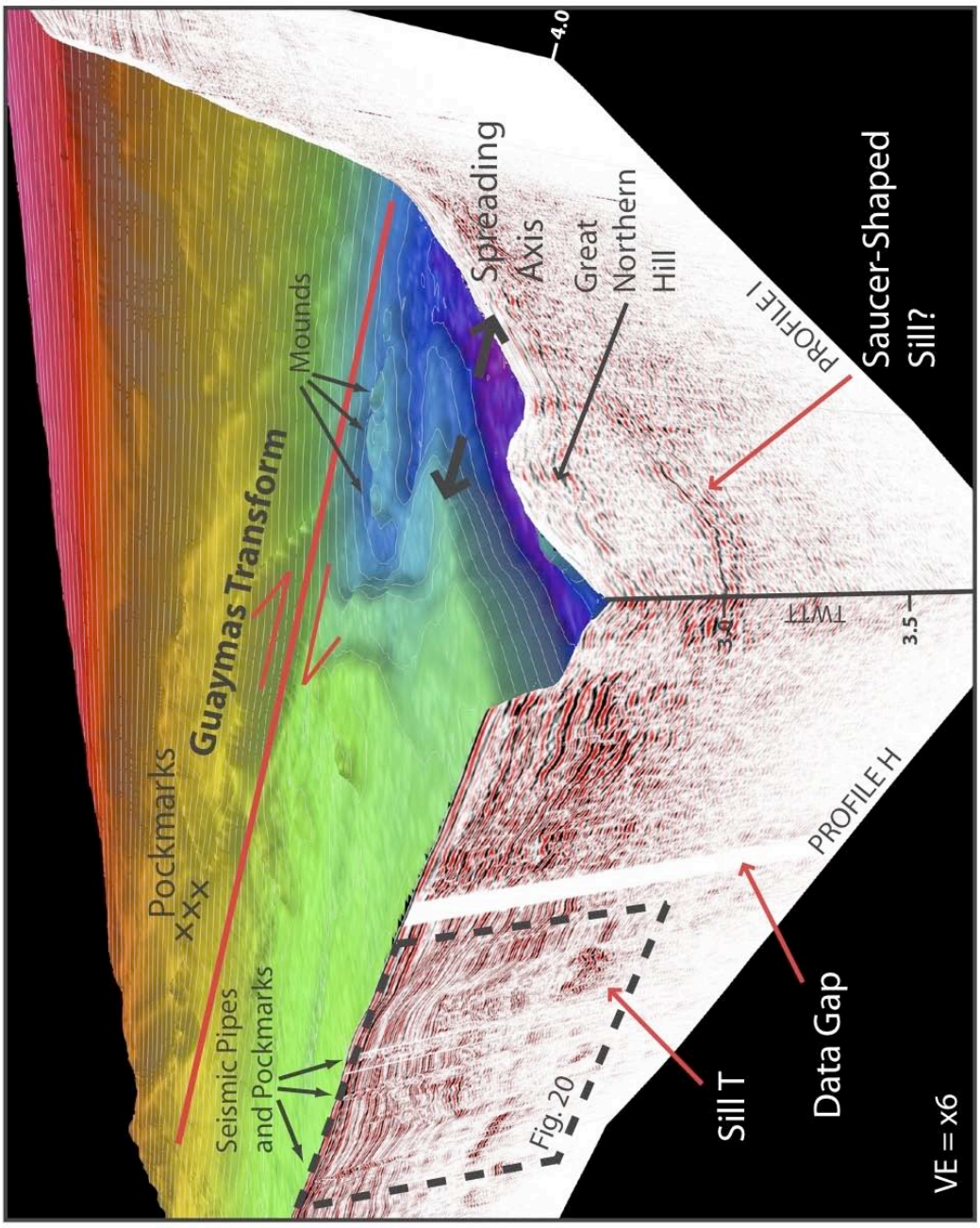
Pockmarks
Guaymas Transform
Mounds
Seismic Pipes
and Pockmarks
Spreading
Axis
Great
Northern
Hill
PROFILE I
Saucer-Shaped
Sill?
4.0
TWTT
3.5
Fig. 20
Sill T
Data Gap
PROFILE H
VE = x6

Figure 3-14. MCS profile M (located on Figure 1) collected near Farallon Transform on the western side of Farallon Basin. Black arrows point out faulted back-tilted continental crust, shallow sills, and the second return (multiple). Grey rectangle represents zone of uncertainty and black zigzag line represents the interpretation of the continental-oceanic boundary. NW = Northwest, SE = Southeast.

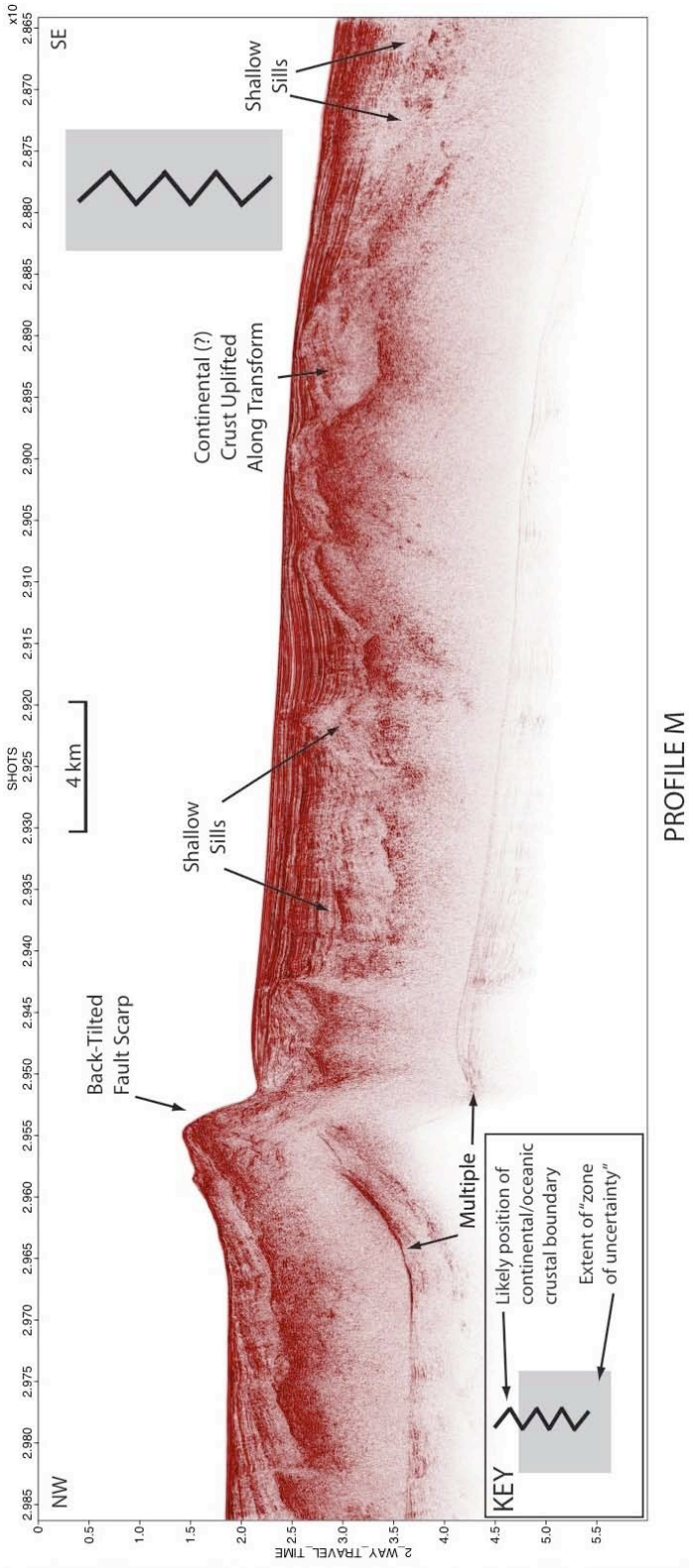
NW
SE
SHOTS
2_WAY_TRAVEL_TIME
x10
4 km
Back-Tilted
Fault Scarp
Shallow
Sills
Continental (?)
Crust Uplifted
Along Transform
Shallow
Sills
Multiple
KEY
Likely position of
continental/oceanic
crustal boundary
Extent of "zone
of uncertainty"

PROFILE M

Figure 3-15. MCS profile N (located on Figure 1) collected near the western edge of the western side of Farallon Basin. Black arrows point out trace of continental crust, shallow sills, gas-rich sediments, and the multiple. Grey rectangle represents zone of uncertainty and black zigzag line represents the interpretation of the continental-oceanic boundary Note the rapid change in sill depth and seismic response southeast of the interpreted boundary zone. NW = Northwest, SE = Southeast.

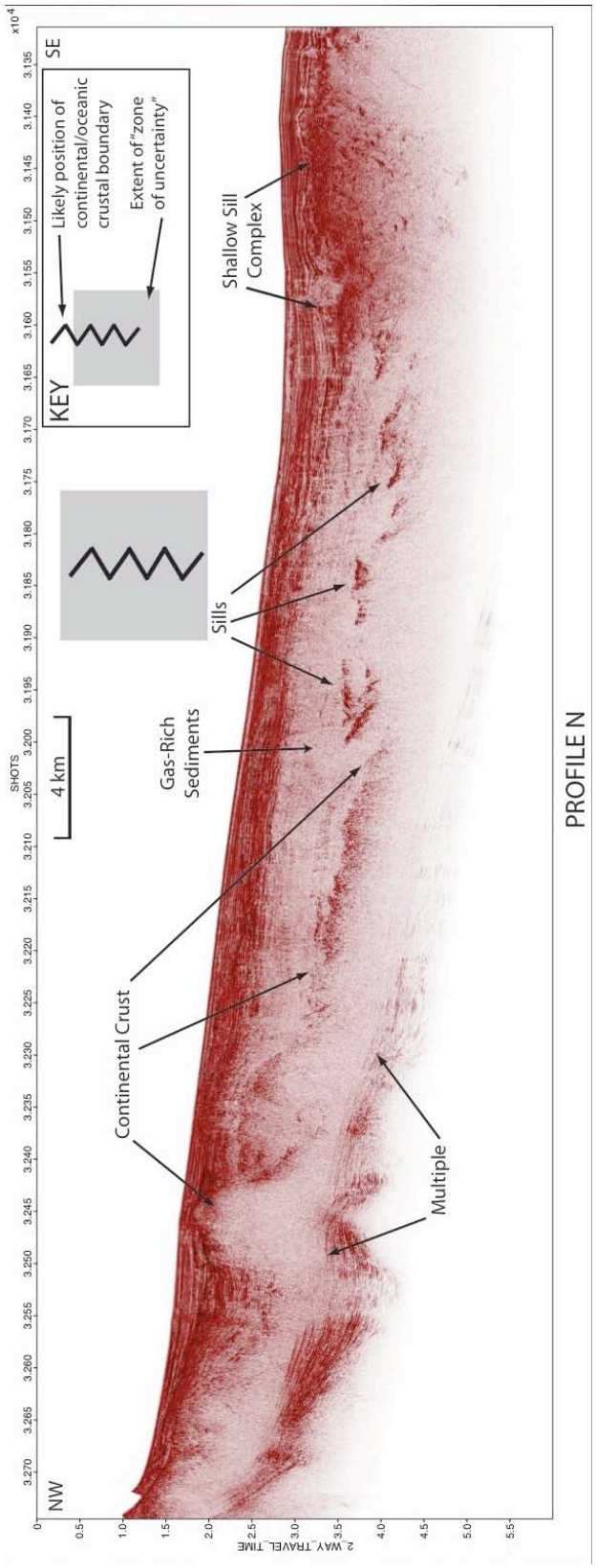
NW
SE
KEY
Likely position of continental/oceanic crustal boundary
Extent of "zone of uncertainty"
Shallow Sill Complex
Sills
Gas-Rich Sediments
Continental Crust
Multiple
4 km
SHOTS
2 WAY TRAVEL TIME
PROFILE N

Figure 3-16. MCS profile O (located on Figure 1) collected across the central part of western Farallon Basin. Black arrows point out trace of continental crust, shallow sills, and the multiple. Grey rectangle represents zone of uncertainty and black zigzag line represents the interpretation of the continental-oceanic boundary. Note the rapid change in sill depth and seismic response southeast of the interpreted boundary zone. NW = Northwest, SE = Southeast.

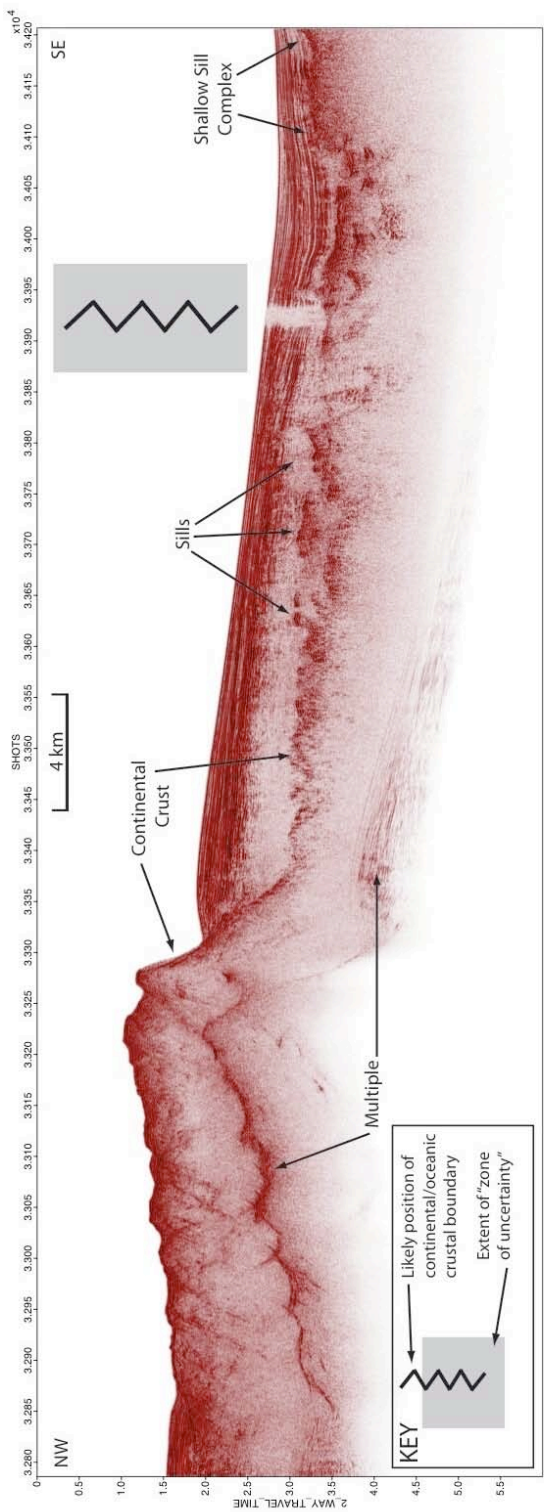
NW
SE
SHOTS
4 km
Continental Crust
Sills
Shallow Sill Complex
Multiple
KEY
Likely position of continental/oceanic crustal boundary
Extent of "zone of uncertainty"
2_WAY_TRAVEL_TIME
PROFILE O

Figure 3-17. MCS profile K (located on Figure 1) crosses a large crater located on a volcanic feature on the southeast side of north Pescadero spreading center. Somewhat continuous and layered high-amplitude reflections extending from the crater are interpreted as lava flows. Within the onlapped sedimentary section is a clear, negative polarity BSR, most likely related to sill-driven gas generation imaged nearby. Low amplitudes on the northeast end of the profile are contributed to a sharp change in course during collected of data. NE =Northeast, SW = Southwest.

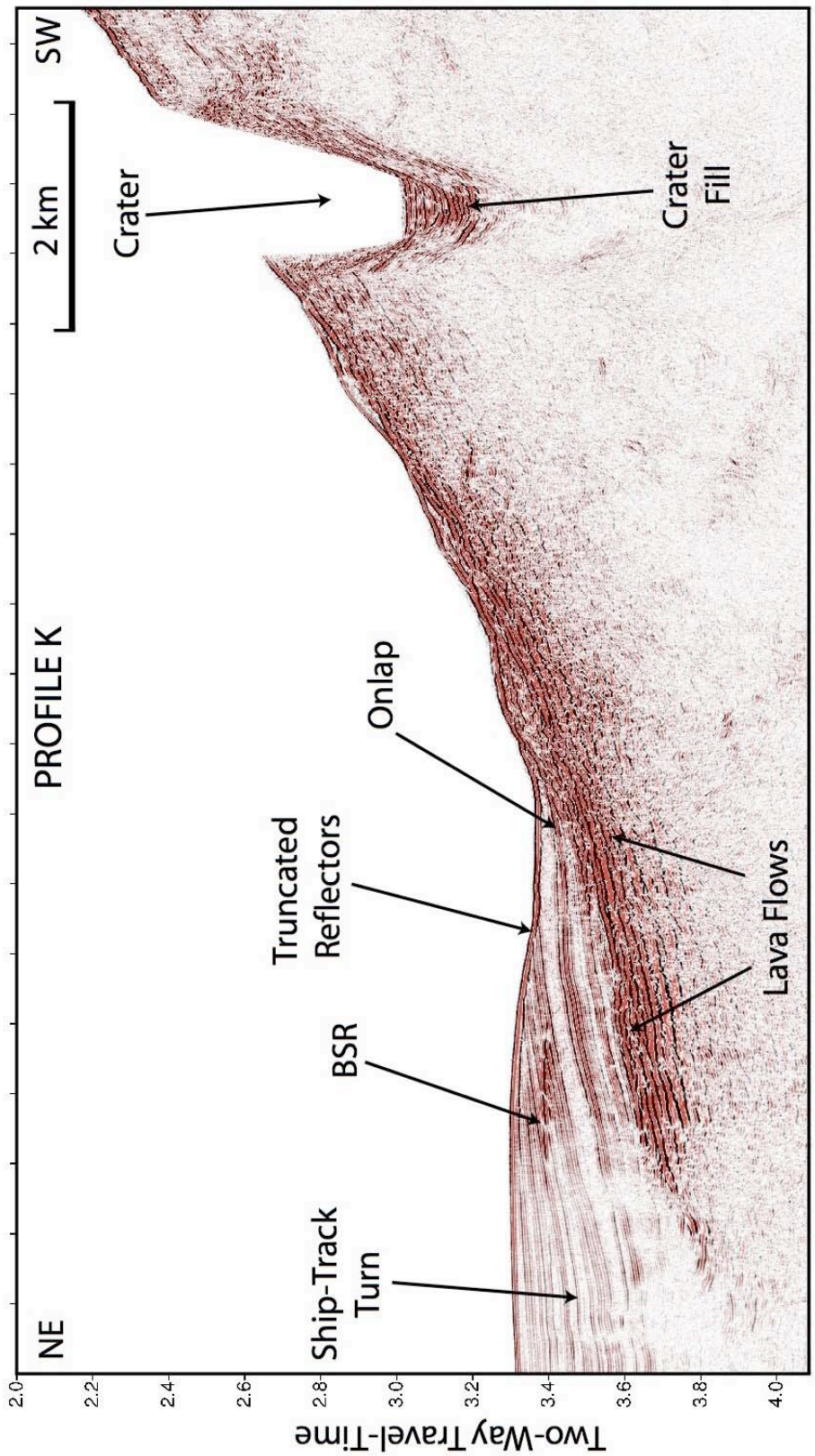
NE
SW
PROFILE K
2 km
Crater
Crater Fill
Onlap
Truncated Reflectors
BSR
Ship-Track Turn
Lava Flows
Two-Way Travel-Time
2.0
2.2
2.4
2.6
2.8
3.0
3.2
3.4
3.6
3.8
4.0

Figure 3-18. Plot of upturned sill width vs. emplacement depth. X and Y-axes are in meters, with Y-axis representing sill width and X-axis representing emplacement depth. As a general trend, sill width increases linearly with depth, with two distinct linear trends (R^2 = 0.8778 and R^2 = 0.75321). Sills (red triangles) appear to be clustered together based on geographic location, suggesting some sort of structural control linked to the basins. Red circles represent stacked sill complexes in which the sill had multiple internal reflections, suggesting a stacked sill complex with inter-bedded sediment layers. Sill locations are identified using colored circles.

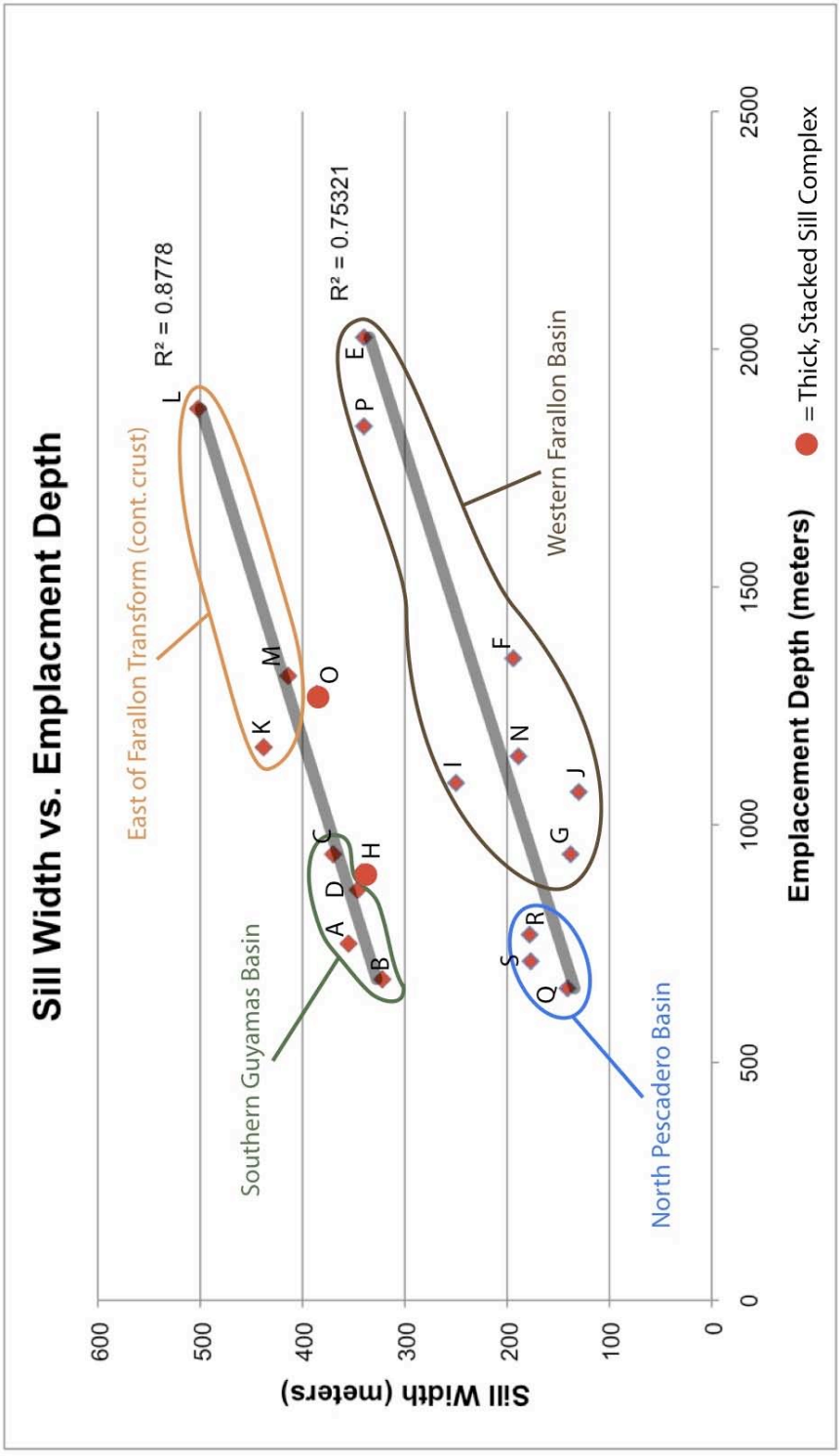
Sill Width vs. Emplacment Depth
Sill Width (meters)
Emplacement Depth (meters)
= Thick, Stacked Sill Complex
R² = 0.8778
R² = 0.75321
East of Farallon Transform (cont. crust)
Southern Guyamas Basin
Western Farallon Basin
North Pescadero Basin
A
B
C
D
E
F
G
H
I
J
K
L
M
N
O
P
Q
R
S
0
100
200
300
400
500
600
0
500
1000
1500
2000
2500

Figure 3-19. Bathymetric map located at the bend in the Northern Trough of Guaymas Basin. Map shows multiple axial uplift mounds, most of which are elongated along the axis. Red line across the axial trough represents the location of MCS profile J (Figure 15) collected onboard the *R/V EWING*. S = sulfur sample and T = talc sample collected by Lonsdale at el. (1980). 10 m isobaths.

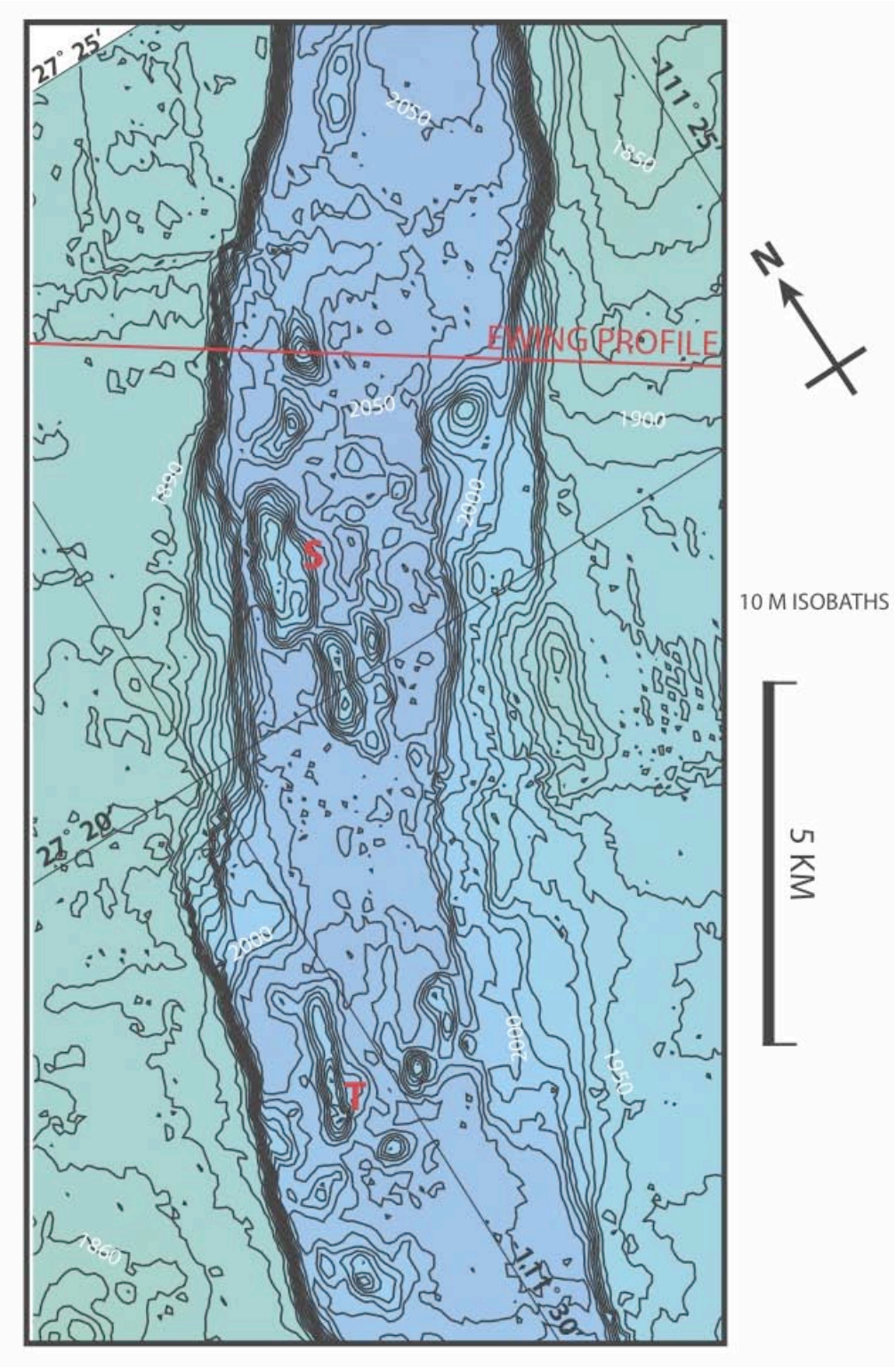
27° 25'
111° 25'
2050
1850
EWING PROFILE
2050
1900
1850
2000
S
10 M ISOBATHS
27° 20'
5 KM
2000
2000
1950
T
1850
111° 30'
N

Figure 3-20. MCS profile J. Seismic profile (location shown on Figure 14) crosses the North Trough of Guaymas Basin and has been taken and modified from Lizarralde et al. (2010). The profile crosses a sediment uplift mound (black arrow) located near the center of the axial floor and images a strong concave-upwards reflection (strong amplitudes in red and blue) directly below the mound, interpreted by Lizarralde et al. (2010) as a saucer-shaped sill. NW = Northwest, SE = Southeast.

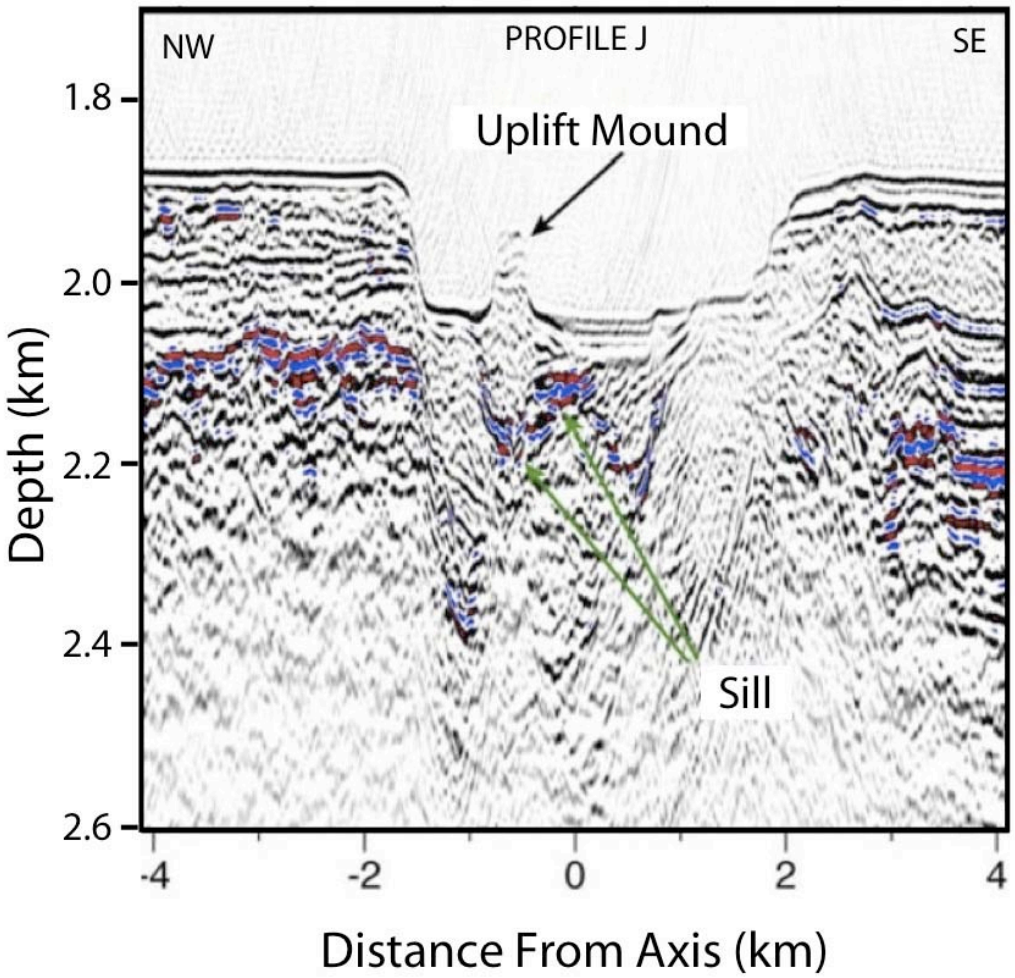
NW
PROFILE J
SE
Uplift Mound
Sill
Depth (km)
1.8
2.0
2.2
2.4
2.6
-4
-2
0
2
4
Distance From Axis (km)

Figure 3-21. Boundary element based model panels A, B and C. A: Perspective view of model setup with circular horizontal sill, 2 km in diameter, described by discrete elements in a boundary element based model. The vertical observation plane cuts through the center of the sill. B: Distribution of opening across the sill, showing maximum dilation (~280 m) at the center (dark orange). C: Vertical displacements at the surface (max. ~230 m above the sill center).

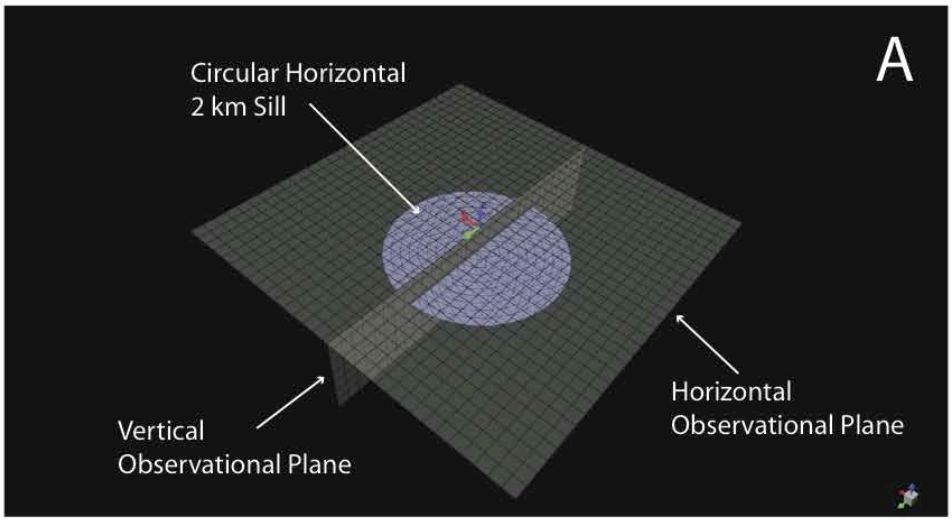
A
Circular Horizontal
2 km Sill
Vertical
Observational Plane
Horizontal
Observational Plane

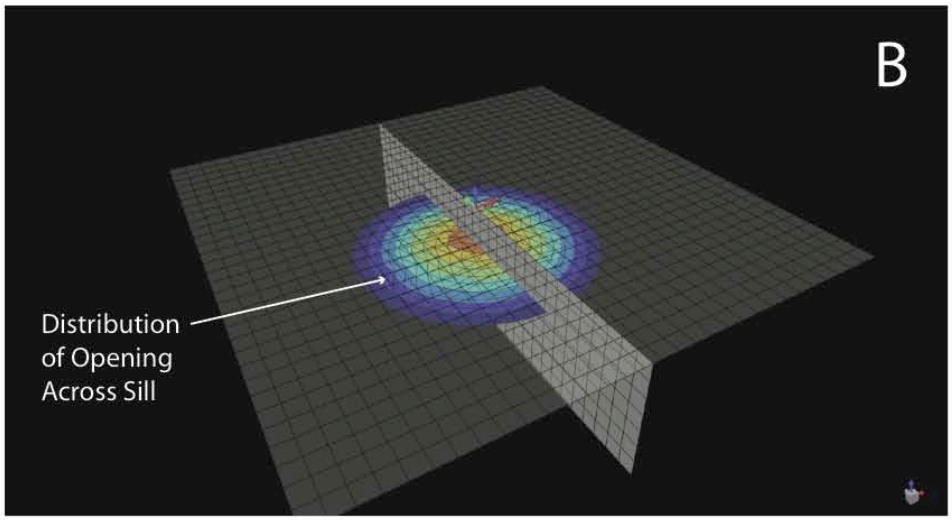
B
Distribution
of Opening
Across Sill

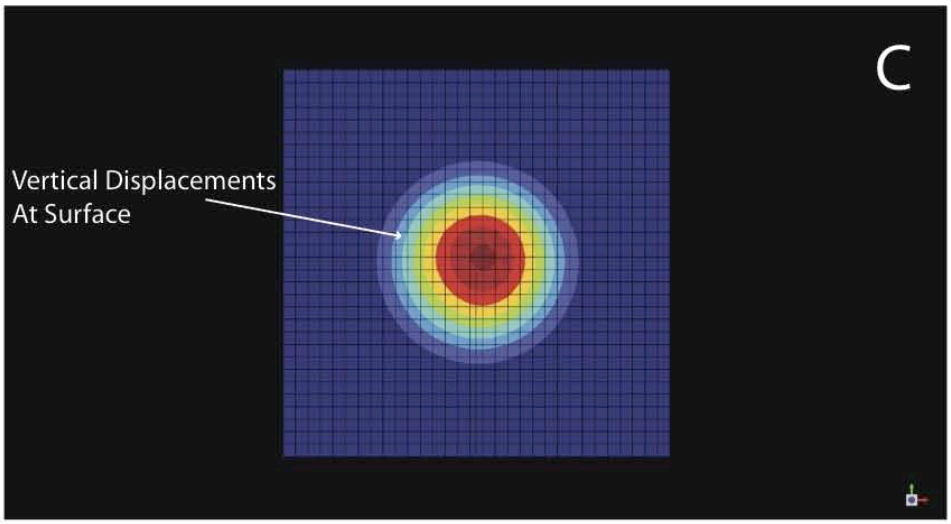
C
Vertical Displacements
At Surface

Figure 3-22. Boundary element based model panels D, E, and F. D: Vertical displacements on the vertical observation plane (outline of sill in profile view visible as black ellipse). E: Distribution of maximum compressive stress (S3) magnitude on the vertical observation plane. Note zones of tension (red colors) slightly above the tip zone of the sill and zones of compression at the surface above the tip zone as well as immediately above the center of the sill (blue colors). Units are megapascals (MPa). F: Distribution of maximum compressive stress (S3) magnitude on the horizontal observation plane at the earth's surface. Note zones of tension (red colors) above the center of the sill and a ring of compression at the surface above the tip zone (blue colors). Units are megapascals (MPa). Additionally, program uses a sign convention in which tensile stresses are positive in magnitude. Maximum compressive stress is S3 and maximum tensile stress is S1

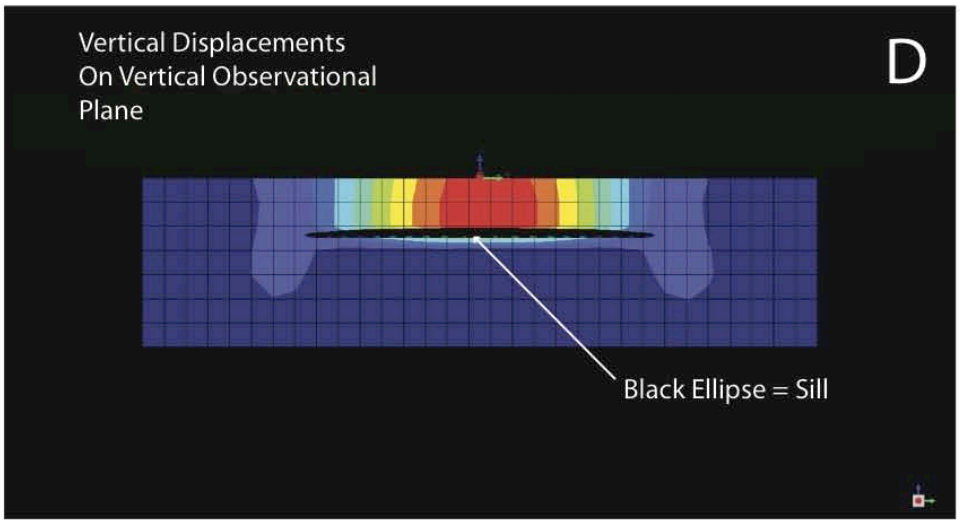
Vertical Displacements
On Vertical Observational
Plane
D
Black Ellipse = Sill

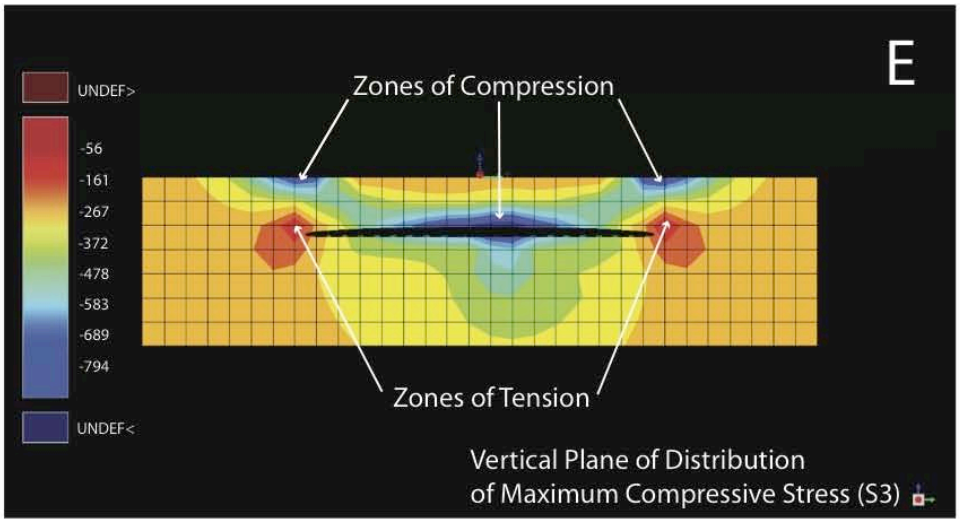
E
UNDEF>
-56
-161
-267
-372
-478
-583
-689
-794
UNDEF<
Zones of Compression
Zones of Tension
Vertical Plane of Distribution
of Maximum Compressive Stress (S3)

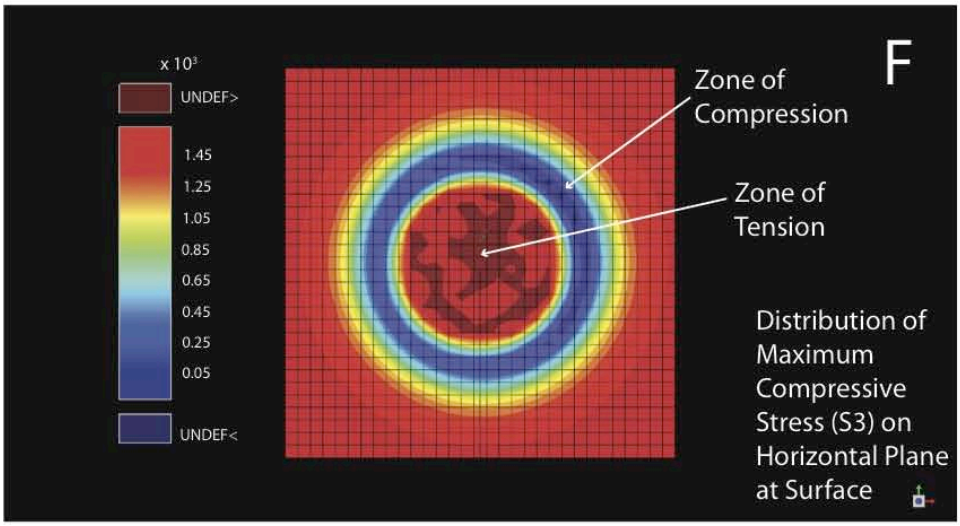
F
x 10³
UNDEF>
1.45
1.25
1.05
0.85
0.65
0.45
0.25
0.05
UNDEF<
Zone of
Compression
Zone of
Tension
Distribution of
Maximum
Compressive
Stress (S3) on
Horizontal Plane
at Surface

Figure 3-23. Sill emplacement model panels A, B, C, D, E, and F. A: Illustration showing the initial stage in sill emplacement. A magmatic feeder rises to a level of neutral buoyancy within the sedimentary cover. B: Once level of neutral buoyancy is reached, magma begins to spread laterally within the host strata forming a sill and a contact aureole (zone of sediment alteration). C: Magma spreads laterally forming a chilled outer layer and the sill thickens. When expulsion of pore-waters can no longer make enough room for the injecting magma the sill displaces the overburden (sedimentary uplift). At this point, stress fields above the sill become asymmetrical and zones of tension form above the sill tips (see Figure 17E) and magma preferentially migrates upwards into the zones of tension, forming inclined “wings”. D: Magma migrates upwards until it is capped by a zone of compression, at which point magma again begins to spread laterally away from the source. E: The process starts over, eventually forming a smaller (based on Figure 13) sill with upturned wings. F: Eventually this system dies and is buried by younger sediments, producing onlap on the uplift mounds.

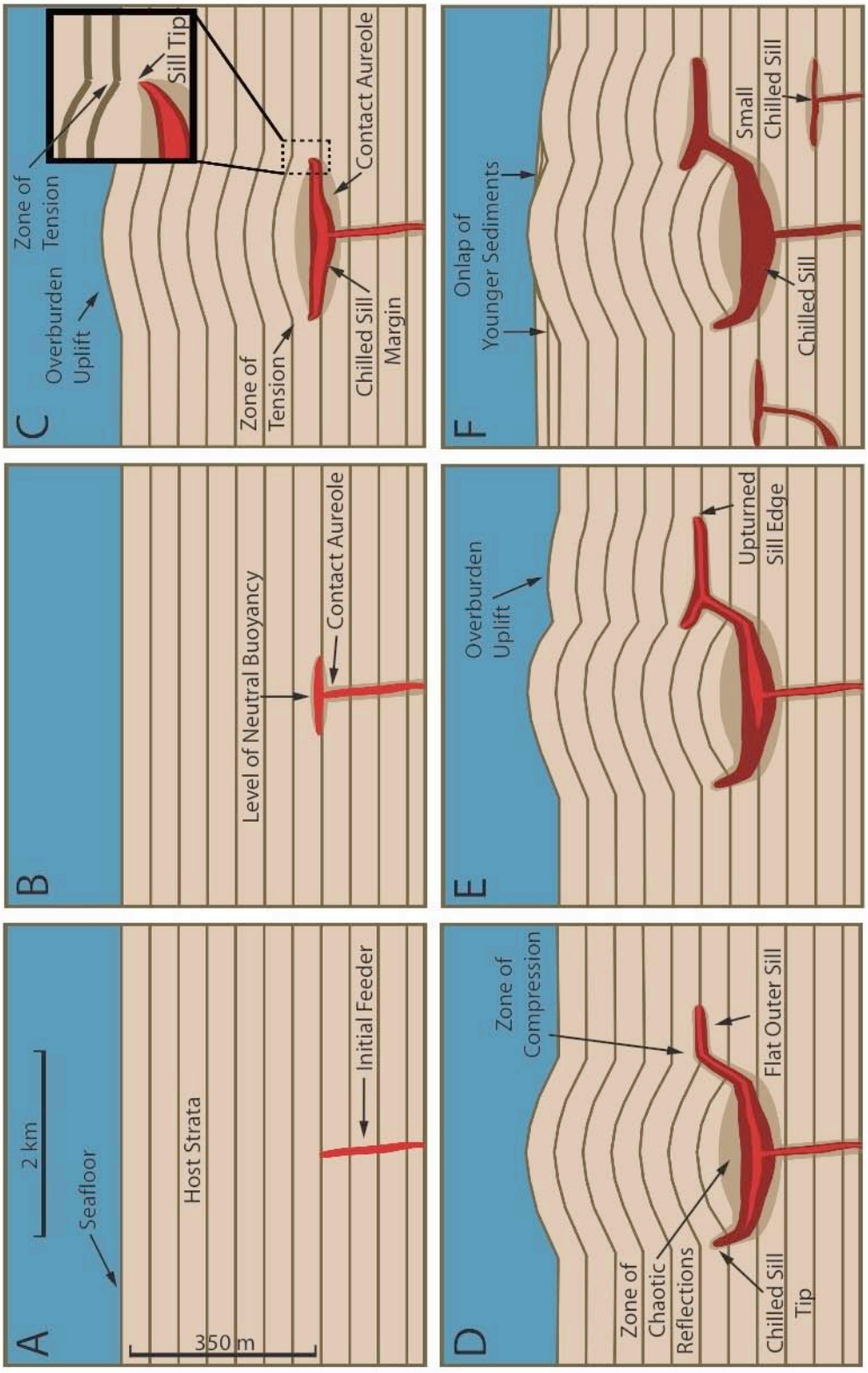
A
2 km
Seafloor
Host Strata
350 m
Initial Feeder
B
Level of Neutral Buoyancy
Contact Aureole
C
Zone of Overburden Uplift
Tension
Sill Tip
Zone of Tension
Contact Aureole
Chilled Sill Margin
D
Zone of Compression
Zone of Chaotic Reflections
Chilled Sill Tip
Flat Outer Sill
E
Overburden Uplift
Upturned Sill Edge
F
Onlap of Younger Sediments
Small Chilled Sill
Chilled Sill

Figure 3-24. MCS profile P (located on Figures 1 and 31) taken across the axial trough of Farallon Basin. Profile shows evidence of shallow sill intrusion bellow the axial floor and asymmetrical sill horizons on the rift shoulder flanks. Note the thick sediment load on the southeast flank of the axis versus the thin sediment cover on the northwest flank. Black lines highlight fault traces. NW = Northwest, SE = Southeast, VE = Vertical Exaggeration.

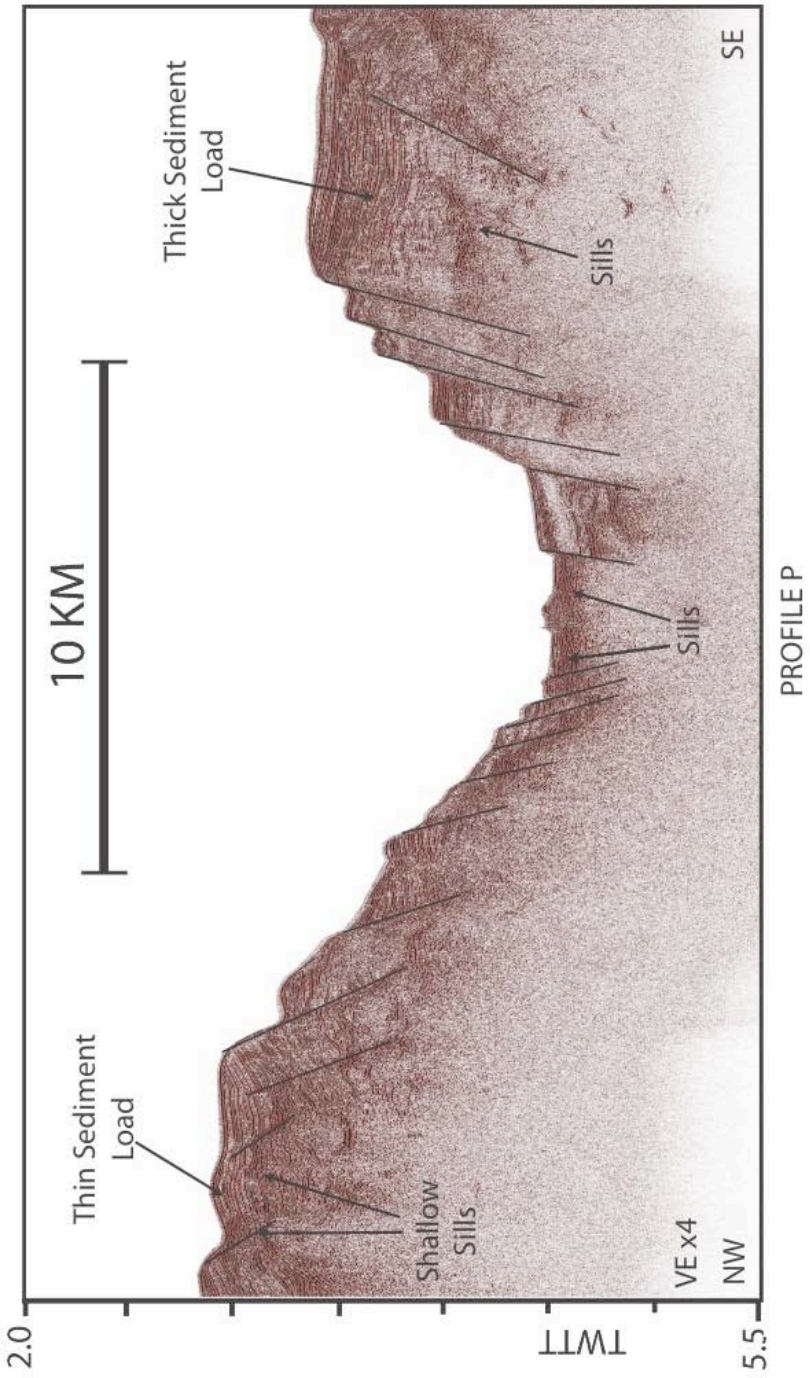
Thin Sediment Load
Shallow Sills
Thick Sediment Load
Sills
Sills
10 KM
NW
VE x4
SE
2.0
TWTT
5.5
PROFILE P

Figure 3-25. MCS profile H and analog 3.5 kHz profile. Below: Reprocessed MCS profile H (located on Figure 1 and shown on Figure 12) collected west of the Northern Trough of Guaymas Basin during the site survey for DSDP Leg 64. Dashed blue box outlines portion shown in Figure 21. Note near-vertical zones of seismic disturbance interpreted as pipe-like fluid-flow conduits. Above: Analog 3.5 kHz profile collected simultaneously with MCS profiles during site survey. Profile shows three pockmarks and acoustic blanking below that linkup with near vertical zones of seismic disturbance below. Note how the seafloor is not imaged across two of the pockmarks, possibly indicating active fluid venting.

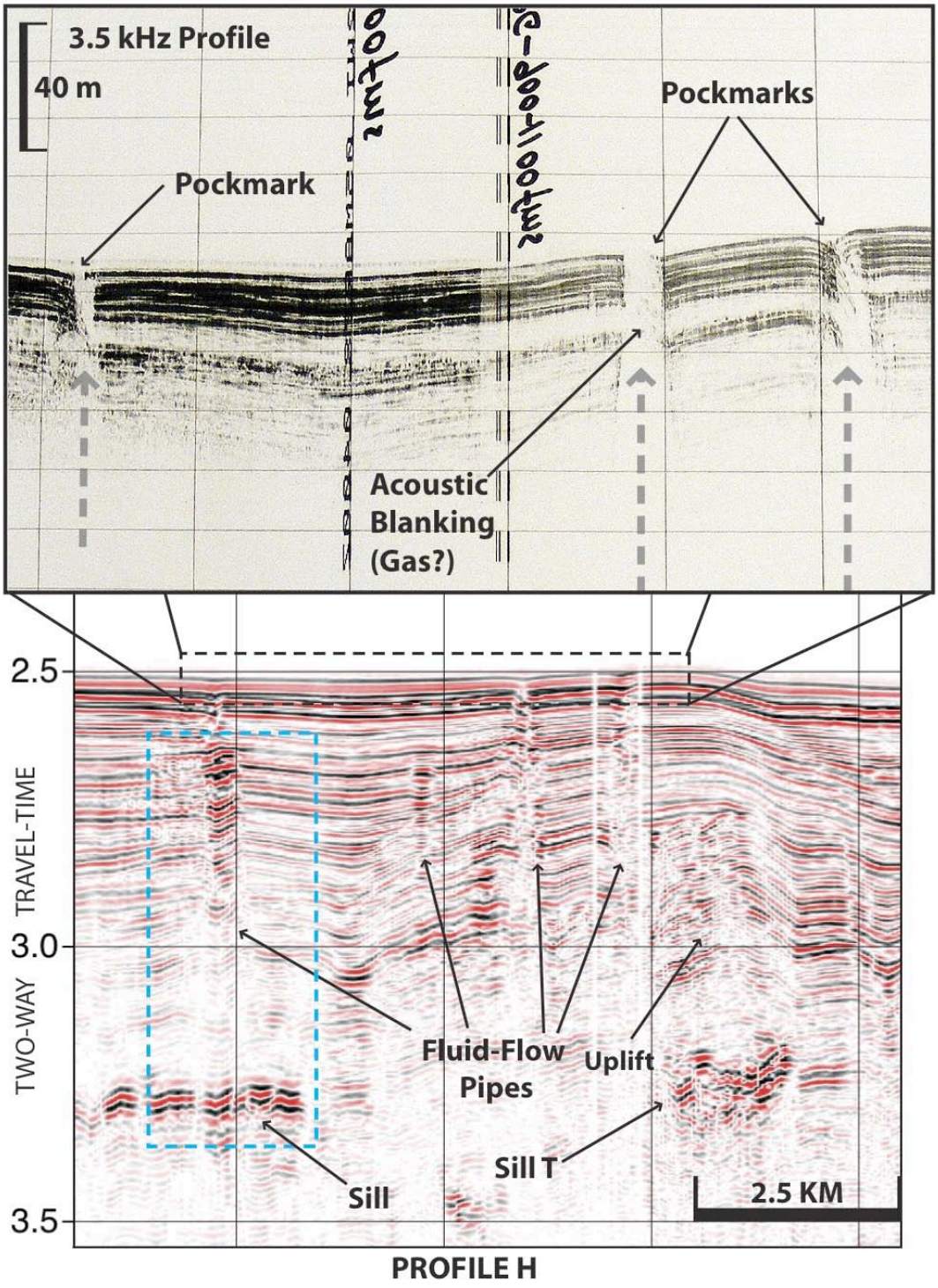
3.5 kHz Profile
40 m
Pockmark
Pockmarks
Acoustic
Blanking
(Gas?)
2.5
3.0
3.5
TWO-WAY TRAVEL-TIME
Fluid-Flow
Pipes
Uplift
Sill
Sill T
2.5 KM
PROFILE H

Figure 3-26. Fluid-flow model panels A, B, C, and D. A: Portion of profile H outlined in Figure 20. Zoomed in image shows a near-vertical zone of disturbance, up to 500 m wide and over 400 m tall, extending upwards from a positive polarity, high-amplitude reflection interpreted as a magmatic sill. Grey ellipse indicates the contact aureole, dashed blue arrows indicate fluid-flow direction, and dashed green line traces a reflector across the zone of disturbance. Note the stacked high-amplitudes near the top of the zone of disturbance and the push-down of reflections directly below. B and C: Time-lapse seismic profiles displaying the effect of prolonged CO_2 injection into the Utsira Formation sandstone (North Sea). Images show pre-CO_2 injection (B) and 5 years post CO_2 injection (C). IP = Injection Point. The second profile (C) was collected in 1999 after 2.3 million tons of CO_2 had been injected. Main change in seismic characteristics after injection of CO_2 was development of stacked high-amplitude reflections in the sandstone layers of the Utsira Formation. Push-down of reflectors below the stacked brights is caused by overlying concentrations of low-velocity CO_2 (Eiken et al., 2000, Løseth et al., 2008). D: Model of proposed sill-driven hydrofracturing and fluid-flow.

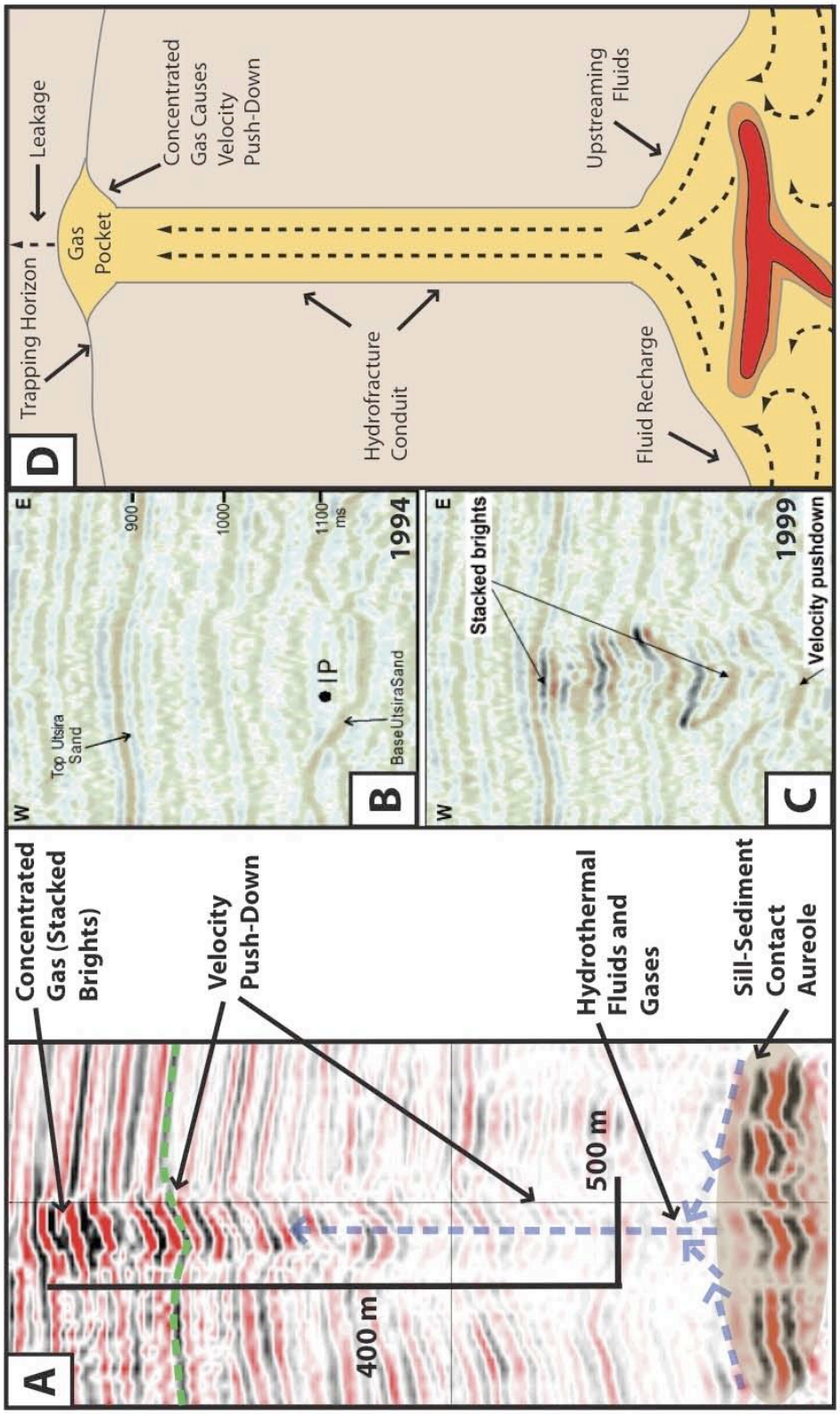
A
Concentrated Gas (Stacked Brights)
Velocity Push-Down
Hydrothermal Fluids and Gases
Sill-Sediment Contact Aureole
500 m
400 m
B
W
E
Top Utsira Sand
900
1000
1100 ms
IP
BaseUtsiraSand
1994
C
W
E
Stacked brights
Velocity pushdown
1999
D
Trapping Horizon
Leakage
Gas Pocket
Concentrated Gas Causes Velocity Push-Down
Upstreaming Fluids
Hydrofracture Conduit
Fluid Recharge

Figure 3-27. 3D cutaway of MCS profile M. A: MCS profile M (located on Figure 1) across the Southern Trough of Guaymas Basin superimposed below a 3D bathymetric grid. Dashed black box outlines zoomed-in portion of profile M displayed to the right. Red Xs indicate location of drilling sites. VE = Vertical Exaggeration. Note extensive faulting along the axial walls and below the rift shoulders. B: Zoomed in section of profile M along the southern rift wall. Black line traces major normal fault and blue arrows indicate direction of hydrothermal fluid migration. Note the high-amplitude, eye-shaped feature imaged alongside the fault trace and the stacked brights below and off to the side.

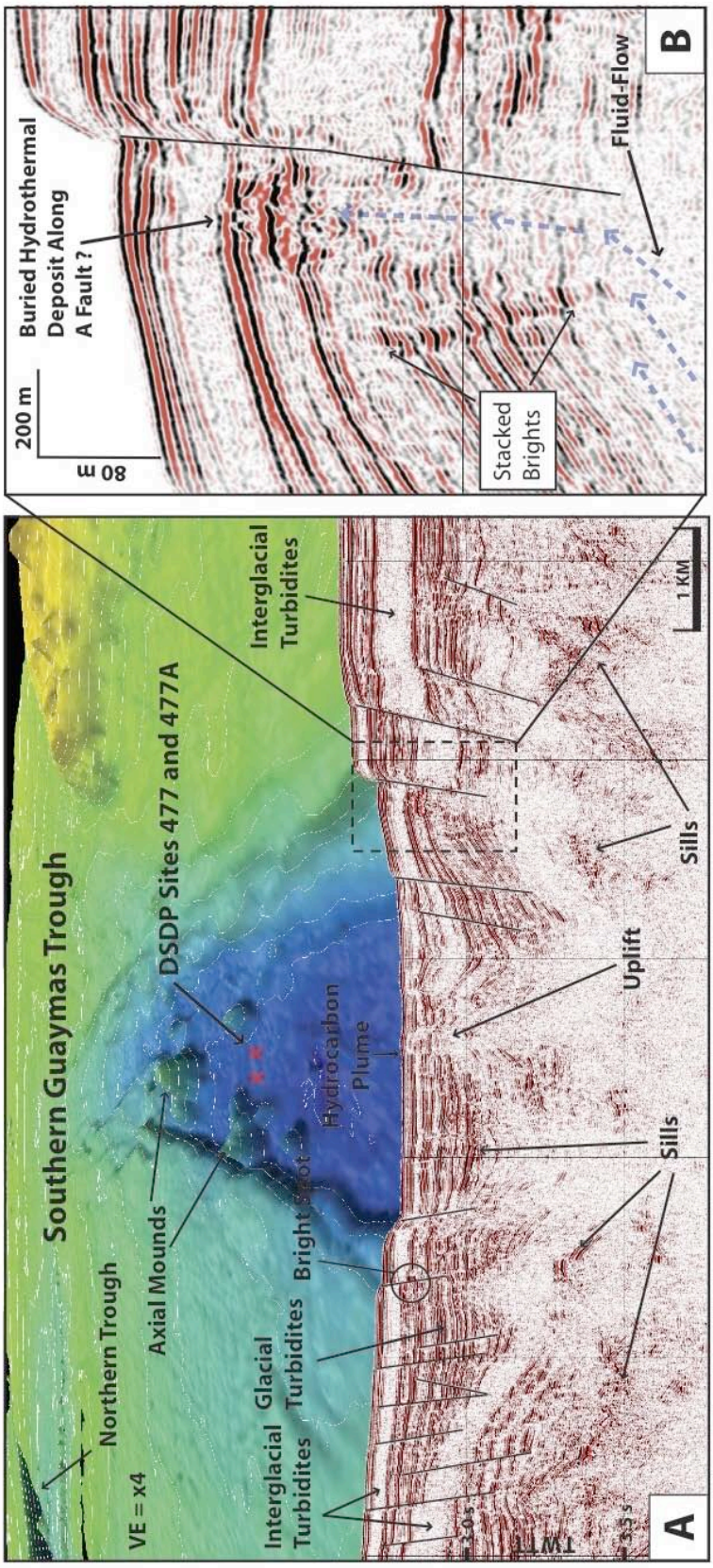
Southern Guaymas Trough
Northern Trough
VE = x4
Axial Mounds
DSDP Sites 477 and 477A
Interglacial Turbidites
Glacial Turbidites
Interglacial Turbidites
Bright Spot
Hydrocarbon Plume
Uplift
Sills
Sills
1 KM
A
TWT
2.0 s
3.0 s
Buried Hydrothermal Deposit Along A Fault ?
200 m
80 m
Stacked Brights
Fluid-Flow
B

PROFILE M

Figure 3-28. MCS profile L. Profile (located on Figure 1) shows evidence of fluid-flow and gas concentrations in La Paz Basin. Blanking in seismic amplitudes along fault traces indicates fluid-flow along fault planes. High-amplitude, negative polarity reflections terminating against fault traces are interpreted as bright spots, most likely caused by concentrations of hydrocarbons and/or other gases.

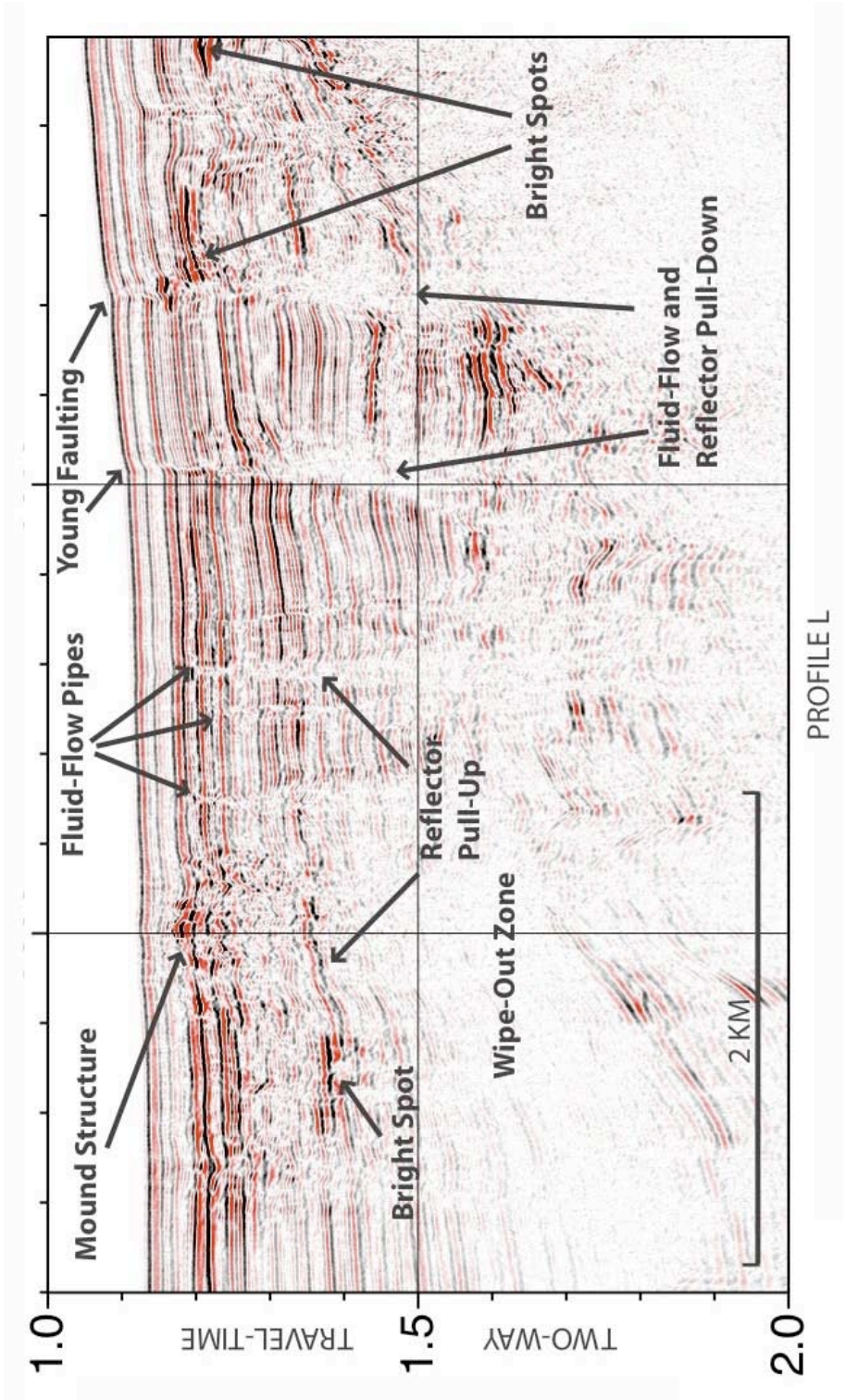
Mound Structure
Fluid-Flow Pipes
Young Faulting
Bright Spots
Fluid-Flow and
Reflector Pull-Down
Bright Spot
Reflector
Pull-Up
Wipe-Out Zone
2 KM
1.0
1.5
2.0
TRAVEL-TIME
TWO-WAY
PROFILE L

Figure 3-29. Subsection of profile F. Dashed green line traces a reflector across the profile, highlighting push-down spots caused by concentrated zones of low velocity material above. Black arrows point out evidence of sill intrusion, fluid-flow, and bright spots (gas/hydrocarbons). Note the clear negative polarity of the labeled bright spots, the flat nature, and associated acoustic turbidity below.

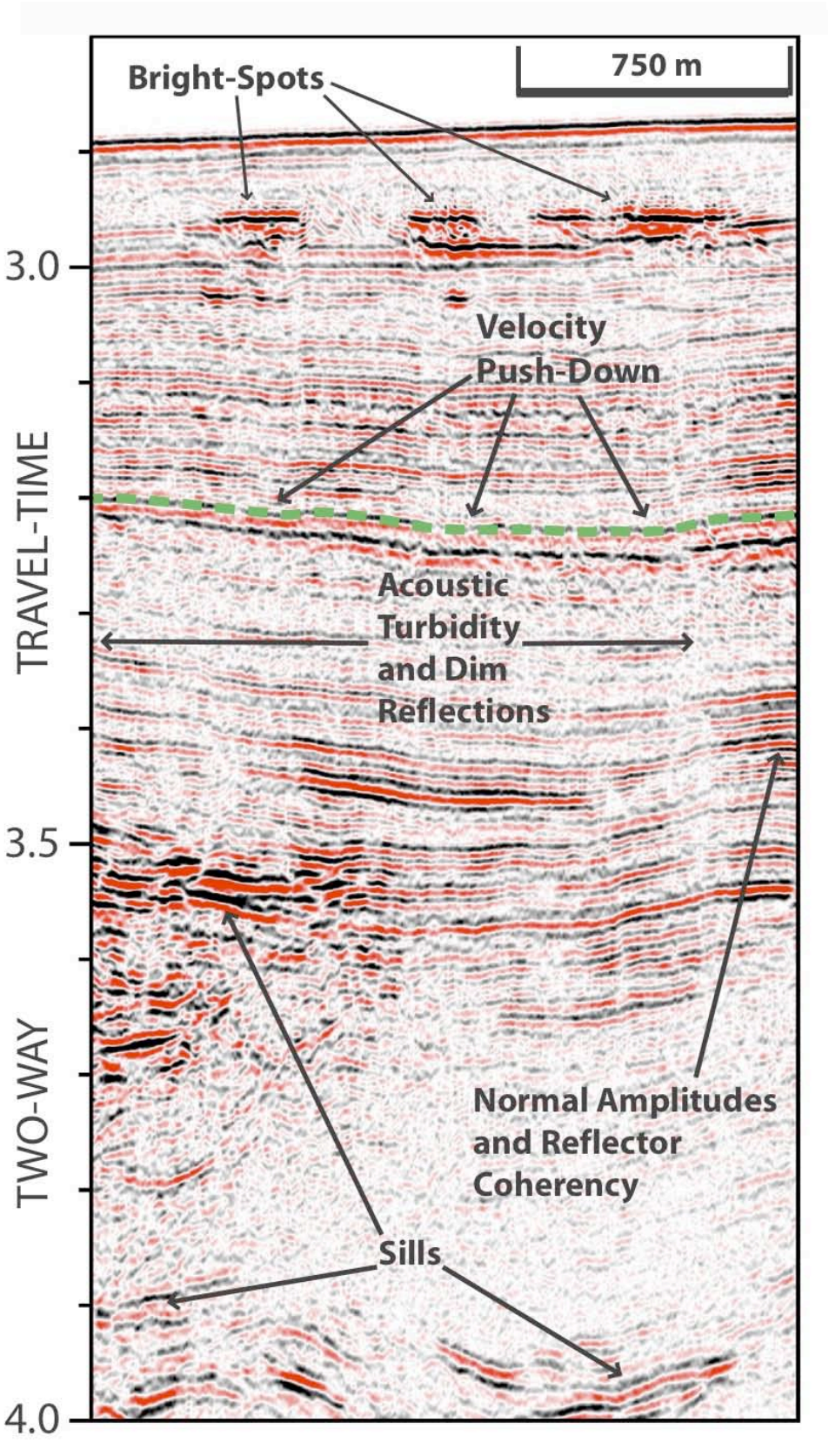
750 m
Bright-Spots
3.0
Velocity
Push-Down
TRAVEL-TIME
Acoustic
Turbidity
and Dim
Reflections
3.5
TWO-WAY
Normal Amplitudes
and Reflector
Coherency
Sills
4.0

Figure 3-30. 3.5 kHz profile southwest of Carmen Axis. Profile shows extensive evidence of fluid-flow and shallow gas concentration in sediments. Note the stair-stepping gas, vertical zones of acoustic blanking, mound-like features, and an “eye” shaped feature just below the seafloor. BSR = Bottom Simulating Reflector.

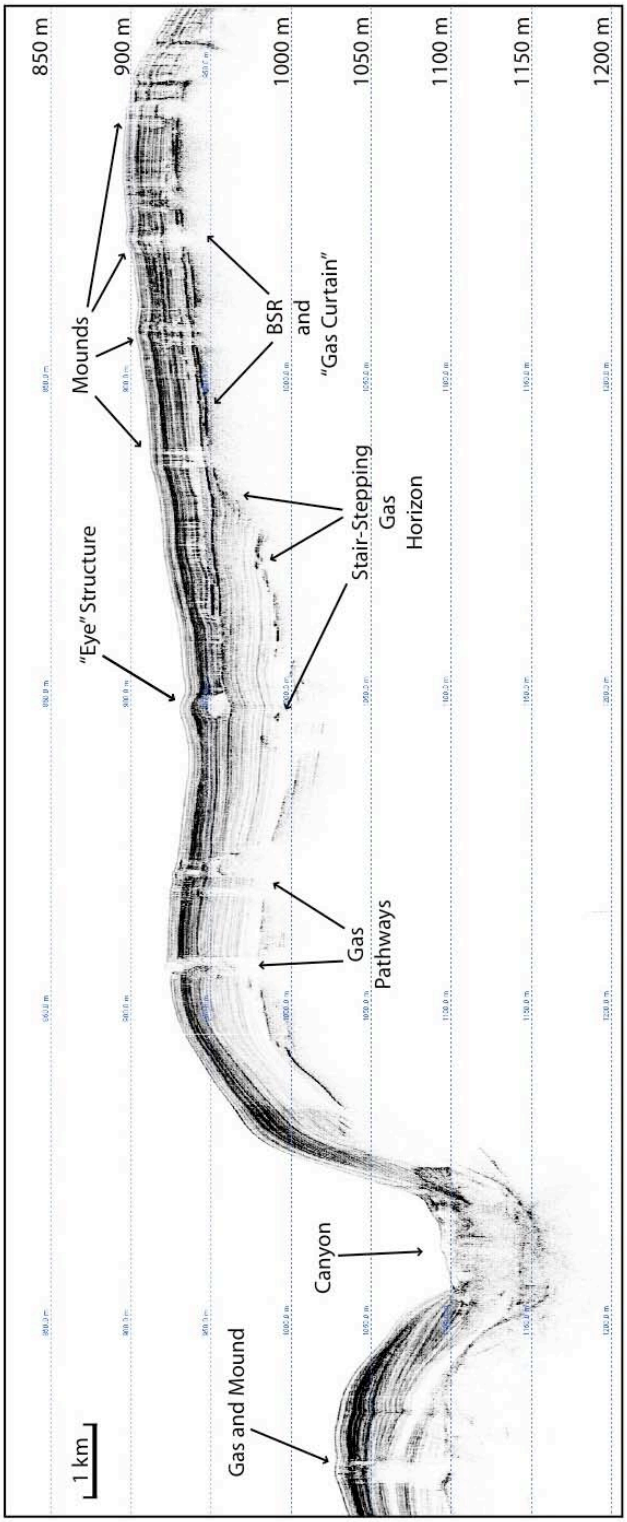
850 m
900 m
1000 m
1050 m
1100 m
1150 m
1200 m
Mounds
BSR
and
"Gas Curtain"
"Eye" Structure
Stair-Stepping
Gas
Horizon
Gas
Pathways
Canyon
Gas and Mound
1 km

Figure 3-31. Multichannel seismic reflection profile collected across Bransfield Strait. Data was downloaded from UIT seismic reflection database (http://www.ig.utexas.edu/sdc/) and displayed using Seismic Unix. Profile shown is among multiple profiles collected across the Bransfield Strait during research cruise EW9101 in 1991 lead by John Mutter and James Austin. Location of profile is shown in Barker and Austin, (1994). Note the high-amplitude reflection interpreted as a magmatic sill with upturned wings.

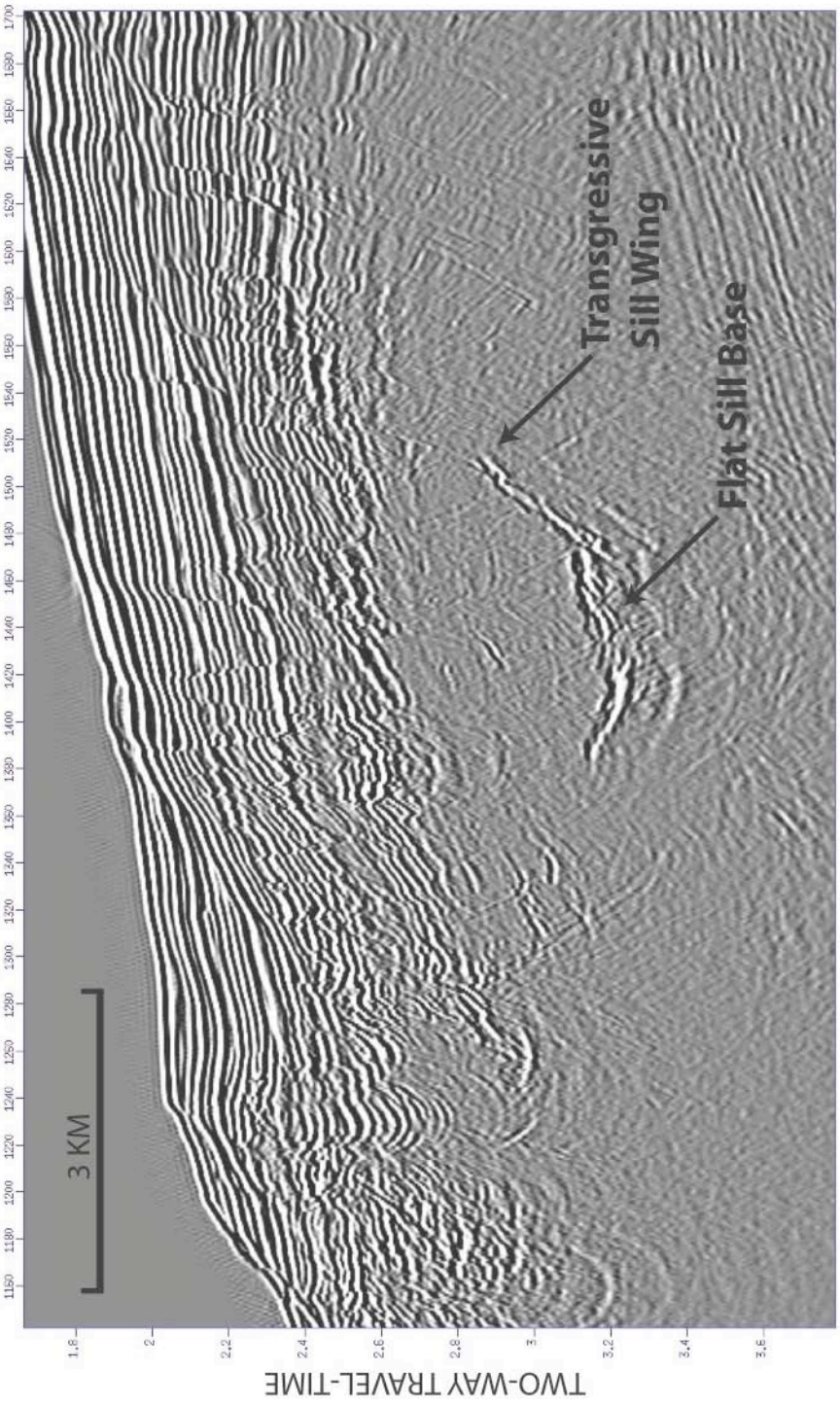
Transgressive
Sill Wing
Flat Sill Base
3 KM
TWO-WAY TRAVEL-TIME

Chapter 4

Conclusions

The research presented in this dissertation has improved the understanding of the relationships between tectonics, climate and erosion, sediment transport, sedimentation, and intrusive magmatism in the central Gulf of California. Unlike old, deeply-buried, passive rifted margins, the central Gulf of California provides a unique setting in which relatively young (and some currently active) rift-to-drift processes can be studied in high-resolution within the uppercrust. A key part of this research was the acquisition, processing, and interpretation of high-resolution geophysical data, including multichannel seismic (MCS) reflection profiles, 3.5 kHz profiles, and multibeam bathymetry. The two preceding studies have presented new geophysical and geological data that illuminated the interactions between processes influence the uppercrustal structure of a young oceanic rift system. The following paragraphs summarize the major results and conclusions of this research.

The first study investigates the effect of 100-kyr climate cyclicity on sedimentation and axial rift relief in southern Guaymas Basin. A high-resolution MCS profile collected across the Southern Trough of Guyamas Basin within the central Gulf of California reveals cyclical changes in reflector units below the adjacent basin floors. Several alternations in acoustically transparent units and close-spaced high-amplitude reflector units below the older flanking crust are correlated to a nearby, reprocessed MCS profile that crosses over Deep Sea Drilling Project (DSDP) Site 478. This allows correlation of basin-floor and trough-floor seismic stratigraphy with sampled sediment; seismically transparent units

correlate with parts of the cored sections where sandy beds at the base of (often subtly) graded diatomaceous mud sequences are very thin or absent (low internal impedance contrasts), whereas thick beds of silty sand terrigenous clastics (high internal impedance contrasts) correlate to high-amplitude reflector units. Sparse biostratigraphic data from the drill-cores is consistent with a match between the cyclic deposition of reflective and transparent units and indicate that alternations in reflector units correlate to glacial/interglacial climatic cyclicity. This correlation is also supported by the spatial extent of the seismic units, with the transparent units intercepting acoustic basement at approximately 100-kyr distance intervals using the half spreading rate (~23 km/Myr). Seismic stratigraphy also shows that while the reflector-rich sandy units were being deposited, turbidite accumulation rates in the southwest part of Guaymas Basin increased significantly, filling the axial trough. With lesser sediment supply during post-glacial periods, continued extension and spreading of the oceanic crust reestablished the axial rift-valley relief. Profiles collected in other pull-apart basins in the central and southern Gulf of California show similar reflector alternations, however lack of nearby drill-cores prevents accurate dating. The results from this study suggest that pronounced changes in sedimentation driven by 100-kyr climate cyclicity may be recorded in a variety of heavily sedimented tectonic settings that are largely affected by orbital-scale climate cyclicity. More specifically, this process may be common to young, oceanic rifted margins in which spreading centers are still located near sources of significant terrigenous

runoff (i.e. river deltas) or continental shelves, which could provide significant sediment input during low-stand (interglacial) periods.

The final study focuses on the relationship between young intrusive magmatism, sedimentation, and fluid-flow in the central Gulf of California. Analysis of MCS profiles in the central Gulf of California that transect across oceanic basins and bounding rifted and sheared continental margins provides extensive evidence of young magmatic sills, and associated host-rock deformation, fluid-flow structures, feeder structures, and hydrocarbon generation. Multiple large (1-2 km in diameter) sills display a characteristic concave-upwards profile and are mostly found as off-axis intrusions into unconsolidated sediments blanketing Guaymas, Carmen, and Farallon Basins, with a few identified within sediment ponded in the northern axial trough of Guaymas Basin. Groups of these satellite sills are also found emplaced into sediments overlying thinned continental crust and the basins' rifted and sheared margins, where they appear to acoustically mask the continental-oceanic boundary. Mutliple sills located in sediments blanketing both off-axis oceanic and continental crust are very young and uplift the present seafloor, disrupting turbidite patterns, providing onlap relationship timing with surrounding intrusions, faults, and sedimentary features. Using the combination of MCS and 3.5 profiles and multibeam bathymetry a large concave-upwards sill located near Farallon Transform is identified as a 3D saucer-shaped sill. Using this evidence, sills exhibiting inclined tips are interpreted as 3D saucer-shaped sills, similar to that found in the North Atlantic

Igneous Province and in multiple outcrop studies. Additionally, uplift features found directly above saucer-shaped sills are identified as sedimentary forced folds. Plotting sill width against emplacement depth reveals an overall linear trend (deeper = wider sill) and elastic modeling results (using Poly3D) reveal the development of an asymmetrical stress field above the sill after sediment uplift, suggesting emplacement depth as a control on the development of inclined tips. Above multiple sills, narrow zones of seismic turbidity and stacked high-amplitudes are interpreted as fluid-flow 'pipes', some of which are connected to pockmarks on the seafloor. Additional MCS profiles located over sills that lack obvious fluid pathways to the seafloor exhibit extensive evidence for concentrated hydrocarbons (i.e. bright spots, negative polarity, phase reversals, reflector pull-down). In the central Gulf of California, widespread evidence of magmatic intrusions into the shallow crust suggest that melt is being delivered not just to spreading centers, but to a much broader area of off-axis oceanic and continental crust. Furthermore, the interaction between sedimentation and volcanism in other heavily sedimented, young oceanic rift systems may play an important role in the distribution of magmatism and uppercrustal structure, as well as associated fluid-flow and hydrocarbon generation.